# Dynamically Linked Two Dimensional / One-Dimensional Hydrodynamic Modelling Program for Rivers, Estuaries and Coastal Waters

| | |
|---|---|
| Prepared For: | |
| Prepared By: | WBM Oceanics Australia |


***Offices***

*Brisbane*
*Denver*
*Karratha*
*Melbourne*
*Morwell*
*Newcastle*
*Sydney*

*Vancouver*

# DOCUMENT CONTROL SHEET


**WBM Oceanics Australia**

Brisbane Office:

WBM Pty Ltd
Level 11, 490 Upper Edward Street
SPRING HILL QLD 4004
Australia

PO Box 203
Spring Hill QLD 4004

Telephone (07) 3831 6744
Facsimile (07) 3832 3627
www.wbmpl.com.au

ABN 54 010 830 421 002


| | |
|---|---|
| ***Document:*** | WJS Thesis (Syme 1991).doc |
| ***Title:*** | Dynamically Linked Two-Dimensional/ One-Dimensional Hydrodynamic Modelling Program for Rivers, Estuaries & Coastal Waters |
| ***Project Manager:*** | |
| ***Author:*** | |
| ***Client:*** | |
| ***Client Contact:*** | |
| ***Client Reference:*** | |
| ***Synopsis:*** | |

## REVISION/CHECKING HISTORY

| REVISION NUMBER | DATE | CHECKED BY | | ISSUED BY | |
|---|---|---|---|---|---|
| 0 | | | | | |

## DISTRIBUTION

| DESTINATION | REVISION | | | | | | | | | | |
|---|---|---|---|---|---|---|---|---|---|---|---|
| | 0 | 1 | 2 | 3 | 4 | 5 | 6 | 7 | 8 | 9 | 10 |
| ???<br>WBM File<br>WBM Library | | | | | | | | | | | |

# CONTENTS

# LIST OF FIGURES

# SUMMARY

Hydrodynamic modelling practices are greatly enhanced by combining one-dimensional (1-D) and two-dimensional (2-D) models into one overall model. The benefits are: greater efficiency; reduced computation time; greater accuracy; impacts from works are registered in all models; and, improved user satisfaction and performance.

To realise these benefits, a dynamically linked 2-D/1-D hydrodynamic modelling program, codenamed TUFLOW, was developed. It is specifically designed for the modelling of long waves in rivers, estuaries and coastal waters.

For the 1-D component, the ESTRY program was used without any significant modification. ESTRY is an established program, based on an explicit finite difference method (FDM) for the 1-D shallow water equations (SWE). For the 2-D component, new computer code was written to emulate the 2-D SWE solution scheme proposed in Stelling (1984). The Stelling scheme is an alternating direction implicit (ADI) FDM based on the well-known Leendertse (1967, 1970) schemes.

The code written for the 2-D scheme was validated and assessed using a range of test models. The results from the testing found that:

1 Mass was conserved 100 % between internal grid elements.

2 The advection terms in the momentum equation were performing correctly.

3 Water level boundaries were extremely stable, but incorrect results can occur where only water level boundaries are specified, as the discharge across the model's boundaries is not defined.

4 Flow boundaries were highly unstable for steady state simulations, and where stable, caused a loss of mass of up to 3 % for large Courant Numbers (> 50). They showed good stability in dynamic simulations.

Incorporated into TUFLOW are three significant developments, namely:

1 A method for wetting and drying of 2-D intertidal flats, which allows the continued draining of perched waters.

2 The dynamic linking of any number of ESTRY 1-D network models to a TUFLOW 2-D model.

3 The stabilisation of water level boundaries lying obliquely to a 2-D orthogonal grid, therefore, providing maximum flexibility for locating the 2-D/1-D interface.

A comprehensive computer graphics system was also developed for the purpose of this study, but is not presented as part of this thesis. Aspects of the above developments have been briefly described in Syme (1989, 1990a), and Syme and Apelt (1990b).

The wetting and drying method developed is shown to calculate the tidal prism more accurately, and to eliminate the occurrence of surges when perched waters are re-connected with the rising tide. Application in practice has shown the method to be a significant improvement over convential methods, especially in models with large areas of intertidal flats.

For dynamically linking the 1-D and 2-D schemes, a simple but effective method is proposed, which utilises the excellent stability properties of the 2-D scheme's water level boundaries.

The 1-D and 2-D boundaries at the interface are treated as normal open boundaries. A flow boundary is specified for the 1-D model and a water level boundary for the 2-D model. At the end of each computation step boundary condition data is transferred from one model to the other. For the 1-D boundary, the flow across the 2-D model boundary is specified, while for the 2-D boundary the water level from the 1-D model is used.

The conditions at the 2-D/1-D interface are that the water level is approximately horizontal, there is negligible variation in the convective acceleration terms and the flow is perpendicular to the 2-D model boundary. These are essentially the same conditions which are applied at the open boundaries of the 1-D and 2-D schemes.

Testing has shown the 2-D/1-D link to conserve mass 100 % and to have no stability problems. Application to more than twenty production models has shown it to be a very useful and powerful facility.

A key aspect in the successful application of the 2-D/1-D link was the development of a method for stabilising water level boundaries which lie obliquely to the orthogonal 2-D grid. This provides maximum flexibility for locating the interface, which in practice is extremely important, because of the irregularity of natural water bodies.

This thesis presents a discussion on the process of selecting the 1-D and 2-D schemes; and the details of: the methodology used for coding the 2-D scheme; the wetting and drying method; the dynamic 2-D/1-D link; and the stabilisation of oblique water level boundaries. Selected results from test cases are also presented.

# LIST OF SYMBOLS

$A$ = *Cross - section Area*

$B$ = *Width of Flow*

$C$ = *Chezy Bed Friction Coefficient*

$C_0, C_1, C_4$ = *C Values on 2 - D Grid (See Figure 3.1)*

$c_f$ = *Coriolis Force Coefficient*

$C_r$ = *Courant Number*

$d_f = 2H_{u/s}(1 - f_f)$

$$\left.\begin{matrix} E_{vv}0, E_{vv}2, E_{vv}4 \\ E_{uv}0, E_{uv}1 \\ E_v0, E_v1 \end{matrix}\right\} = \left\{\begin{matrix} \text{Computation Coefficients} \\ \text{Stage 1, Step 1 of 2 - D Scheme} \end{matrix}\right.$$

$$\left.\begin{matrix} E_u, E_{vu}, E_{uu} \\ E_{10}, E_{13}, E_{20}, E_{23} \\ E_{30}, E_{33}, E_{40}, E_{43} \end{matrix}\right\} = \left\{\begin{matrix} \text{Computation Coefficients} \\ \text{Stage 1, Step 2 of 2 - D Scheme} \end{matrix}\right.$$

$$E_{50}, E_{53}\rangle = \left\{\begin{matrix} \text{Additional E Coefficients} \\ \text{for Free Overfall Method} \end{matrix}\right.$$

$$f_0, f_3 = \left\{\begin{matrix} \text{Factors at } u_0 \text{ and } u_3 \text{ points} \\ \text{Oblique Water Level Boundary Method} \end{matrix}\right.$$

$f_f$ = *Free Overfall Factor*

$f_{ob}$ = Oblique Water Level Boundary Weighting Factor

$f_x, f_y$ = { Distance Factors in X and Y Directions; Oblique Water Level Boundary Method }

$F_x, F_y$ = Components of External Forces in X and Y Directions

$g$ = Acceleration due to Gravity

$H$ = Total Water Depth = $h + z$ (2 - D Scheme)

$h$ = Water Depth Below Datum (positive downwards)

$h_1, h_2, h_3, h_4$ = h Values on 2 - D Grid (See Figure 3.1)

$h_{0'}, h_{3'}$ = Adjusted h Values at $u_0$ and $u_3$ points

$H_f$ = Free Overfall Depth

$h_u$ = h Value at a u point

$H_{u/s}$ = Upstream Water Depth

$H_v$ = H Value at a v point

$h_v$ = h Value at a v point

(Free Overfall Method)

$H_{vy}$ = Computation Coefficient - Stage 1, Step 2

$k$ = Energy Loss Coefficient

$m$ = 2 - D Element Grid Reference in X Direction

$n$ = 2 - D Element Grid Reference in Y Direction

$p$ = Sweep Number (2 - D Scheme)

$p'$ = Computation Control Variable (2 - D Scheme)

$Q$ = Discharge

$q$ = Iteration Counter (2 - D Scheme)

$q$ = Discharge per Unit Depth

$q, r, s, t$ = Coefficients for Tri - diagonal Matrix Solution

$S$ = Water Surface Gradient

$t$ = Time

$u$ = { Depth and Width Averaged Velocity (1 - D Scheme); Depth Averaged Velocity in X Direction (2 - D Scheme) }

$u_0$, $u_1, u_3, u_4$, $u_8, u_{10}, u_{12}$ = u Values on 2 - D Grid (See Figure 3.1)

$\bar{u}$ = Mean u Value at a v point

$V$ = Velocity Magnitude

$v$ = Depth Averaged Velocity in Y Direction (2 - D Scheme)

$v_0$, $v_1, v_2, v_3, v_4$, $v_6, v_9, v_{11}$ = v Values on 2 - D Grid (See Figure 3.1)

$\bar{v}$ = Mean v Value at a u point

$x$ = { Distance (1 - D Scheme); Distance in X Direction (2 - D Scheme) }

$y$ = Distance in Y Direction (2 - D Scheme)

*A superscript on $u, v$ or $z$ indicates its computational level as follows :*

*0 - Beginning of Timestep*

*1 - End of Stage 1*

*2 - End of Stage 2*

*p - 0, or Sweep 1 or 2*

*q - $q^{th}$ Iteration on the Variable*

** - Indicates either p or p - 1*

$\Delta t$ = *Computation Timestep*

$\Delta x = \begin{cases} \text{Length of 1 - D Model Element} \\ \text{Length of 2 - D Model Element in X Direction} \end{cases}$

$\Delta y$ = *Length of 2 - D Model Element in Y Direction*

$d$ = *Computation Control Variable in 2 - D Scheme*

$z$ = *Water Surface Elevation Relative to Datum*

$z_0, z_1, z_2, z_3, z_4$ = $z$ *Values on 2 - D Grid (See Figure 3.1)*

$z_{bv}$ = *Pre - defined Boundary Water Level*

$m$ = *Horizontal Diffusion of Momentum Coefficient*

$f$ = *Angle of Oblique Water Level Boundary Line*

# ACKNOWLEDGEMENTS

The author wishes to acknowledge the following persons and organisation, who gave the support, encouragement and patience necessary for the completion of this study.

- WBM Pty Ltd (Oceanics Australia).
- Professor Colin Apelt (The University of Queensland).
- Dean Patterson, Craig Witt and Tony McAlister (whom the author can fully recommend for providing constructive suggestions and finding "bugs" in "user-friendly" software).
- Georgina Warrington.

This study was funded by WBM Pty Ltd and The University of Queensland.

# QUALIFICATION

All that is presented and discussed in the content of this thesis, including any reference to computer code (except for the ESTRY program), was the work of the author.

# 1 INTRODUCTION

## 1.1 General

Quantifying the hydraulic behaviour of natural and artificial watercourses is often essential for (a) understanding hydraulic, biological and other processes, (b) predicting impacts of works and natural events, and (c) environmental management. Numerical hydrodynamic models are presently the most efficient, versatile and widely used tools for these purposes. There are, however, opportunities for development, amelioration and refinement of the mathematical methodologies used.

A hydrodynamic model aims to represent numerically the topography and roughness of a watercourse, so as to be a sufficiently accurate approximation of the real situation. Along the boundaries of the model, estimates of the hydraulic conditions need to be specified prior to a simulation. These boundary conditions could be the water levels of an ocean tide or the flow in a river. A computer program simulates the hydraulic behaviour over time throughout the domain of the model using the free surface fluid flow equations.

The general purpose computer software used for developing, calculating and displaying the results of hydrodynamic models can be classified into two areas. Firstly, the coding for the solution scheme and, secondly, for processing the input and output data. There is a need for continued improvement and optimisation of the solution schemes so more complex and detailed hydrodynamic systems can be modelled. In conjunction with this, the development of user-friendly, menu driven, graphic environments has many benefits.

The development of computer graphic systems for data input and output is being driven by further advances in computer hardware. This must not be brushed aside as fancy trimming, but as the opportunity to develop easily and efficiently hydrodynamic models of great complexity, and to enhance the visualisation and understanding of model results. To realise these opportunities the development of computer software in this area is necessary and should be given a high priority.

The solution schemes must be accurate, robust and versatile to be of use in practice. No one universal scheme has yet been developed because of a combination of factors such as the complexity and range of scale of natural waterways, limitations of computer hardware, and cost versus benefit considerations. Schemes are therefore varied in their complexity, accuracy and robustness, and are designed for specific areas of application.

The schemes are approximate solutions of the partial differential equations of mass and momentum conservation for unsteady free-surface flow of long waves. These equations are known as the shallow water equations (SWE), and are typically used for modelling floods, ocean tides or storm surges.

SWE schemes are categorised as either one-dimensional (1-D), two-dimensional (2-D) or three-dimensional (3-D). A 1-D scheme is based on a form of the 1-D SWE, a 2-D scheme on the 2-D SWE, and so on. 1-D schemes are the simplest and most economical, while 3-D schemes are complex and highly demanding on computational effort and computer memory. 1-D and 2-D schemes are by far the most widely used and are those which we are concerned with in this study.

1-D schemes are typically used for rivers and estuaries as the flow is essentially channelised or one-directional. In these schemes the water velocities are calculated as a cross-sectional average in the direction of flow. 1-D solution schemes are often networked to give a quasi 2-D representation and to model branching of water courses. These models are widely used for modelling the flooding of rivers and floodplains, and tidal flows in estuaries.

2-D schemes are normally in plan view with the velocities averaged over the depth of the water column. They are mostly used for coastal waters where the water moves in a horizontal plane and also in sections of rivers and estuaries where a more detailed study of the flow patterns is required. 3-D schemes are occasionally adopted where the study requires consideration of density and temperature variations in the water column or the flows are sufficiently complex to warrant the third dimension. 2-D schemes can be layered to give a quasi 3-D effect.

Clearly, the domains of 1-D and 2-D models must meet and overlap. For example, the river (1-D model) discharging into a coastal bay (2-D model), or when modelling on a fine scale the 2-D flow patterns in a section of an estuary.

Representing such scenarios as one overall model composed of a combination of 1-D and 2-D models, has numerous benefits relating to greater flexibility, accuracy, efficiency and performance. To realise these benefits a dynamic link between the 1-D and 2-D schemes is required. The dynamic link transfers hydrodynamic variables from one model to the other as the computation proceeds, thus removing the need to simulate 1-D and 2-D models separately. An example of how a dynamically linked 2-D/1-D model would be schematised is illustrated in Figure 1.1.

The 2-D/1-D dynamic link, despite its many benefits, is only mentioned in the literature a few times (Stelling 1981, Danish Hydraulic Institute 1983 and Crean et al 1988). The development of a robust and widely applicable 2-D/1-D dynamically linked scheme for use in practice does not appear to have been publicised. To realise the benefits of a 2-D/1-D link a study was initiated by the author, the results of which are presented herein.

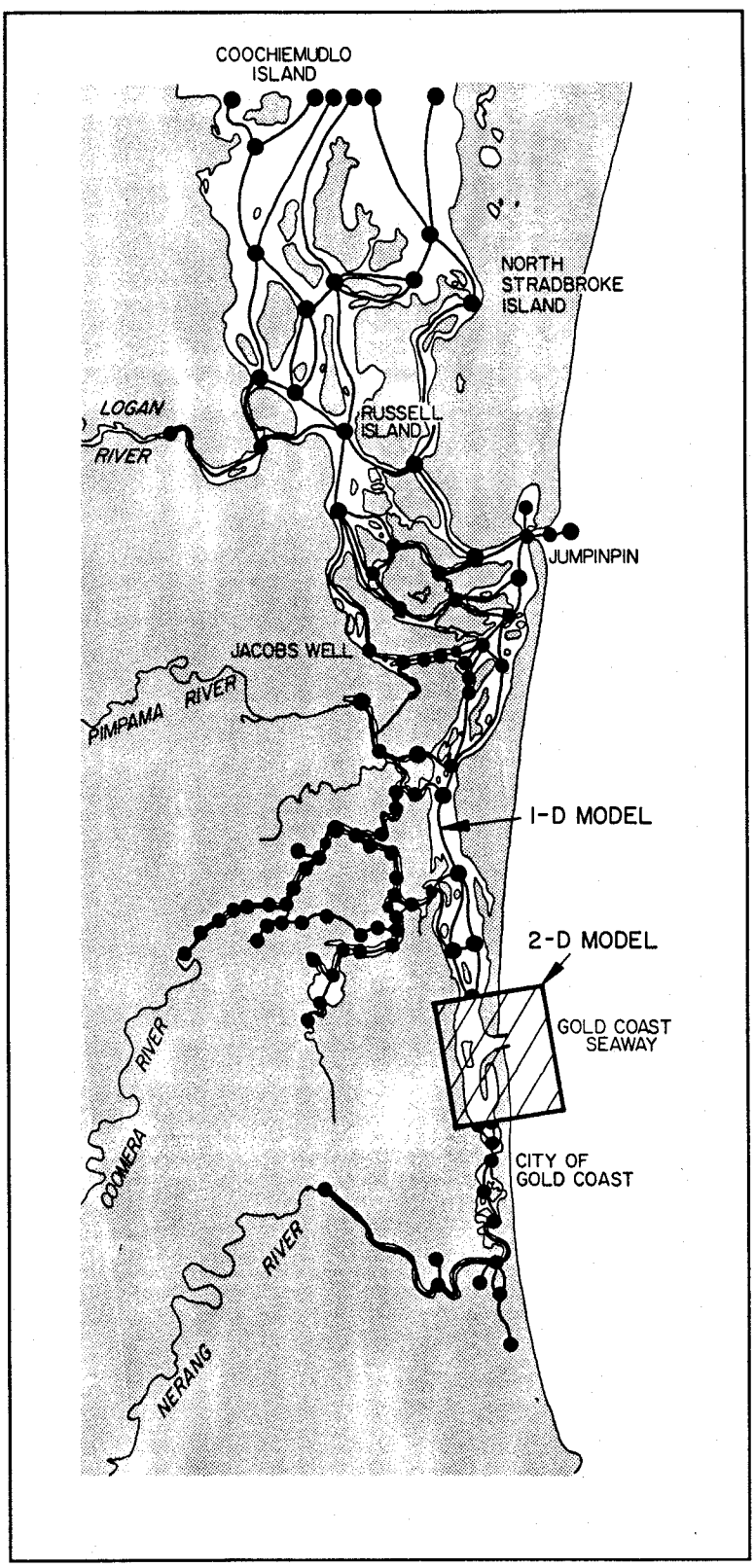


**Figure 1.1 Linked 2-D/1-D Model Layout**

## 1.2 Benefits and Limitations of Dynamically Linked 2-D/1-D Models

The benefits of representing a hydrodynamic system as a combination of 1-D and 2-D models dynamically linked together are:

(a) greater flexibility and versatility when developing a hydrodynamic model,

(b) the hydrodynamic response resulting from a change to one model is registered in all other models (this is particularly important for assessing hydraulic impacts),

(c) greater computational efficiency and accuracy, and

(d) user satisfaction and performance.

A more general discussion of the benefits is presented in point form below.

(i). Most hydrodynamic systems of coastal regions are best represented by a combination of 1-D and 2-D models. For example, in the case of a river (1-D model), flowing into a coastal bay (2-D model). In such situations, the traditional approach has been to use separate models. This can lead to uncertainties and inaccuracies if the boundary conditions of the models where they interface are not clearly defined. If the 1-D and 2-D models can be dynamically linked these uncertainties and inaccuracies would be eliminated.

(ii). A 2-D model of an estuary can often not cover the whole tidal waterway because of limitations on the model dimensions and computation time. This necessitates that the neglected waterways must be (a) represented by artificially created areas within the 2-D model domain, (b) represented by a separate 1-D model as discussed above, or (c) ignored. If significant areas of a tidal waterway are ignored or poorly represented, a tide model will produce inaccurate results as it is essential that the full tidal compartment be modelled. By being able to link 1-D models dynamically onto a 2-D model, the entire tidal waterway area outside the 2-D model domain can be simply and easily represented.

(iii). The majority of hydrodynamic modelling exercises are carried out to establish the impacts of works and natural events, and to provide engineering solutions to minimise these impacts. If impacts extend outside the domain of a model, their full extent can not be assessed accurately. The ability to represent easily a greater area with dynamically linked 1-D and 2-D models would largely overcome this problem as the impacts would be registered in all models. This is not the case where separate 1-D and 2-D models are used.

(iv). The domain of a 2-D model may also have to be extended well away from the area of interest to define an open boundary adequately. If part of this extension of the 2-D model can be represented by a 1-D model, the coverage of the 2-D model can be reduced allowing decreased computational times and/or a finer spatial discretisation.

(v). The greater flexibility, accuracy and versatility associated with a 2-D/1-D dynamic link would provide indirect benefits of user satisfaction and performance. These benefits would result from

those benefits already mentioned such as reduced data input; higher turnover of simulations because of faster computations; greater flexibility and greater confidence in the results.

Limitations of the 2-D/1-D dynamic link would be:

(a) Stability constraints at the 2-D/1-D interface which override those of either the 1-D or 2-D schemes.

(b) Loss of accuracy caused by assumptions built into the 2-D/1-D link.

(c) Numerical disturbances caused by the 2-D/1-D link.

## 1.3 Available Computer Software

Suitable computer software code which was freely available is briefly discussed in this section. The computer programs were developed by WBM Pty Ltd or The University of Queensland.

It is noted that software which resulted from this project was to be used for both consulting and research purposes. Some preliminary investigations showed that this essentially excluded software from other organisations as there was generally a major cost involved if it was to be used for consulting. Also some organisations only offer executable code, not source code as was required.

The other consideration is the benefits gained from developing in-house software. This should not be over-looked, and was the preferred approach at all times.

### 1-D Hydrodynamic Programs

WBM Pty Ltd has developed and used extensively the 1-D hydrodynamic network program, ESTRY (Morrison and Smith, 1978) since 1974. It can be regarded as a proven program, having been widely used in practice, and scrutinised.

The University of Queensland has also developed a 1-D hydrodynamic program (Apelt, 1982). Although not widely used in design applications it has had many research applications and can be regarded as capable and accurate.

For the purposes of this project, ESTRY was given preference for the following reasons:

- the author's familiarity with the program coding and his involvement in ESTRY's development.
- ESTRY has had far wider use in practice with a large bank of developed and calibrated models available for use if required.

### 2-D Hydrodynamic Programs

WBM Pty Ltd has available the 2-D hydrodynamic modelling program, TWODIM, which is based on the well-known method described in Leendertse (1967). This method has found widespread use in the consulting and research fields because of the public availability of the computer code and Leendertse's good documentation. It has, however, a number of limitations relating to numerical stability and accuracy and is today regarded as somewhat outdated. During the 1980's a number of alternative solution schemes for the 2-D SWE have been presented in the literature and are claimed to be superior to the Leendertse scheme.

The University of Queensland developed an explicit 2-D hydrodynamic program (Apelt et al, 1974). This program is fairly limited and has been used only for research applications and was therefore given minor consideration. Also for reasons to be discussed later it was desirable to have an implicit or unconditionally stable 2-D scheme.

As the above 2-D hydrodynamic programs are not representative of the present level of world expertise, it was decided to investigate the possibility of developing new computer code. If it became apparent that this could not be achieved in the given timeframe, the TWODIM code would be used for developing the 2-D/1-D dynamic link. Consideration was also given to purchasing suitable software.

## 1.4 Study Objectives

The main objective of the study was to develop a computer program capable of modelling long waves using 1-D and 2-D solution schemes dynamically linked together. As discussed above, it was also highly desirable to develop a new computer program for the 2-D component, noting that the development of such a program would be a major exercise in itself. Consideration was also to be given towards the development of a computer graphics system for 2-D models to enhance data entry and output.

After initial investigations and literature reviews the objectives were broadly defined as:

1a. Develop a new computer program based on one or more 2-D schemes described in the literature.

1b. In parallel to 1a above, develop a computer graphics system for 2-D models.

2. Research and develop an algorithm for dynamically linking the 1-D scheme of the ESTRY program with the 2-D scheme resulting from 1a above.

During the course of the project it became apparent that further research and development of improved methods for modelling wetting and drying of intertidal flats in a 2-D model, and for handling oblique water level boundaries on an orthogonal 2-D grid was advantageous. The latter was especially required for allowing maximum flexibility when locating the 2-D/1-D link interface.

## 1.5 Thesis Layout

### Chapter 2

Chapter 2 contains a discussion of the preliminary investigations carried out so as to form a solid research basis and establish methodologies prior to software development. Literature reviews and general notions on the dynamic linking of 1-D and 2-D schemes are presented. Guidelines for selecting 1-D and 2-D schemes are set down.

Based on these guidelines, the suitability of the ESTRY program for the 1-D component is established. Several of the more prominent 2-D schemes presented in the literature are reviewed and assessed for the purpose of developing a new 2-D hydrodynamic program. One of these 2-D schemes is selected.

## Chapter 3

The mathematical methods used in the new 2-D hydrodynamic program are presented in Chapter 3. The performance of the methods are discussed and illustrated through computer graphic output. Not presented in any detail is the considerable effort which went into data administration and the numerous features, such as error messages and flexibility in specifying boundary values, which make a program highly user-friendly and easy to apply in practice.

The mathematical solution, which is based on Stelling (1984), is an alternating direction implicit (ADI) finite difference method over an orthogonal grid. A brief description of the computation procedure and the treatment of model boundaries as proposed by Stelling is presented. The methodology used by the author for coding the scheme is detailed.

The more interesting results of the many test cases used to validate the 2-D scheme are illustrated and examined. The scheme's performance under different conditions is established.

To enhance the performance of the 2-D scheme in practical situations a new wetting and drying method is proposed. The results of test cases highlighting the performance of the method is presented.

## Chapter 4

The method proposed for linking dynamically the 1-D and 2-D schemes is described in Chapter 4. The logic behind selecting the types of open boundaries at the interface is discussed followed by the details of the transfer of data from one model to the other.

The results of two of a range of test cases, which were used to validate the method and assess its performance, are presented. These tests show a comparison of results for idealised situations which are modelled in both a 1-D and a 2-D/1-D form.

To allow maximum flexibility in locating the 2-D/1-D interface, investigations into calculating the flow across a line oblique to a 2-D orthogonal grid, and for improving the stability of water level boundary conditions along an oblique line were made. Methods to handle these situations are proposed and detailed. The results of a test case highlighting their performance are presented.

# 2 SELECTION OF SCHEMES

## 2.1 Summary

A discussion on the preliminary investigations carried out to establish the basis for the research and development of the 2-D/1-D hydrodynamic program is presented.

Firstly some base considerations are addressed, namely, whether to use finite differences or finite elements, the definition of the Courant Number, and the merits of explicit and implicit schemes.

Secondly, a literature review and some general aspects of dynamically linking 1-D and 2-D schemes are presented. Based on this, broad guidelines are established for the selection of the 1-D and 2-D SWE solution schemes.

As discussed earlier, the program ESTRY was preferred for the 1-D component primarily because of the availability of its computer code and its widespread application. The ESTRY program is briefly described and is shown to be suitable for implementation into the 2-D/1-D hydrodynamic program based on the guidelines.

The 2-D SWE scheme is addressed. A selection of the more suitable schemes are reviewed based on reports in the literature and private communication. The scheme described in Stelling (1984) was selected for the development of a new 2-D hydrodynamic modelling program on the grounds of a good level of documentation and high standard of performance.

## 2.2 Base Considerations

### 2.2.1 Finite Differences versus Finite Elements

Only finite difference methods (FDM) have been considered for the purposes of this project as opposed to other methods such as that of finite elements (FEM). The reason for this is that FDM have tended to dominate the literature in the free-surface hydrodynamic modelling field and are by far the most popular for use in practice. Also, the ESTRY solution scheme is a FDM, and a practical link to it would require using a FDM for the 2-D scheme.

The domination of the FDM originates from their simplicity making them the only real option when computers were far more limited. In more recent times the FEM has found greater application for large scale models, but is still cumbersome and more expensive for the finer detail models (Benque et al 1982b). For a program to be of wide application, the FDM is still the preferred option. This has become even more so with the use of curvilinear grids which provide the same benefit that the FEM offers, namely better geometrical representation of a model's boundaries.

### 2.2.2 Courant Number / Computation Timestep

The Courant Number, $C_r$, extends from the 'Courant-Friedrichs-Lewy (CFL) condition' (Abbott 1979). An implication of the CFL condition is that the stability of an explicit scheme is conditional on $C_r$ being less than 1.0. Only approximate solutions will occur for $C_r$ less than 1.0, while for $C_r$

greater than 1.0 the solution will bear little or no resemblance to the true solution, ie an unstable simulation. A true solution will occur if $C_r$ is equal to 1.0.

Implicit schemes are generally not conditional on $C_r$ being less than 1.0 and are referred to as unconditionally stable. The inaccuracy (phase error) of an implicit scheme, however, increases with increasing $C_r$. The degree of inaccuracy can be established for simple cases using phase portraits (Abbott 1979), but is difficult to ascertain in practice other than by comparing with simulations which used lower values of $C_r$.

In practice the Courant Number is used as a guide for calculating the computation timestep for a simulation. Assuming the mean water velocity to be small compared with the wave celerity, the formula for $C_r$ is given by Equations 2.2.1 (1-D) and 2.2.2 (2-D). In the case of a 2-D square grid Equation 2.2.2 reduces to Equation 2.2.3.

$$C_r = \frac{\Delta t \sqrt{gH}}{\Delta x} \qquad \textbf{1-D Scheme (2.2.26)}$$

*where*

$\Delta t = timestep, s$

$\Delta x = length\ of\ model\ element, m$
$g = acceleration\ due\ to\ gravity, ms^{-\frac{1}{2}}$

$H = depth\ of\ water, m$

$$C_r = \Delta t \sqrt{gH} \left( \frac{1}{\Delta x^2} + \frac{1}{\Delta y^2} \right)^{\frac{1}{2}} \qquad \textbf{2-D Scheme (2.2.2)}$$

$$C_r = \frac{\Delta t \sqrt{2gH}}{\Delta x} \qquad \textbf{2-D Square Grid (2.2.3)}$$

In reality the value of $C_r$ varies over the computational domain, as either the element lengths and/or depths vary (the timestep usually being constant). Usually when a Courant Number is quoted it is the largest value over the model domain. This is referred to as the critical Courant Number as it is used to determine the most suitable computation timestep. For 2-D models of constant element size, the average depth is sometimes used.

All Courant Numbers quoted in this thesis are critical values for the models considered. For tidal simulations, the critical Courant Number was calculated on the basis of water depths at mid tide (at mean water level).

### 2.2.3 Explicit versus Implicit Schemes

Explicit schemes allow the calculation of results in one analytical step based entirely on parameter values from the previous time step. Implicit schemes use formulations incorporating two or more unknown time dependent parameter values. They therefore require the use of iterative procedures and matrix solution methods, and are more difficult to formulate.

Mathematical stability analyses generally show that explicit schemes are restricted to Courant Numbers less than unity which requires the use of small computation timesteps. Explicit schemes are, however, generally easier to formulate and use less computational effort per timestep than implicit schemes.

The advantage of using implicit schemes is that they are not restricted to Courant Numbers less than unity, and can therefore use larger timesteps than explicit schemes. Clearly there must be an upper limit to the timestep, the determination of which varies depending on the scheme and complexity of the flow. A too large a timestep is generally characterised by either instabilities and/or inaccuracies. For most implicit schemes in use today, a critical Courant Number between 2 and 15 is typically used.

The preference for an explicit or an implicit scheme is partly a personal issue dependent on the type of schemes the person is familiar with. Historically, implicit schemes were often preferred because of their capability to provide stability at large time steps, thereby reducing computational effort.

For 1-D schemes the issue of computation speed superiority of implicit schemes is less important with today's level of computing power except for extremely large models or simulations over a long period of time. Thus, with regard to the 1-D scheme, either an explicit or implicit method would suffice for this study.

For 2-D SWE schemes, explicit methods can be satisfactory for large grid sizes as the number of timesteps per tidal cycle is not prohibitive. An example given in Benque et al (1982b) for a model of the English Channel with a grid spacing of 10 km required 200 timesteps per tide. In comparison, a model with a grid spacing of 20 m would require in excess of 100,000 timesteps per tidal cycle which can be prohibitive depending on the computer hardware. As the 2-D scheme was to be as wide ranging as possible in its application, it was decided that an implicit 2-D scheme would be preferable to an explicit one.

## 2.3 Linking 1-D and 2-D Schemes

### 2.3.1 General

This section presents a general discussion on the dynamic linking of 1-D and 2-D schemes. Firstly a literature review is given followed by consideration of a number of key aspects as given below.

- methodology of 2-D/1-D dynamic link,
- timestep compatibility of 1-D and 2-D schemes,
- Courant number/stability criteria of 1-D and 2-D models,
- oblique orientation of 2-D/1-D interface to a 2-D orthogonal grid.

### 2.3.2 Literature Review

A review of Stelling (1981), Danish Hydraulic Institute (1983) and Crean et al (1988) with regard to the linking of 1-D and 2-D SWE schemes is given below.

## Stelling (1981)

Stelling (1981) examines several methods for coupling or linking 1-D and 2-D schemes. The schemes used are both implicit with the 2-D scheme being based on that of Leendertse (1970).

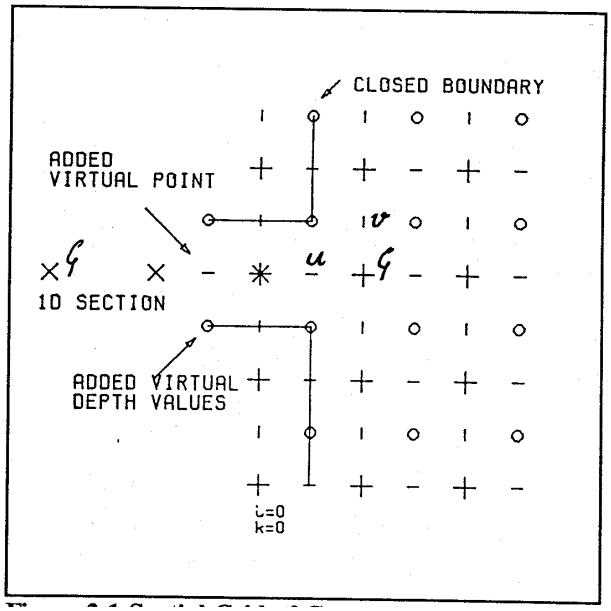


**Figure 2.1 Spatial Grid of Coupled Model, (Figure 4.1, Stelling 1981)**

Three methods are proposed and are briefly described below. They are based on the prescription of internal boundary conditions at the interface of the two models in conjunction with the governing equations. The internal boundary conditions are based on a common water surface level and equivalence of flow in the direction perpendicular to the internal boundary of the 2-D model. The governing equations at the interface need only be expressed in a 1-D form in the direction of the flow.

For the methods presented, Figure 2.1 illustrates the spatial grid of the coupled 1-D/2-D model arrangement. A virtual velocity point is created which is where the equivalence of flow condition is applied.

Method 1 Uses the virtual flow point and a one-sided difference form of the continuity equation.

Method 2 As for Method 1 but the characteristic equations are used. In the case examined only the outgoing characteristic equation is used. The advantage of this method appears to be the capacity to overcome the one-sided differencing used in Method 1 by using either the out-going or in-going form of the equations as applicable.

Method 3 This method, which is different to the above two, uses an overlapping of the 1-D non-staggered grid with the 2-D staggered grid. The internal boundary conditions and forms of the continuity and momentum equations can then be applied at the overlap.

The accuracy of each method is assessed through simple model test cases. In each case spurious waves or numerical disturbances were generated as a wave passed through the internal boundaries of the two models. Method 2 was shown to produce by far the most accurate results. Stelling concludes that:

'A coupling between existing 1-D and 2-D models can be established indeed. Coupling schemes based upon characteristics are likely to give the most accurate results.'

### Danish Hydraulic Institute (1983)

A coupling of the Danish Hydraulic Institute S11 (1-D scheme) and S21 (2-D scheme) computer programs in an application to the Gambia estuary and river is given in Danish Hydraulic Institute (1983). No detail or reference is provided other than that the 'coupling is led through a special component that is comprised of a set of parallel one-dimensional channels with constraints imposed upon lateral exchanges between them'.

### Crean et al (1988)

Crean et al (1988) describes the development of a combined 1-D and 2-D model codenamed GF2 of the Strait of Georgia, Juan de Fuca Strait, and adjoining passages and inlets. The 2-D scheme is solved explicitly over a square mesh. Two 1-D schemes are used, the first being explicit and an adaptation of the 2-D scheme, the second being implicit. The 1-D explicit scheme does not include the advective accelerations.

At each junction the width of the channel in the 1-D model is assumed to be the same as the 2-D square mesh size. To obtain the correct cross-sectional area the depth of the 1-D channel is adjusted.

The linking of the 2-D and explicit 1-D schemes was carried out as follows. When solving the 1-D continuity equation for the water level adjacent to the 2-D model, the adjoining 2-D grid element is treated as an extension to the 1-D model. This allows the flow into/out of the 1-D model to be defined. For calculating the boundary water level of the 2-D model a Lagrangian interpolation of the adjacent water levels in both the 1-D and 2-D models was used. This appears to be necessary as the spatial location of the 1-D and 2-D water level boundary values are not coincident.

For linking the 2-D and implicit 1-D schemes a similar approach was adopted, but the need for the Lagrangian interpolation is removed by defining the length of the first element of the 1-D model as equal to the mesh size of the 2-D model. This allows the 2-D continuity equation to be used at the boundary of the 2-D model by adopting the first element of the 1-D model to be an extension of the 2-D model in a similar manner to that used for the 1-D model as described above.

## 2.3.3 Comments on the Literature

The three sources listed above all present or illustrate one or more methods for linking 1-D and 2-D schemes. Comments on these methods and their suitability are presented below:

(i). All of the methods appear to be limited in that only one 2-D grid element can be connected to a 1-D model as opposed to any number of 2-D elements. This problem is overcome to some extent in the Danish Hydraulic Institute example where the 1-D model is branched into a number of parallel channels with each of these connecting to a single 2-D grid element. Such a procedure is, however, somewhat cumbersome.

(ii). Stelling (1981) applies the proposed methods to idealised situations only. The performance of the methods when applied to practical situations does not seem to have been presented in the

literature and is therefore uncertain. Some concern must be expressed over the occurrence of the numerical disturbances and instabilities mentioned.

(iii). The methods described in Crean et al (1988) appear limited because of the restrictions on the linkage of 1-D and 2-D schemes.

(iv). The use of two different solution schemes for the 1-D and 2-D models is plausible.

### 2.3.4 Methodology of 2-D/1-D Dynamic Link

There are essentially two types of methodologies that can be used for linking 1-D and 2-D schemes. They are:

1. The 1-D and 2-D schemes are solved independently, with each scheme "feeding" the other boundary values after each computation step. Such an arrangement allows the 1-D and 2-D schemes to be autonomous. However, both schemes must have "non-reflective" characteristics at an open boundary so the conveyance of mass from one model to another is accurately represented.

2. The 1-D and 2-D schemes use a similar solution technique so that both the 1-D and 2-D equations are solved simultaneously. In this situation, the 1-D sections would essentially be an extension of the 2-D grid.

Most of the methods described in Section 2.3.2 are of the first type. Variations on this methodology are used however, such as overlapping models so they have common computation points or the use of virtual points outside the model domains.

The first type was selected in this project in preference to the second as it allowed greater freedom when selecting the 1-D and 2-D schemes and has potentially more flexibility and a wider range of applicability. Limitations may be "reflective" boundaries at the 2-D/1-D interface and harsher stability constraints.

### 2.3.5 Computation Timestep

To avoid extrapolation of boundary values at the 2-D/1-D interface, it is necessary for the computation timestep to be the same for both schemes. Extrapolation of boundary values would require an iterative procedure to ensure convergence occurred. This is unlikely to provide any benefits in computation efficiency.

A common computation timestep for both the 1-D and 2-D schemes implies that one of the schemes would be running inefficiently as it would be using a smaller timestep than that which would be used to run the scheme on its own.

### 2.3.6 Courant Number Constraints

By adopting a common computation timestep, the critical Courant Number of each of the 1-D and 2-D models would differ greatly, with the value for a 2-D model being typically greater than that of a 1-D model because of the finer or smaller spatial discretisation in the 2-D model. Adopting this as being the norm, the issue of whether the solution schemes should be explicit or implicit is discussed

below. For the purposes of the discussion, an explicit scheme implies the critical Courant Number is less than unity, while for an implicit scheme a value no greater than fifteen is implied.

If both the 1-D and 2-D schemes are implicit the computation timestep would be controlled by the 2-D model. This necessitates that the simulation of the 1-D model would be computationally inefficient because of the comparatively short timestep. However, this would generally be of minor consequence as the majority of computational effort would be for the 2-D model. With both schemes being implicit this arrangement offers the maximum flexibility and is preferred for this reason.

The same logic applies if both schemes are explicit. However, an explicit 2-D scheme can be limited in its practical application because of the large computation requirements when modelling with small grid lengths (Section 2.2.3).

An implicit 2-D scheme linked to an explicit 1-D scheme is also practicable. Where the timestep is controlled by the 2-D solution, this is the optimum combination, as an explicit 1-D scheme is more computationally efficient per timestep than an implicit one. This is, however, of only minor benefit unless the computational effort for the 1-D model is significant in comparison to that for the 2-D model. Where the timestep is controlled by the explicit 1-D scheme, however, this arrangement would be computationally inefficient.

An explicit 2-D scheme / implicit 1-D scheme combination would be limiting except in the rare situation where the Courant Number for the 2-D scheme is much lower than that of the 1-D scheme.

The above implies that the order of preference for the schemes would be:

1. Implicit 2-D / Implicit 1-D

2. Implicit 2-D / Explicit 1-D

3. Explicit 2-D / Explicit 1-D

4. Explicit 2-D / Implicit 1-D

The first two arrangements are much preferred over the last two as it was desirable not to have an explicit 2-D scheme as discussed previously.

The arrangement of schemes finally adopted was the implicit 2-D / explicit 1-D combination.

### 2.3.7 Length and Orientation of 2-D/1-D Interface

The methods presented in the literature for linking 1-D and 2-D schemes (Section 2.3.2) appear to allow only the connection of one 2-D grid element to one 1-D element for each link. This is restrictive as it would clearly be desirable for the 2-D/1-D interface to extend over more than one 2-D element as shown in Figure 2.2.

There is also the problem that for an orthogonal 2-D grid difficulty can occur in representing accurately an open boundary along a line which is oblique to the X and Y axes of the grid. This is due to the irregularity of the boundary line as boundary values can only be specified at fixed grid points. It would therefore be necessary to test the accuracy and performance of open boundaries lying obliquely to orthogonal grid axes because of the irregularity of natural water courses. There

would be significant practical benefits if a 2-D/1-D interface can be located at an oblique boundary as is illustrated in Figure 2.3.

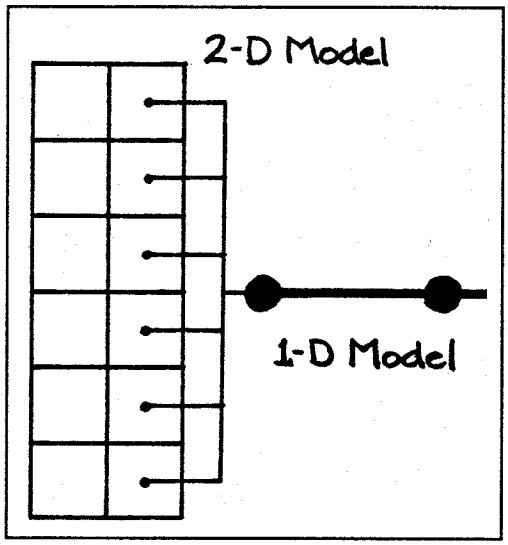


**Figure 2.2 A 1-D Element Linked to Multiple 2-D Grid Elements**

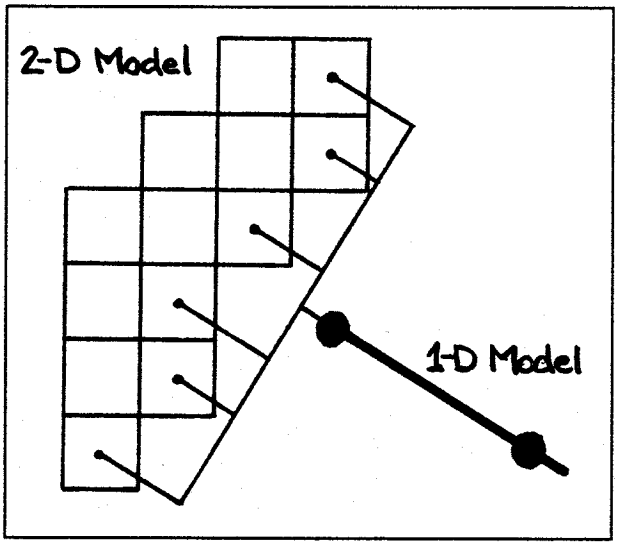


**Figure 2.3 2-D/1-D Link at an Oblique Boundary**

## 2.4 1-D Scheme of ESTRY

### 2.4.1 General

ESTRY, which has been developed by WBM Pty Ltd since 1974, is a proven and established program for modelling floods and tides using 1-D network schematisations. During ESTRY's development, it has been subject to validation testing (Collins 1988) and scrutinised by WBM employee's and others. It has been shown to be reliable and accurate for a wide range of tidal and flood applications, as demonstrated by calibration and verification to recorded level and flow data, and by rigorous assessment in various "test case" situations.

Because of ESTRY's recognition, capabilities and availability, it was decided to incorporate its code into the 2-D/1-D program.

### 2.4.2 Description

ESTRY, by default, uses an explicit finite difference, second-order, Runge-Kutta solution technique (Morrison and Smith, 1978) for the 1-D SWE of continuity and momentum as given by Equations 2.4.1 and 2.4.2. An implicit scheme was also developed, however, testing and experience has shown the explicit scheme to be preferred for production simulations. The equations contain the essential terms for modelling periodic long waves in estuaries and rivers, that is: wave propagation; advection of momentum (inertia terms) and bed friction (Manning's equation).

$$\frac{\partial(uA)}{\partial x} + B\frac{\partial z}{\partial t} = 0 \qquad \textbf{(2.4.1)}$$

$$\frac{\partial u}{\partial t} + u\frac{\partial u}{\partial x} + g\frac{\partial z}{\partial x} + k|u|u = 0 \quad \textbf{(2.4.2)}$$

*where*

$u$ = *depth and width averaged velocity*

$z$ = *water level*

$t$ = *time*

$x$ = *distance*

$A$ = *cross sectional area*

$B$ = *width of flow*

$k$ = *energy loss coefficient* $= \dfrac{gn^2}{R^{4/3}}$

$n$ = *Manning's n*

$R$ = *Hydraulic Radius*

$g$ = *acceleration due to gravity*

The spatial discretisation of an area of interest is carried out as a network of interconnected nodes and channels. The nodes represent the storage or pondage characteristics of a river, floodplain or estuary, while the channels model the hydraulic conveyance characteristics. An example of an ESTRY network was shown in Figure 1.1 of Chapter 1.

Nodes are relatively simple to construct. Each node is defined as a table of "still water" surface areas at selected elevations. From this, the volume or storage capacity of the river or estuary is defined. Intermediate values are interpolated linearly.

The channels represent the flow conveyance paths between the nodes. They are defined, in their simplest form, as a table of flow width versus elevation. In more complex forms, the cross-sectional area, wetted perimeter and/or Manning's n are specified as a function of the elevation to allow more appropriate calculation of the channel conveyance.

Channels also require details such as length, Manning's n value, and form loss coefficient (a dynamic head loss factor). A channel maybe specified as either a gradient channel, weir, bridge, culvert or the default which is a conventional channel. Gradient channels are designed for overbank flowpaths or where steep water gradients occur. They require an upstream and downstream channel bed level and include an algorithm for free-overfall such as which occurs when flood waters return to a river across a levee as the river waters recede. Weir and bridge channels have essentially zero length. Algorithms for these channels are based on standard engineering design publications and practices. Allowances

are made for submergence of bridge decks and downstream control for flow over a weir. The culvert algorithms, which represent all flow regimes, are based on standard formulae and have been tested successfully against manufacturers standards.

The continuity equation is solved at the nodes, while the momentum equation is solved for conventional and gradient channels. The output consists of water levels at the nodes, and flows, velocities and integral flows (flow integrated over time) at the channels.

All boundary conditions for an ESTRY model are applied at the nodes. These may be a constant flow, flow versus time, flow versus water level, harmonic water level, water level versus time or water level versus flow (a stage-discharge curve). Flow boundary values are applied at nodes when the continuity equation is solved, while water level boundary values are used during the solution of the momentum equation.

### 2.4.3 Suitability

The reasons for and against using ESTRY for the 1-D scheme are discussed below.

4 The main possible drawback of using ESTRY was that its explicit scheme requires the Courant Number to be less than unity. As discussed in Section 2.3.6 an explicit 1-D scheme is acceptable, and even preferred where the timestep is controlled by the 2-D scheme but is limiting where it is controlled by the 1-D scheme. Careful consideration was given to this, upon which it was concluded that in the majority of cases:

   (a) The timestep would be controlled by the 2-D scheme because of its finer spatial resolution.

   (b) The area of interest would lie in the 2-D model, so that if the ESTRY explicit scheme was imposing a limitation on the timestep, the spatial resolution in the constraining areas of the 1-D model could be made coarser, thus allowing a longer timestep without any likely loss of accuracy in the 2-D model.

An explicit 1-D scheme was therefore not considered to be a limitation in practice.

5 ESTRY is well suited in terms of its application of boundary conditions as both water level and flow boundaries are located at nodes. This simplifies to some extent any problems associated with the spatial location of water level and flow points at the 2-D/1-D interface.

6 There are of course the benefits already discussed of using a scheme which is widely accepted and proven in practice.

On the basis of the above it was decided to adopt the 1-D scheme of ESTRY.

## 2.5 Two-Dimensional Scheme Selection

### 2.5.1 Summary

The majority of 2-D schemes which have found widespread practical application use the alternating direction implicit (ADI) FDM. Other schemes have utilised finite elements FEM, the fractional step approach, explicit FDM and fully implicit FDM.

The prime objective in selecting the 2-D scheme was that it was designed for use in practice, and had been successfully applied in this area. Only implicit finite difference schemes were considered for reasons discussed in earlier sections. In the following sections the ADI FDM schemes of Leendertse (1967 and 1970) and Stelling (1984) are reviewed. Other ADI schemes of note are described in Falconer (1986) and Abbott et al (1973). A general discussion of the limitations of ADI schemes in general is also given. Other schemes reviewed are the fractionary step method of Benque et al (1982a) and the fully implicit scheme of Wilders (Floyd 1988).

The scheme of Stelling (1984) was finally selected, because of its performance and the detail of the documentation. On a performance basis it was difficult to differentiate between the more suitable schemes given the limited information on real time application.

### 2.5.2 ADI Schemes

ADI (Alternating Direction Implicit) schemes use an alternating direction algorithm for solving the 2-D SWE. The procedure is to first perform a double sweep in the X (or Y) direction to take the variables half a timestep forward to an intermediate time level. A second double sweep, this time in the Y (or X) direction, is then performed to take the variables to the end of the timestep. During a double sweep in one direction the variables of the other direction remain frozen.

Abbott (1979) provides a theoretical discussion of the alternating direction algorithm and of several 2-D SWE ADI schemes. Leendertse (1967) gives a good first description of practically applying the alternating direction algorithm to the 2-D SWE.

#### Limitations of ADI Schemes

The prime limitation of ADI schemes is the inaccuracy which occurs at high Courant Numbers. Benque et al (1982a) shows a case where highly inaccurate results can be obtained when using a high Courant Number. Weare (1979) also presents a case where errors are due to too high a Courant Number. Stelling et al (1986) provides a possible explanation for these inaccuracies and guidelines for determining the critical Courant Number.

Stelling et al (1986) propose that 'a tidal signal cannot be transferred more than once through an angle of 90° in one complete ADI step. Hence, in one timestep a signal cannot travel more than once through two bends in e.g., a zigzagging channel, halfway around an island or tidal flat, or around a peninsula shaped projection of the coastline.' If large Courant Numbers are used in such areas the instability of the solution is not affected but inaccuracies may occur. To increase the accuracy the timestep has to be reduced. Stelling et al illustrate for practical problems that to establish the level of accuracy of a simulation, the simulation must be compared with other simulations using lower timesteps until there is negligible difference in the results.

A review of ADI schemes in Benque et al (1982a) was summarised as follows.

1 The RAND or Leendertse scheme (Leendertse 1967, 1970) is widely used and fairly representative of ADI schemes.

2 The schemes described in Leendertse (1967, 1970) usually have stability problems for Courant numbers greater than 3 to 5.

3 ADI schemes of the Leendertse type can be stabilised by the use of a weighting factor which decentralises space derivatives backward in time, permitting the use of higher Courant numbers (up to 20). This, however, can decrease the accuracy of the results.

Benque et al (1982a) also gives an explanation for the poor performance of ADI schemes at high Courant numbers which is briefly explained as follows. The ADI method was developed as an iterative solution for elliptic problems, ie. problems without time dependence. They are therefore characterised by requiring only a few iterations for convergence at small Courant numbers, while for Courant numbers from 20 to 40 several hundred iterations may be required. Also in the case of a small Courant number the convergence can be enhanced where the boundary conditions do not change greatly, as the computations of the ensuing timestep act to some extent as a corrective iteration of the present timestep. For higher Courant numbers, however, the ADI's single iteration produces a solution further from the correct one and the following timestep does not act to the same degree as an iterative correction of the previous one. This leads to convergence problems and inaccuracies.

## Leendertse Schemes

The Leendertse or RAND scheme (Leendertse 1967, 1970) has been the most widely used 2-D scheme and has formed the basis for most ADI schemes in use today. This has been due to the computer code being publicly available and the good quality of the documentation. It has, however, become outdated because of further developments by others.

The main technical deficiencies of the Leendertse scheme are listed below. They are based on comments in the literature (Stelling 1984, Benque et al 1982a and Weare 1979) and have been experienced by the author.

(i) There is a fundamental difficulty in maintaining stability for $C_r$ less than about five, especially for complex models with rapidly changing geometry, thus significantly reducing its applicability to practical problems.

(ii) The use of an unrealistically high coefficient for the horizontal diffusion of momentum may be required to achieve a stable simulation. This is referred to as artificial viscosity and has a very dispersive effect on eddies and jets.

(iii) Without the use of artificial viscosity, simulations are usually restricted to Courant Numbers of no more than three to five for stability and accuracy reasons.

(iv) Algorithms for wetting and drying of grid elements were not developed by Leendertse for the 1967 scheme. A simple functional algorithm was developed for the 1970 scheme.

(v) At the open boundaries, only water levels could be specified, although Leendertse discusses how a flow boundary could be implemented.

After reviewing several schemes, Stelling (1984) states that

> 'the Leendertse scheme seems to be the most efficient, because of the fully staggered grid and the simple implicit equations. Another advantage is the widespread experience with this method for practical applications.

> Disadvantages are (i) formal instability because of the approximation of the advection operator, (ii) second order accuracy is obtained only if more than 2 iterations are used, (iii) stable results could imply a large number of iterations which decrease the efficiency.'

Despite the above, the Leendertse scheme has been and is continuing to be applied successfully to many practical situations when used by those who understand and appreciate its limitations.

### Stelling (1984)

Stelling (1984) proposes an ADI scheme which is essentially a more robust, accurate and stable version of Leendertse's (Leendertse 1967, 1970).

Initially Stelling goes to some length to examine various key aspects of the SWE with regard to the stability and convergence characteristics of alternative solution schemes with particular emphasis on the treatment of the advection terms.

A scheme for the non-linear 2-D SWE is finally proposed which is claimed to be accurate, stable and suitable for a wide range of applications. Special emphasis is given to the treatment of open and closed boundaries. A method for modelling intertidal flats is also provided.

The Stelling scheme still suffers from the main limitation inherent in ADI schemes, namely inaccuracies at high Courant Numbers. It appears, however, not to have any need for artificial viscosity or for any form of stabilisation from backward differencing, and is stable for Courant Numbers greater than five for both steady state and dynamic models, making it a potentially marked improvement over the Leendertse schemes.

Discussions with Mr John Floyd (private communication) who had recently implemented the Stelling scheme confirmed that it was a major improvement over the original Leendertse scheme and was showing excellent results in its practical application.

Stelling also provides a relatively detailed documentation of the scheme compared with others (except for possibly Leendertse). For this reason and also its apparent superiority to other ADI schemes and successful use in practice, it was adopted as that on which to base the 2-D scheme. There were also other, less important reasons such as the ability to extend the scheme to use curvilinear coordinates, and its close ties to the Wilders fully implicit scheme as discussed in Section 2.5.3.

## 2.5.3 Other Schemes

### Benque et al (1982a and 1982b)

Benque et al (1982a and 1982b), describe a method for computation of 2-D tidal currents which aims to overcome some of the limitations of the ADI schemes. The scheme is based on a fractional step approach where the terms of the governing equations are separated into three groups, with each group representing the physical processes of wave propagation, advection of momentum and horizontal diffusion of momentum.

Before reviewing the scheme, Benque et al make a number of comments regarding schemes described in the literature and general problems associated with the computation of 2-D free surface flows. They claim that the two most frequently occurring problems of 2-D schemes are:

'1. Parasitic oscillations and artificial numerical attenuation due to inadequate treatment of the non-linear advection terms.'

'2. Poor reproduction of wave propagation when large time steps are used.'

They also make the comment that few of the available program codes provide a satisfactory treatment of the wetting and drying of intertidal flats. The proposed scheme by Benque was developed largely to overcome these problems.

The equations of each group are solved in three separate steps. The momentum advection is calculated first using the method of characteristics. This is followed by the horizontal diffusion of momentum which is computed using an implicit finite difference scheme. Lastly, wave propagation is calculated using an iterative implicit solution.

Stelling (1984) briefly reviews the Benque scheme stating that there is thought to be a timestep limitation imposed by the advection step for dynamic simulations and a 'much more severe accuracy limitation for steady state problems'. Stelling concludes that

> 'In view of this, the method does not seem to be very effective (although excellent results for practical problems were reported) especially if one takes into account the computational work needed to solve the fully implicit propagation step'

and that

> 'The timestep limitation due to the advection step of their (Benque et al) method is probably even more restrictive than the restrictions due to the ADI structure. Also taking into account the increased computational effort, with respect to both storage and computing time, required by the iterative method to solve the fully implicit equations, it is questionable if this method is efficient compared with an ADI method, despite smaller timesteps needed in the latter for accuracy'

Despite these comments it was difficult to establish the true extent of these restrictions based on the limited information available.

Inquiries had been previously made by Professor Apelt (The University of Queensland) into purchasing the computer code, codenamed CYTHERE. The response was that the code itself was available at no cost for research purposes only and of the order of A$60,000 for commercial purposes. In either case someone would be required to visit Grenoble, France, for an extensive training period. This option was rejected on the grounds of cost.

## Wilders Scheme (Floyd 1988)

The Wilders scheme is a fully implicit method for the 2-D SWE, and is an extension of the work by Stelling (1984). A description of implementing the Wilders scheme is given by Floyd (1988) which also includes a method for wetting and drying of intertidal flats for the scheme.

The Wilders scheme is based on the same spatial discretisations as for the Stelling (1984) scheme with only changes to the time discretisations required. The treatment of closed and open boundaries is also as per the Stelling scheme.

The Wilders scheme offers a fully implicit solution allowing the use of much higher Courant Numbers. Floyd (1988) states that the scheme:

> 'appears to be 3 to 8 times slower per time step than the equivalent ADI scheme per time step' ... 'The Wilders scheme produced results of a similar accuracy to an explicit scheme with Courant Numbers in the range 40 to 100' ... 'in cases with complex bathymetry, the Wilders scheme will give a good accuracy with a Courant Number of about 60, whereas the HR (Hydraulics Research Ltd) ADI scheme may have to be run with a Courant Number as low as 2.'
>
> (No details are given regarding the explicit and ADI schemes mentioned.)

The Wilders scheme appears to have the most potential of all of the schemes discussed. It has, however, yet to be tested rigorously in practice. The Wilders scheme was not adopted for this reason. Since it uses virtually the same discretisations as the Stelling scheme, it was decided that a logical progression would be to develop first the Stelling scheme, followed by inclusion of the Wilders scheme as an alternative at a later date.

# 3 TWO-DIMENSIONAL HYDRODYNAMIC MODELLING PROGRAM

## 3.1 Summary

A new computer program for modelling 2-D hydrodynamics of long waves was developed based on the 2-D SWE. As discussed in Chapter Two, the solution scheme selected was that proposed by Stelling (1984).

The methodology for the development of the program was as follows.

(i) Formulate finite difference equations including boundary conditions.

(ii) Devise architecture of the computer code.

(iii) Establish formats for the input and output of data in collaboration with the development of a computer graphics system.

(iv) Write computer code.

(v) Debug and validate code using idealised test cases.

(vi) Establish the accuracy of the mass transfer across the open boundaries for the 2-D/1-D link.

(vii) Develop and test methods for wetting and drying of grid elements.

(viii) Apply the code in practice to establish limitations and improve on the above points where applicable.

This chapter addresses only points (i), (v), (vi) and (vii) above, namely the mathematical methods developed for handling the Stelling finite difference approximations, validation and testing of the computer coding, and a method for wetting and drying of intertidal flats.

The Stelling scheme is described herein only briefly. The reader is referred to the original reference for details of the scheme's development and finite difference formulations.

The computer code was validated to a range of idealised test cases and to several cases presented in the literature. In all, approximately thirty models were developed, from which more than one hundred simulations were performed. The purpose of the simulations ranged from simple checks (eg. uniform flow) to more complex ones for assessing the scheme's performance and potential. Particular emphasis was given to testing different open boundary arrangements for the purposes of the 2-D/1-D dynamic link. The results from a selection of the more interesting simulations are presented.

The majority of tests were steady state problems in idealised models as these proved to be the hardest to stabilise. The stability problems, which were encountered when using steady state flow boundaries, pose some concern. Stelling (1984) briefly mentions that stability problems were experienced, and were overcome by the use of Riemann invariants to adjust the boundary values artificially. Further assessment of these problems was very difficult, as no details or results from fundamental test cases (such as those in Section 3.4) are presented in Stelling (1984). The author can

not guarantee that the computer code is "bug free", and that an exact reproduction of the Stelling scheme was achieved, but on the basis of the validation tests, the author is confident that the code is performing as designed.

Mass was found to be conserved 100 % between internal grid elements, however, a loss of up to 2 to 3 % was experienced across flow boundaries when high Courant Numbers were used ($C_r$ = 50). This and the stability problems associated with flow boundaries are, at least in part, due to the condition of a horizontal surface gradient across a flow boundary. Stelling implies that this condition is necessary as the extrapolation of the water surface gradient across the boundary is highly prone to instabilities. Testing by the author confirmed this to be the case.

If further research and development is to be carried out in this area, it would be well advised to have discussions with Stelling, or with J Floyd (Public Works Department, NSW) who has also developed the Stelling scheme. Such action was not taken by the author because, as discussed later, the 2-D/1-D link was best achieved by using water level boundaries (which show excellent stability properties) for the 2-D model. Also, the flow boundary appears to have good stability properties in dynamic simulations, as can be seen during the "warm-up" period of steady state tests, and as evidenced in their application in practice.

Specification of water level boundaries at both the upstream and downstream boundaries showed excellent stability properties in all cases, however, a fundamental problem exists in that the mass entering or leaving the model is not defined. A solution to this problem, which resulted from the development of the 2-D/1-D dynamic link, is to connect a small 1-D model to the 2-D model and specify a flow boundary in the 1-D model. This approach has been applied very successfully to practical 2-D flow problems which require a flow boundary.

For dynamic simulations, excellent stability properties have been observed. Application to a number of practical cases has shown the program to perform extremely well and to calibrate models successfully using standard friction coefficients. In this regard, the scheme is certainly a major improvement over the well-known Leendertse schemes.

Testing and practical application of the program has shown that the use of a large diffusion coefficient is not necessary for stability purposes as is used in other schemes, except for where a flow boundary is used in a steady state simulation. In this case the simulation can be stabilised by using a diffusion coefficient typically between 1.0 and 10 $m^2/s$, however, the results will be unrealistic.

The issue of modelling the wetting and drying of intertidal flats was addressed and is presented in Section 3.5. During several applications it became clear that in certain situations a more robust method was required. This was particularly apparent for large flats which take a long time to drain. A new method is proposed to handle such situations. The results from two test cases are presented.

The new method, called the Free Overfall Method, allows perched waters on tidal flats to continue to drain until the flat is dry, as opposed to more convential methods which tend to pond water once the grid elements on the edge of the flat have dried. This allows a more correct representation of the storage of a tidal system. The Free Overfall Method is also more computationally efficient because it allows perched tidal waters to drain, therefore, reducing the number of active computational points. Other benefits are the non-occurence of a surge which is experienced by convential methods when the

ponded waters are re-connected with the rising tide, and also greater stability in regions of steep water surface gradients.

A key component in the program development was the in-parallel development of the computer graphics system, which minimised the development time of test models and markedly enhanced the analysis and interpretation of results. The system allows the majority of input data to be entered using "pop-up" menus and a pointing device (digitiser / mouse), thus greatly improving upon traditional methods. Displaying the results of a simulation is carried out in a similar manner. All models and results presented in this thesis were generated using the graphics system written by the author.

## 3.2 Solution Scheme for the 2-D SWE

### 3.2.1 Overview

Firstly the partial differential equations representing the 2-D SWE as used by the solution scheme are presented. This is followed by a brief description of the general scheme and the treatment of open and closed boundaries as proposed in Stelling (1984).

### 3.2.2 2-D Shallow Water Equations (SWE)

The shallow water equations (SWE) are the equations of fluid motion used for modelling long waves such as floods, ocean tides and storm surges. They are derived using the hypotheses of vertically uniform horizontal velocity and negligible vertical acceleration (ie. a hydrostatic pressure distribution). These assumptions are valid where the wave length is much greater than the depth of water. In the case of the ocean tide the SWE are applicable everywhere.

The 2-D SWE in the horizontal plane are described by the following partial differential equations of mass continuity (Equation 3.2.1) and momentum conservation in the X and Y directions (Equations 3.2.2a and b) for an in-plan cartesian coordinate frame of reference.

$$\frac{\partial z}{\partial t} + \frac{\partial (Hu)}{\partial x} + \frac{\partial (Hv)}{\partial y} = 0 \quad \textbf{(3.2.3)}$$

$$\frac{\partial u}{\partial t} + u\frac{\partial u}{\partial x} + v\frac{\partial u}{\partial y} - c_f v + g\frac{\partial z}{\partial x} + g\,u\frac{\sqrt{u^2+v^2}}{C^2 H} - m\left(\frac{\partial^2 u}{\partial x^2} + \frac{\partial^2 u}{\partial y^2}\right) = F_x \quad \textbf{(3.2.2a)}$$

$$\frac{\partial v}{\partial t} + u\frac{\partial v}{\partial x} + v\frac{\partial v}{\partial y} + c_f u + g\frac{\partial z}{\partial y} + g\,v\frac{\sqrt{u^2+v^2}}{C^2 H} - m\left(\frac{\partial^2 v}{\partial x^2} + \frac{\partial^2 v}{\partial y^2}\right) = F_y \quad \textbf{(3.2.2b)}$$

*where*

$z$ = *Water surface elevation*

$u$ *and* $v$ = *Depth averaged velocity components in* $X$ *and* $Y$ *directions*

$H$ = *Depth of water*

$t$ = *Time*

$x$ *and* $y$ = *Distance in* $X$ *and* $Y$ *directions*

$c_f$ = *Coriolis force coefficient*

$C$ = *ChÇzy coefficient*

$m$ = *Horizontal diffusion of momentum coefficient*

$F_x$ *and* $F_y$ = *Sum of components of external forces in* $X$ *and* $Y$ *directions*

The terms of the SWE can be attributed to different physical phenomena. These are propagation of the wave due to gravitational forces, the transport of momentum by advection, the horizontal diffusion of momentum, and external forces such as bed friction, rotation of the earth, wind, wave radiation stresses, and barometric pressure.

The 2-D SWE scheme adopted incorporates all of the above physical processes. External forces such as wind, wave radiation stresses, and barometric pressure were incorporated into the code by the author but are not discussed in the present work.

### 3.2.3 Computation Procedure

The computation procedure used is an alternating direction implicit (ADI) finite difference method, and is referred to by Stelling as a 'stabilisation of the Leendertse scheme'. The treatment of the model boundaries is also given particular attention.

The method involves two stages each having two steps, giving four steps overall. Each step involves solving a tri-diagonal matrix for which the method in van Rosenberg (1969) was adopted.

Stage 1, step 1 solves the momentum equation in the Y-direction for the Y-velocities. The equation is solved using a predictor/corrector method which involves two sweeps. For the first sweep, the calculation proceeds column by column in the Y-direction, sweeping in the dominant direction of flow in the X-direction. If the signs of all velocities in the X-direction are the same the second sweep is not necessary, otherwise the calculation is repeated sweeping in the opposite direction.

The second step of Stage 1 solves for the water levels and X-direction velocities by solving the equations of mass continuity and of momentum in the X-direction. A tri-diagonal equation is obtained by substituting the momentum equation into the mass equation and eliminating the X-velocity. The water levels are then calculated and are back substituted into the momentum equation to calculate the X-velocities. This process is repeated for a recommended two iterations. Testing by the author on a number of models showed there to be little benefit in using more than two iterations.

Stage 2 proceeds in a similar manner to Stage 1 with the first step using the X-direction momentum equation and the second step using the mass equation and the Y-direction momentum equation. Of note is that the same computer code can be used for both stages if desired.

The above procedure is relatively straightforward although somewhat complex to code. The complexity arises, however, when the boundary conditions are included. These boundary conditions are described briefly below. The formulation of the Stelling scheme by the author for the computer code is presented in Section 3.3.

### 3.2.4 Open Boundaries

The open boundary conditions for the Stelling scheme are described in brief below. For hydrodynamic models, an open boundary can be defined as either a water level time, or a flow time history. A flow can be specified as either a discharge or a velocity.

#### Water Level Boundaries

At a water level boundary, only the discretisation of the advection terms poses a problem, as a value for the velocity on the outside of the computation domain is required.

The conditions imposed are:

1. The water level at the boundary is defined prior to each computation step.

2. There is no flow between water level boundary elements which have a common side (ie. the velocity component parallel to the boundary is zero).

3. For the first velocity point inside the boundary the advection term is approximated by upstream differencing if the flow is outwards, and is set to zero if flow is inwards.

4. For the second velocity point inside the boundary upstream differencing is used for the advection term if flowing outwards or inwards.

The types of water level boundaries incorporated into the code were:

(a) Sinusoidal water level defined by a mean water level, period, amplitude and phase. Any number of sinusoidal curves may be specified at an element. A constant water level may be defined by specifying zero amplitude.

(b) A table of water level versus time with an option to use a cubic interpolation in preference to a linear interpolation. Any number of tables may be specified at an element and there is no limitation on the size of the tables.

#### Flow Boundaries

In the case of flow boundaries, a condition has to be defined for the water level outside the model domain. As for the water level boundaries, special discretisations are also required for the advection terms. The conditions imposed are:

1. The velocity or discharge at the boundary is defined prior to each computation step.

2. A zero water surface gradient across the boundary.

3. For the first velocity point inside the boundary upstream differencing is used for the advection term if flowing outwards or inwards.

The types of flow boundaries incorporated into the code were:

(a) Constant discharge or velocity.

(b) A table of discharge or velocity versus time in a specified direction with an option to use a cubic interpolation in preference to a linear interpolation. Any number of tables may be specified at an element and there is no limitation on the size of the tables.

### 3.2.5 Closed Boundaries

Closed boundaries represent the dry land / water interface. The treatment of these boundaries is briefly discussed below.

The conditions applied are:

1. The velocity perpendicular to a closed boundary is zero.

2. The velocity parallel to a closed boundary is (a) defined as equal to zero (ie. a no slip condition), (b) defined by setting its spatial derivative normal to the boundary as zero (ie. a perfect slip condition implying there is no variation across the grid element of the velocity component parallel to the closed boundary), or (c) a combination of (a) and (b) giving a partial slip effect. Typically, the perfect slip condition is applied and is that which was adopted.

   (Only the discretisations of the momentum equations are affected by the above conditions as follows.)

3. For the advection term's spatial derivatives along the line perpendicular to the boundary downstream differences are used where the flow is towards the boundary, or are set to zero for flow away from the boundary.

4. For the cross advection terms, the situation is more complex as the full discretisation involves more grid points. This is overcome by reducing the order of accuracy near both closed and open boundaries, but the complexity remains because of the number of checks required in the coding.

5. For the diffusion terms, the discretisations are reduced in order of accuracy near the boundary and are relatively simple for the perfect slip situation as mentioned above.

## 3.3 Coding Finite Difference Equations

### 3.3.1 Overview

Prior to writing the computer code, much effort was placed on producing a set of structured, easy to interpret equations, and to construct algorithms in a logical progression. The end result was to have a highly structured code, which was relatively easy to read, change and debug. Overall this has been the case, although, there are parts which could have been more streamlined.

No computer code is presented as part of this thesis because of ownership rights. The methodology used for streamlining the finite difference formulations including the boundary conditions is, however, described below.

Figure 3.1 illustrates the spatial location of the hydraulic variables. A variable's subscript solely defines its location in space relative to a central element according to Figure 3.1. These subscripts were adopted to reduce the length of computer code. For example, the variables $?_0$, $u_0$, $v_0$, $C_0$ and $h_1$ are associated with the central grid element [n,m], the variables $?_3$, $u_3$, $v_3$ and $h_4$ are associated with element [n,m-1], and in the case of element [n-1,m-1] the only variable applicable is $h_3$.

Superscripts refer to the computation stage at which the value of the variable was or is being calculated. For example, $u^o$ refers to the value of $u$ calculated at the end of the previous timestep, $u^1$ that after Stage 1 is complete and $u^2$ that after Stage 2, which is the end of the current timestep. Note that a 'p' or a 'q' superscript indicates the iteration number on the variable. For example, $v^p$ is the $p^{th}$ iteration of the value $v$ at the stage under consideration.

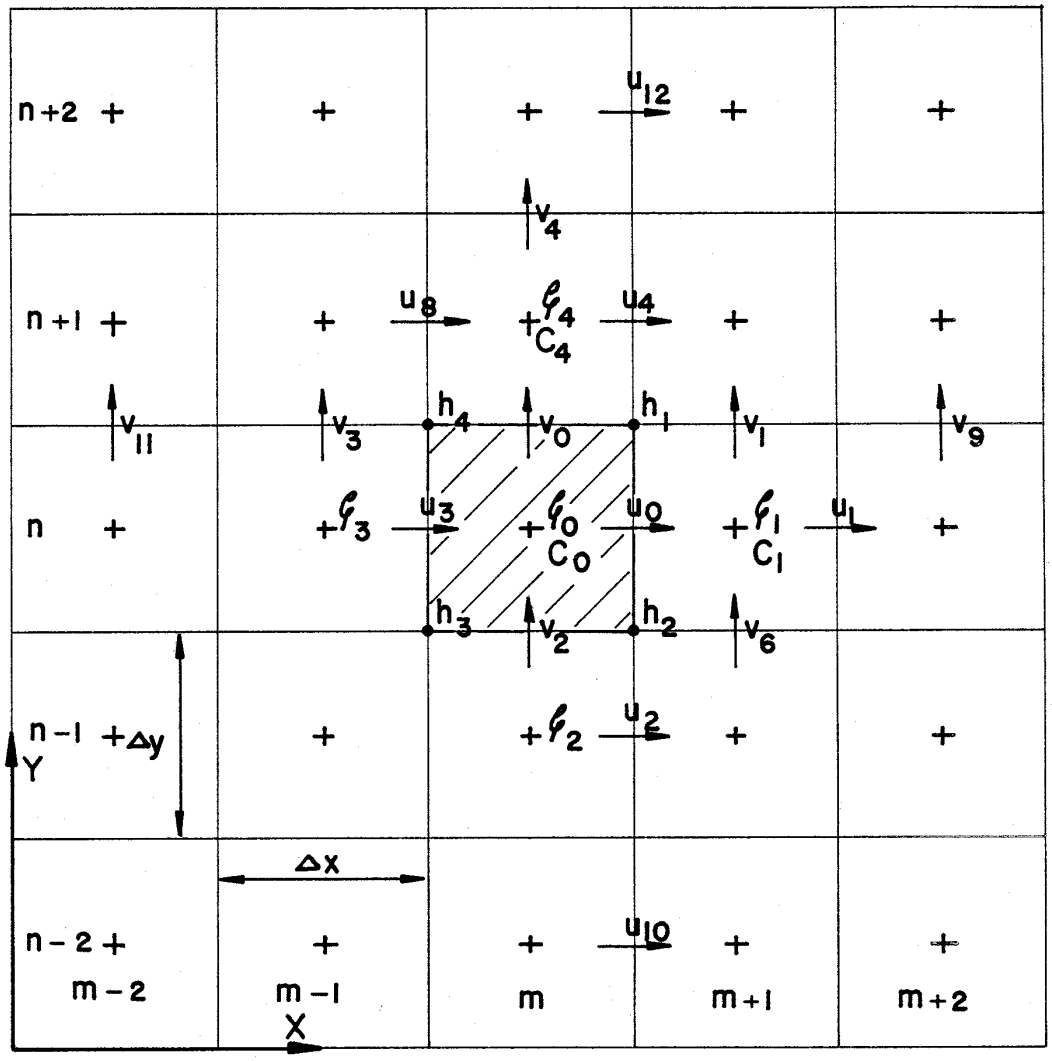


ζ – Water level relative to a datum.
u – Depth averaged velocity in X direction.
v – " " " " Y direction.
h – Water depth relative to a datum.
C – Chézy coefficient.
Δx – Length of element in X direction.
Δy – " " " " Y direction.

Note ζ is tve above zero and h is tve below zero.

**Figure 3.1 Spatial Location of Variables Relative to a Grid Element**

### 3.3.2 Stage One - Step One

Stage 1 - Step 1 of the scheme solves implicitly for the *v* velocities using the Y-momentum equation. As described in Section 3.2.3, this equation is solved column by column in the Y-direction, sweeping first in the dominant direction of flow in the X-direction and secondly in the other direction. For the case where the net flow overall, and average flow locally is in the positive X direction, Equation 3.3.1 results.

$$\frac{2(v_0^p - v_0^0)}{\Delta t} + v_0^0 \frac{(v_4^p - v_2^p)}{2\Delta y} + \bar{u} \frac{(3v_0^p - 4v_3^p + v_{11}^p)}{2\Delta x} + c_f \bar{u} + g \frac{(z_4^0 - z_0^0)}{\Delta y}$$
$$+ g v_0^p \frac{[(\bar{u})^2 + (v_0^0)^2]^{\frac{1}{2}}}{C^2 H} - m \frac{(v_1^{p-1} - 2v_0^p + v_3^p)}{\Delta x^2} - m \frac{(v_4^p - 2v_0^p + v_2^p)}{\Delta y^2} = 0 \quad \textbf{(3.3.1)}$$

A general form of the Y-momentum equation, which takes into account all conditions, including those of the open and closed boundaries, was developed. The resulting formulation yields a tri-diagonal coefficient matrix as given by Equation 3.3.2 with the coefficients defined in Equations 3.3.3a to g.

$$q v_2^p + r v_0^p + s v_4^p = t \quad \textbf{(3.3.2)}$$

$$q = E_{vv2} - \frac{m}{\Delta y^2} \quad \textbf{(3.3.3a)}$$

$$r = \frac{2}{\Delta t} + E_{vv0} + E_{uv0} + g \frac{[(\bar{u})^2 + (v_0^0)^2]^{\frac{1}{2}}}{C^2 H} + E_{v0} + \frac{2m}{\Delta y^2} \quad \textbf{(3.3.3b)}$$

$$s = E_{vv4} - \frac{m}{\Delta y^2} \quad \textbf{(3.3.3c)}$$

$$t = \frac{2v_0^0}{\Delta t} - c_f \bar{u} - E_{uv1} - g \frac{(z_4^0 - z_0^0)}{\Delta y} + E_{v1} \quad \textbf{(3.3.3d)}$$

$$\bar{u} = \frac{u_0^0 + u_3^0 + u_4^0 + u_8^0}{4} \quad \textbf{(3.3.3e)}$$

$$C = \frac{C_0 + C_4}{2} \quad \textbf{(3.3.3f)}$$

$$H = \frac{h_1 + h_4}{2} + \frac{z_0^0 + z_4^0}{2} \quad \textbf{(3.3.3g)}$$

#### *E* Coefficients - General

In Stelling (1984) the general equations are presented for an internal grid element, but no set of equations are provided which take into account the boundary conditions. To improve upon this and to offer a complete set of equations which include all boundary conditions, it was necessary to isolate

those terms in the general equations which can be affected by a boundary condition and replace them by a set of coefficients. These coefficients are the $E$ coefficients in Equations 3.3.3a to d. They include all the boundary conditions and also reduce the length of the main equations for easier coding. Their formulations are dependent on the status of the surrounding grid elements as described below and given on the following pages.

The status of the surrounding grid elements is described by a set of symbols given to the left of each equation. These symbols indicate for example whether the point under consideration (in this case $v_0$) is next to a closed boundary, open boundary, etc. They are positioned as if viewed in the same frame of reference as in Figure 3.1. The arrows, which are orientated in the positive direction of flow, are illustrative only and do not imply the flow is in that direction. The symbols and other variables are defined below.

*Symbol Definitions :*

⇑ *is the computational point under consideration*

↑ *is an active or wet computational point*

_ *is an inactive or dry computational point*

*h is a water level boundary point*

*q is a flow boundary point*

♦ *is one of h, q or _*

*Variable Definitions*

$$d = \frac{1 + (-1)^{p + p'}}{2}$$

$p = 1, 2$ *ie. Sweep 1 and 2*

$p' = 0$ *if* $\sum u > 0$

$p' = 1$ *if* $\sum u \le 0$

*(* $\sum u$ *is the sum of u over all grid points )*

$$v_1^* = v_1^{p-1},\ v_3^* = v_3^p,\ v_9^* = v_9^{p-1},\ v_{11}^* = v_{11}^p \quad \text{if } d = 0$$

$$v_1^* = v_1^p,\ v_3^* = v_3^{p-1},\ v_9^* = v_9^p,\ v_{11}^* = v_{11}^{p-1} \quad \text{if } d = 1$$

The $E_{vv}$ coefficients (Equations 3.3.4a to e) represent the advection term operators, $E_{uv}$ (Equations 3.3.5a to f) the cross advection terms and $E_v$ (Equations 3.3.6a to d) the diffusion terms. The number in the subscript for the $E_{vv}$ coefficients refers to the $v$ velocity it operates on. For example $E_{vv2}$ operates on the $v_2$ velocity. In the case of the $E_{uv}$ and $E_v$ coefficients the number is arbitrary with 0 referring to Equation 3.3.3b and 1 to Equation 3.3.3d.

## $E_{vv}$ Coefficients

↑
⇑ $E_{vv}2 = \frac{-v_0^0}{2\Delta y},\ E_{vv}4 = \frac{v_0^0}{2\Delta y},\ E_{vv}0 = 0$ **(3.3.4a)**
↑

↑ ↑
⇑ or ⇑ $E_{vv}2,\ E_{vv}4,\ E_{vv}0 = 0\ \ if\ v_0^0 > 0$
_ h

**(3.3.4b)**

$E_{vv}2 = 0,\ E_{vv}4 = \frac{v_0^0}{\Delta y},\ E_{vv}0 = \frac{-v_0^0}{\Delta y}\ \ if\ v_0^0 \le 0$

↑ q h ↑
⇑ or ⇑ or ↑ or ⇑ $E_{vv}2 = \frac{-v_0^0}{\Delta y},\ E_{vv}4 = 0,\ E_{vv}0 = \frac{v_0^0}{\Delta y}\ \ if\ v_0^0 > 0$
q ↑ ⇑ ↑
↑ h

**(3.3.4c)**

$E_{vv}2 = 0,\ E_{vv}4 = \frac{v_0^0}{\Delta y},\ E_{vv}0 = \frac{-v_0^0}{\Delta y}\ \ if\ v_0^0 \le 0$

_ h
⇑ or ⇑ $E_{vv}2 = \frac{-v_0^0}{\Delta y},\ E_{vv}4 = 0,\ E_{vv}0 = \frac{v_0^0}{\Delta y}\ \ if\ v_0^0 > 0$
↑ ↑

**(3.3.4d)**

$E_{vv}2,\ E_{vv}4,\ E_{vv}0 = 0\ \ if\ v_0^0 \le 0$

_ h _
⇑ or ⇑ or ⇑ $E_{vv}2,\ E_{vv}4,\ E_{vv}0 = 0$ **(3.3.4e)**
_ _ h

### $E_{uv}$ Coefficients

$\uparrow \uparrow \Uparrow$ $E_{uv}0 = \frac{3\bar{u}(1-d)}{2\Delta x}$, $E_{uv}1 = \frac{\bar{u}(3d\, v_0^0 - 4v_3^* + v_{11}^*)}{2\Delta x}$ $if\ \bar{u} > 0$ **(3.3.5a)**

$\blacklozenge \uparrow \Uparrow$ $E_{uv}0 = \frac{\bar{u}(1-d)}{\Delta x}$, $E_{uv}1 = \frac{\bar{u}(d\, v_0^0 - v_3^*)}{\Delta x}$ $if\ \bar{u} > 0$ **(3.3.5b)**

$\blacklozenge \Uparrow$ $E_{uv}0$, $E_{uv}1 = 0$ $if\ \bar{u} > 0$ **(3.3.5c)**

$\Uparrow \uparrow \uparrow$ $E_{uv}0 = \frac{-3\bar{u}d}{2\Delta x}$, $E_{uv}1 = \frac{\bar{u}(3(d-1)v_0^0 + 4v_1^* - v_9^*)}{2\Delta x}$ $if\ \bar{u} \le 0$ **(3.3.5d)**

$\Uparrow \uparrow \blacklozenge$ $E_{uv}0 = \frac{-d\,\bar{u}}{\Delta x}$, $E_{uv}1 = \frac{\bar{u}\,[(d-1)v_0^0 + v_1^*]}{\Delta x}$ $if\ \bar{u} \le 0$ **(3.3.5e)**

$\Uparrow \blacklozenge$ $E_{uv}0$, $E_{uv}1 = 0$ $if\ \bar{u} \le 0$ **(3.3.5f)**

### $E_v$ Coefficients

$\uparrow \Uparrow \uparrow$ $E_v0 = \frac{2m}{\Delta x^2}$, $E_v1 = \frac{m(v_1^* + v_3^*)}{\Delta x^2}$ **(3.3.6a)**

$\uparrow \Uparrow \blacklozenge$ $E_v0 = \frac{m}{\Delta x^2}$, $E_v1 = \frac{m\, v_3^*}{\Delta x^2}$ **(3.3.6b)**

$\blacklozenge \Uparrow \uparrow$ $E_v0 = \frac{m}{\Delta x^2}$, $E_v1 = \frac{m\, v_1^*}{\Delta x^2}$ **(3.3.6c)**

$\blacklozenge \Uparrow \blacklozenge$ $E_v0$, $E_v1 = 0$ **(3.3.6d)**

The procedure for Stage 2, Step 1 is the same as described above except the momentum equation in the X-direction is used.

## 3.3.3 Stage One - Step Two

Using the same approach as above a tri-diagonal coefficient equation for the water levels was established by substituting the X-momentum equation into the equation for conservation of mass as given by Equations 3.3.7 and 3.3.8a to 3.3.9f. Another set of $E$ coefficients, which are given on the following pages, have also been defined for these equations. A $q$ in a superscript refers to the iteration level on a variable (ie $q$ = 1,2,...$N_q$ where $N_q$ normally equals 2). A q-1 superscript indicates the value from the previous iteration. For the first iteration q-1 equals zero and the value of the variable will be that from the previous half timestep.

$$q z_3^q + r z_0^q + s z_1^q = t \quad \textbf{(3.3.5)}$$

$$q = \frac{-E_{43} g}{\Delta x} - \frac{u_3^{q-1}}{2\Delta x} \quad \textbf{(3.3.8a)}$$

$$r = \frac{2}{\Delta t} + g \frac{E_{40} + E_{43}}{\Delta x} + \frac{u_3^{q-1} - u_0^{q-1}}{2\Delta x} \quad \textbf{(3.3.8b)}$$

$$s = \frac{-E_{40} g}{\Delta x} + \frac{u_0^{q-1}}{2\Delta x} \quad \textbf{(3.3.8c)}$$

$$t = \frac{2 z_0^0}{\Delta t} - E_{10} E_{40} + E_{13} E_{43} - H_{vy} \quad \textbf{(3.3.8d)}$$

$$H_{vy} = \frac{v_0^0 \left( \frac{z_0^0 + z_4^0}{2} + \frac{h_1 + h_4}{2} \right) - v_2^0 \left( \frac{z_0^0 + z_2^0}{2} + \frac{h_2 + h_3}{2} \right)}{\Delta y} \quad \textbf{(3.3.8e)}$$

The $H_{vy}$ coefficient (Equation 3.3.8e) can be calculated prior to iterating to reduce computation time, however, computer memory will have to be allocated to store the values of $H_{vy}$.

### $E_{10}$, $E_{20}$ and $E_{40}$ Coefficients

The $E_{10}$ and $E_{20}$ coefficients (Equations 3.3.9a and b) originate from the X-direction momentum equation which has been substituted into the continuity equation. They are used when back substituting to calculate $u^q$ (described further on by Equation 3.3.13) and must therefore be retained in memory for each sweep in the X-direction. The $E_{40}$ coefficient (Equation 3.3.9f) has been adopted solely to allow for easier coding of Equations 3.3.8a to d in which $E_{40}$ appears several times. Note: $E_{13}$, $E_{23}$ and $E_{43}$ are equal to $E_{10}$, $E_{20}$ and $E_{40}$ at element [n,m-1] respectively.

$$E_{10} = \frac{2u_0^0}{\Delta t} - E_{vu} + c_f \bar{v} + E_u + \frac{m(u_1^0 - 2u_0^0 + u_3^0)}{\Delta x^2} \quad \textbf{(3.3.9a)}$$

$$E_{20} = \frac{2}{\Delta t} + E_{uu} + g \frac{\left[ (\bar{v})^2 + (u_0^0)^2 \right]^{\frac{1}{2}}}{C^2 H} \quad \textbf{(3.3.9b)}$$

$$C = \frac{C_0 + C_1}{2} \quad \textbf{(3.3.9c)}$$

$$\bar{v} = \frac{v_0^1 + v_1^1 + v_6^1 + v_2^1}{4} \quad \textbf{(3.3.9d)}$$

$$H = \frac{z_0^0 + z_1^0}{2} + \frac{h_1 + h_2}{2} \quad \textbf{(3.3.9e)}$$

$$E_{40} = \frac{\left( h_{u_0} + z_0^{q-1} \right)}{\Delta x} \frac{1}{E_{20}} \quad \textbf{(3.3.9f)}$$

The $E_{uu}$, $E_{vu}$ and $E_u$ coefficients (Equations 3.3.10a to 3.3.12d) take into account the boundary conditions which affect the advection, cross advection and diffusion terms respectively in the X-direction momentum equation. As for Stage 1 - Step 1 the symbols on the left of each equation represent the status of the surrounding computation points.

### $E_{uu}$ Coefficient

→ _ → $E_{uu} = \dfrac{u_1^{q-1} - u_3^{q-1}}{2\Delta x}$ **(3.3.10a)**

_ _ →

or $E_{uu} = \begin{cases} 0 & \text{if } u_0^{q-1} > 0 \\ \dfrac{u_1^{q-1} - u_0^{q-1}}{\Delta x} & \text{if } u_0^{q-1} \le 0 \end{cases}$ **(3.3.10b)**

h _ →

→ _ _

or $E_{uu} = \begin{cases} \dfrac{u_0^{q-1} - u_3^{q-1}}{\Delta x} & \text{if } u_0^{q-1} > 0 \\ 0 & \text{if } u_0^{q-1} \le 0 \end{cases}$ **(3.3.10c)**

→ _ h

q _ →

or

→ _ q

or $E_{uu} = \begin{cases} \dfrac{u_0^{q-1} - u_3^{q-1}}{\Delta x} & \text{if } u_0^{q-1} > 0 \\ \dfrac{u_1^{q-1} - u_0^{q-1}}{\Delta x} & \text{if } u_0^{q-1} \le 0 \end{cases}$ **(3.3.10d)**

h → _ →

or

→ _ → h

### $E_{vu}$ Coefficient

→

→

_ $E_{vu} = \dfrac{\bar{v}\,(u_{12}^{q-1} + 4u_4^{q-1} - 4u_2^{q-1} - u_{10}^{q-1})}{12\Delta y}$ **(3.3.11a)**

→

→

♦ → ♦
→ → →
_ or _ or _ $E_{vu} = \frac{\bar{v}\,(u_4^{q-1} - u_2^{q-1})}{2\Delta y}$ **(3.3.11b)**
→ → →
♦ ♦ →

♦ → ♦
_ or _ or _ $E_{vu} = 0$ **(3.3.11c)**
♦ ♦ →

### $E_u$ Coefficient

→
_ $E_u = \frac{m\,(u_4^{q-1} - 2u_0^{q-1} + u_2^{q-1})}{\Delta y^2}$ **(3.3.12a)**
→

♦
_ $E_u = \frac{m\,(u_2^{q-1} - u_0^{q-1})}{\Delta y^2}$ **(3.3.12b)**
→

→
_ $E_u = \frac{m\,(u_4^{q-1} - u_0^{q-1})}{\Delta y^2}$ **(3.3.12c)**
♦

♦
_ $E_u = 0$ **(3.3.12d)**
♦

Finally the *u* velocity is calculated by back substituting as given by Equation 3.3.13.

$$u_0^q = \frac{E_{10} - g\frac{(z_1^q - z_0^q)}{\Delta x}}{E_{20}} \quad \textbf{(3.3.5)}$$

The above process is repeated for a second iteration. More iterations can be made, but testing has shown this to provide little benefit.

The procedure for Stage 2, Step 2 is the same as described above except that the momentum equation in the Y-direction is used.

## 3.4 Validation and Testing

### 3.4.1 Summary

All computer software must be validated to ensure that it is correctly performing the task for which it was designed. Where mathematical equations are being solved to simulate physical phenomena, the validation process should be sufficiently exhaustive so as to illustrate the accuracy of the scheme and to establish its pitfalls and limitations.

For the 2-D SWE scheme so far discussed a validation testing programme was carried out. The testing programme consisted of a range of tests using idealised models which were either developed by the author or based on cases presented in the literature. Some thirty models were developed and over one hundred different simulations were performed. The purpose of the tests varied from simple checks on the hydrodynamic computations to more complex flow patterns to assess the performance of the Stelling scheme.

Not surprisingly though, the true test of the program's capabilities was established during its application on a number of practical cases. It was not uncommon for a test model to be developed based on part of a practical model where difficulties were being experienced.

In all the idealised models, either a steady state or a sinusoidal tide simulation was carried out. All steady state simulations were "warmed up" from a cold start, ie. a horizontal water surface and zero velocities at all velocity points, by adjusting the appropriate boundary values by a cosine function as given by Equation 3.4.1. This allows steady state conditions to be reached relatively smoothly. It was almost impossible to achieve steady state by using a linear adjustment or with no adjustment unless a very small timestep was used because of the large numerical disturbances which would occur.

$$x(t) = x_{ss}\left[1 - \cos^2\left(\frac{p\,(t - t_s)}{2\,t_{ec}}\right)\right] \quad if\ (t - t_s) < t_{ec}$$

$$x(t) = x_{ss} \quad if\ (t - t_s) \geq t_{ec} \qquad \textbf{(3.4.6)}$$

*where*

$x(t)$ = *Boundary value as a function of* $t$

$t$ = *time*

$x_{ss}$ = *Steady state boundary value*

$t_s$ = *Start time of computation*

$t_{ec}$ = *Entry time constant*

The sinusoidal tide simulations, which were also started "cold", were usually run for a few tide cycles until equilibrium was reached.

For all steady state simulations plots of flow versus time were examined at selected locations to check the mass conservation properties. Also, the flows leaving and entering a model were calculated at locations immediately inside each open boundary to establish whether mass was being conserved across them.

For tide simulations with a purely periodic ocean boundary, flow was integrated over time for the same purposes as described above. The expectation here being that the integral of flow over time (the tidal prism) for the ebb tide equals that for the flood tide.

Steady state was easily achieved through the use of Equation 3.4.1 except in cases which developed an instability. These instabilities, which were confined to flow boundary cases, are not dependent on the model warm-up, but are believed to originate from the Stelling boundary conditions. Water level boundaries were observed to be highly stable.

In all cases which remained stable mass was shown to be conserved with varying degrees of inaccuracy depending on the boundary arrangement and Courant Number. The worst situation was when using a flow boundary and a high Courant Number ($C_r = 50$) when a loss of mass of 2 to 3 % would occur. For small Courant Numbers ($C_r < 5$) the loss would be less than 0.5 %. Where only water level boundaries were specified, the correct flow would be computed with less than 0.1 % inaccuracy for uniform flow situations, but in cases where the flow must be defined totally incorrect results would occur (eg. Diverging Flow Case, Section 3.4.3).

The reason for the loss of mass and instabilities across a flow boundary are believed due to the condition of a horizontal water surface. Stelling (1984) states that this condition is necessary as the extrapolation of the water surface gradient across the boundary is highly prone to instabilities. Testing by the author confirmed this to be the case. Mass was always conserved 100 % internally and across water level boundaries.

The majority of model tests undertaken were steady state simulations because of their stability problems, ease of analysis and simplicity. They therefore dominate the results presented below. Dynamic simulations were used for testing the wetting and drying method for which some model test results are presented (Section 3.5.4).

The sections following present and discuss some of the more interesting results from four of the test models:

1. **Uniform Flow** - Comparison of different boundary arrangements for steady state uniform flow.

2. **Diverging Flow** - Modelling the rise in water level due to a decrease in the dynamic head.

3. **Flow Past a Solid Wall** (after Stelling 1984) - Modelling the formation of eddies behind a solid wall.

4. **S-Shaped Channel** (after Benque et al 1982a) - A model to highlight the inaccuracies of ADI schemes at large Courant Numbers.

### 3.4.2 Uniform Flow

Initial testing of the 2-D scheme was undertaken to evaluate its performance under steady state uniform flow conditions. A variety of models were developed and tested. The results from one of the models are discussed and illustrated below.

The model represents a rectangular channel with a bed slope, ***S***, equal to the theoretical water surface slope as given by Equation 3.4.2. For the model simulations described below, a Chézy coefficient of 60 $m^{½}/s$, depth of 10 m, and a velocity of 1.0 m/s were adopted. Over a 100 m length this corresponds to a change in water surface elevation of 0.002778 m. The model layout and bathymetry for the orientation of water flowing in the negative Y-direction is illustrated in Figure 3.2.

$$S = \frac{v^2}{C^2 H} \quad \textbf{(3.4.2)}$$

Simulations were carried out for the following open boundary conditions.

| BC | Upstream | Downstream |
|---|---|---|
| bhh | water level (.06944 m) | water level (zero) |
| bqh | discharge (5000 $m^3/s$) | water level (zero) |
| bhq | water level (.06944 m) | discharge (5000 $m^3/s$) |
| bqq | discharge (5000 $m^3/s$) | discharge (5000 $m^3/s$) |
| bvh | velocity (1 m/s) | water level (zero) |
| bhv | water level (.06944 m) | velocity (1 m/s) |
| bvv | velocity (1 m/s) | velocity (1 m/s) |

The boundary values given above were determined in accordance with the calculated water surface slope. If the model is performing correctly a steady state water surface gradient of 0.06944 m over the length of the model, a uniform velocity of 1 m/s and a discharge of 5000 $m^3/s$ should result once steady state conditions were reached. Note that the sign of the velocity and discharge from the computations should be negative as they are in the negative Y-direction. A cold start was used with all initial water levels and velocities set to zero.

Several computation timesteps were used to test a range of Courant Numbers. The results presented below are for timesteps of 15 and 360 seconds, corresponding to Courant Numbers of 2 and 50. Each simulation was run for 5 h using a 0.5 h entry time constant.

Figures 3.3a to 3.3d show time history plots of the water level at Location A and the flow across Line 1 as defined in Figure 3.2. The flow time histories are repeated in Figures 3.3e and f using a much finer scale on the flow axes for examination of mass conservation properties. Figures 3.3g and h present the longitudinal water surface profiles along the direction of flow once steady state was reached. The bhh results are shown in each graph for ease of comparison, except for Figure 3.3f where the plots have been re-arranged because of the different scalings used on the flow axes.

Examination of the results gave the following conclusions:

**bhh** bhh was the boundary arrangement which produced the best results and stability properties for all timesteps tested. The flow through the model takes longer to reach the steady state value of 5,000 $m^3/s$ compared to the other arrangements. Observation of the fine scale flow time histories (Figures 3.3e and f) show the results for the 15 s and 360 s simulations to be virtually the same (Figure 3.3f). As can be seen a flow of 4,995.5 $m^3/s$ was computed at time 4 h and a value of 5,000.9 $m^3/s$ at 5 h.

**bqh** For low Courant Numbers (< 5) this arrangement performed correctly with the initial oscillations diminishing over time. For high Courant Numbers, however, the simulation became unstable as can be seen in the plot for a timestep of 360 s. The 15 s simulation gave a steady state flow of 4,994.7 $m^3/s$ which corresponds to a 0.1 % loss of mass.

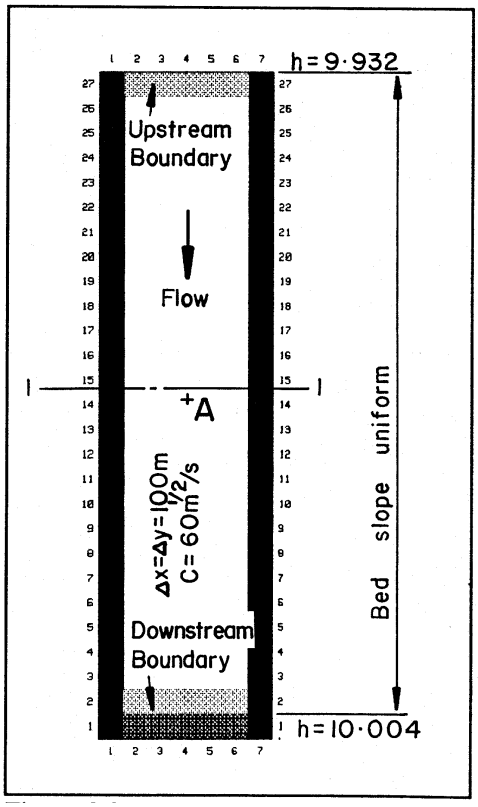


**Figure 3.2 Uniform Flow Model Layout**

**bvh** The bvh arrangement for low Courant Numbers nearly reaches steady state just prior to the development of severe oscillations and instabilities. For higher Courant Numbers the process is the same except the instabilities occur later. In the case of the timestep of 360 s the run became unstable after 16 h. At 5 h this simulation had achieved a steady state discharge of approximately 4,885 $m^3/s$ (2.3 % loss).

**bhq** bhq showed good results for low and high Courant Numbers with only small initial oscillations and long term stability. A loss of mass occurs however, with the higher the Courant Number the greater the loss. For the 15 s simulation the steady state flow was 4,994.7 $m^3/s$ (0.1 % loss) and for 360 s, approximately 4,880 $m^3/s$ (2.4 % loss).

**bqq** bqq showed similar characteristics to bqh, with the 15 s simulation also giving a steady state flow of 4,994.7 $m^3/s$ (0.1 % loss).

**bhv** bhv showed similar characteristics to bhq. The steady state discharges were approximately 4,997 $m^3/s$ (0.06 % loss) and 4,885 $m^3/s$ (2.3 % loss) for the 15 s and 360 s simulations.

**bvv** bvv showed similar characteristics to bvh, but in the case of the 15 s simulation managed to contain the severe oscillations for the duration of the 5 h simulation time. The flow at 5 h (approximately 4,930 $m^3/s$) in the 360 s case was still increasing slightly at about 9 $m^3/s/h$, and the size of the oscillations were also increasing.

The general conclusions which were reached are:

(i) For the upstream boundary a water level condition provides stability regardless of the downstream boundary.

(ii) A water level specified at both boundaries produced very accurate results (to within 0.1 % inaccuracy), but were slow to reach steady state flow conditions.

(iii) Mass was conserved 100 % between internal grid elements. Losses of mass were experienced across flow boundaries, especially for high Courant Numbers. Typically, less than 0.5 % loss was calculated for $C_r < 5$ and a 2 to 3 % loss for $C_r$ of around 50.

(iv) The instabilities and loss of mass associated with using flow boundaries are believed to be due to the boundary condition of a horizontal water surface level. Stelling (1984) gives a brief discussion on the problem of instabilities experienced with velocity boundaries, which he overcomes by using Riemann invariants to adjust the boundary values artificially. Further consideration of these problems at this stage was not taken, as it was believed to be undesirable to use such an adjustment at a 2-D/1-D interface.

(v) The preferred boundary configuration is clearly an upstream and downstream water level, however, the major problem associated with this is that the flow is not defined. Although this was not a problem in the model described above, it would be where the change in water level across a model is unknown as is commonly the case.

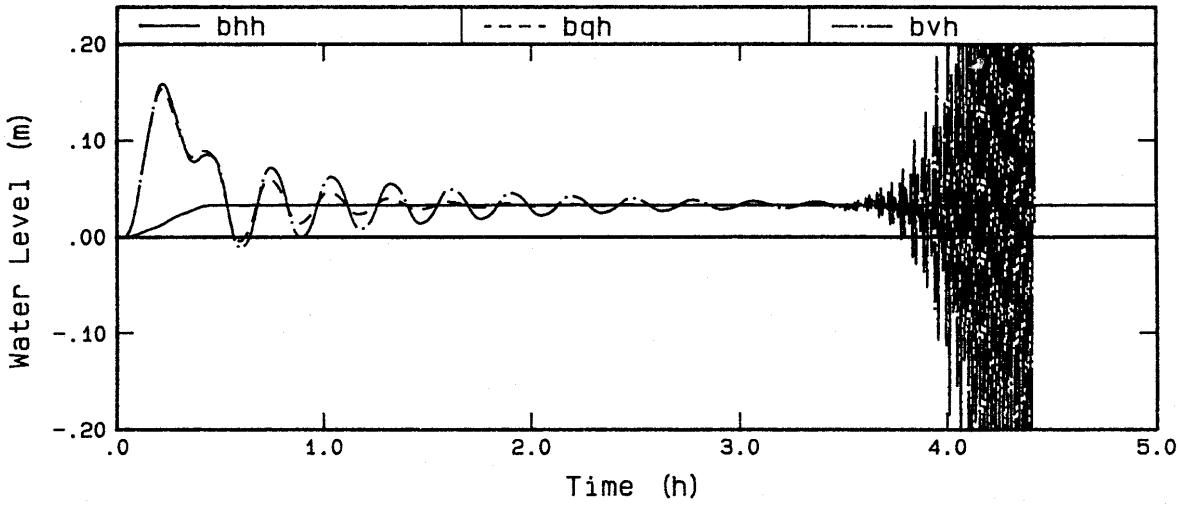


bhh, bqh & bvh Water Levels at Loc A (dt = 15 s)

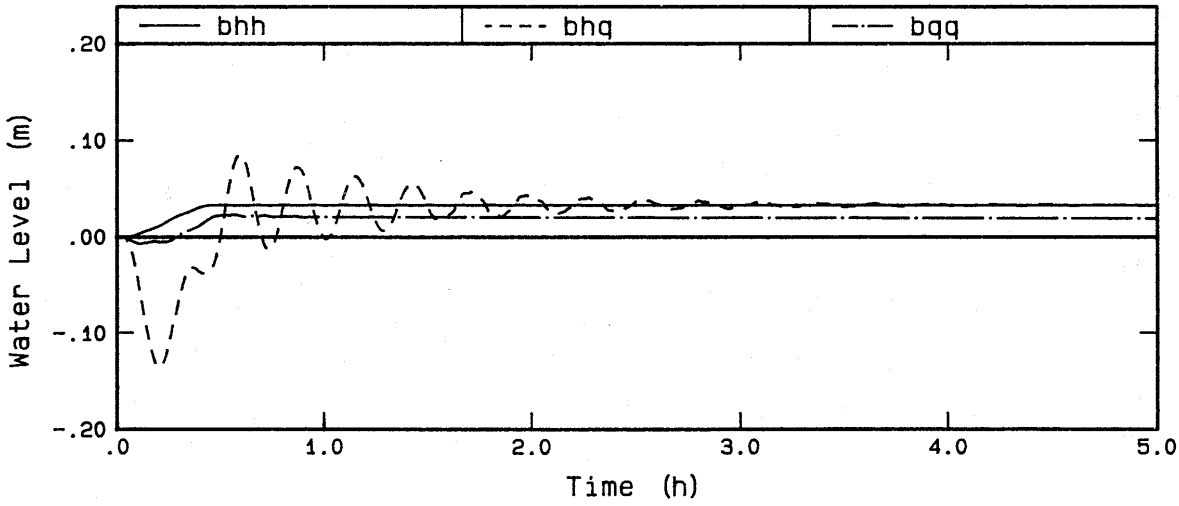


bhh, bhq & bqq Water Levels at Loc A (dt = 15 s)

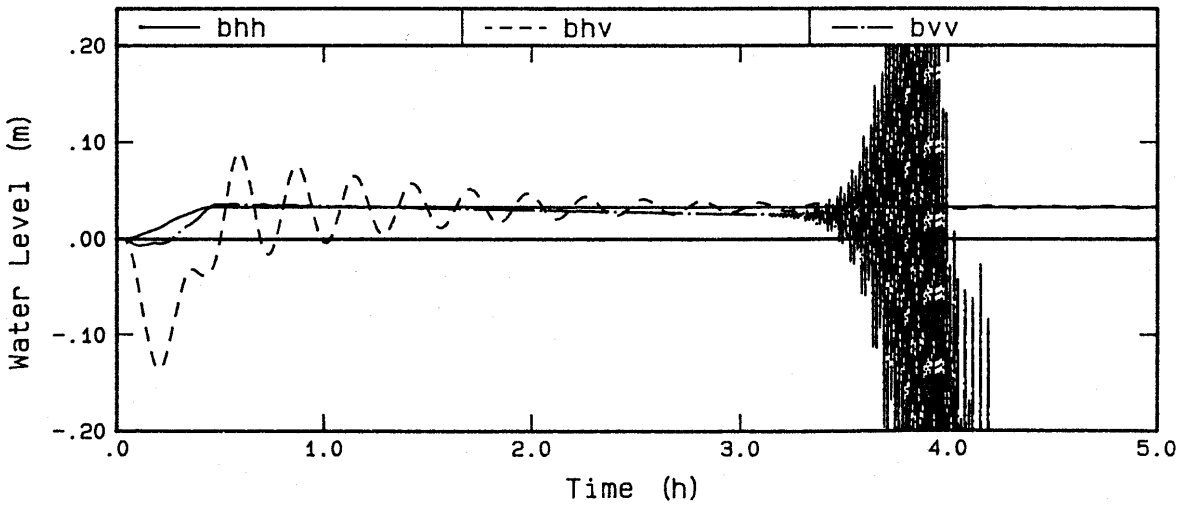


bhh, bhv & bvv Water Levels at Loc A (dt = 15 s)

**Figure 3.3a Water Level Time Histories - Uniform Flow - ?t = 15 s**

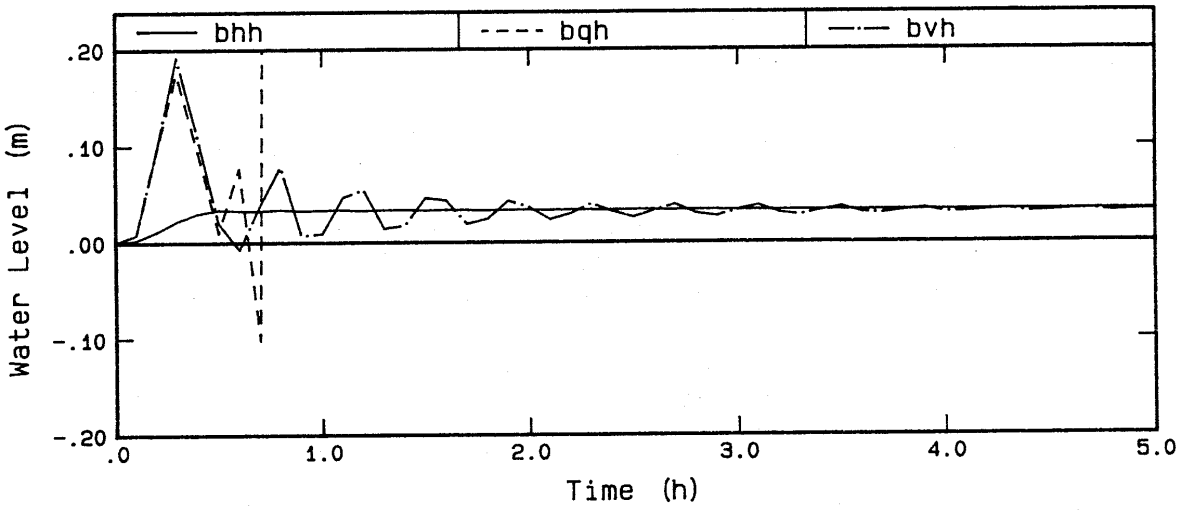


bhh, bqh & bvh Water Levels at Loc A (dt = 360 s)

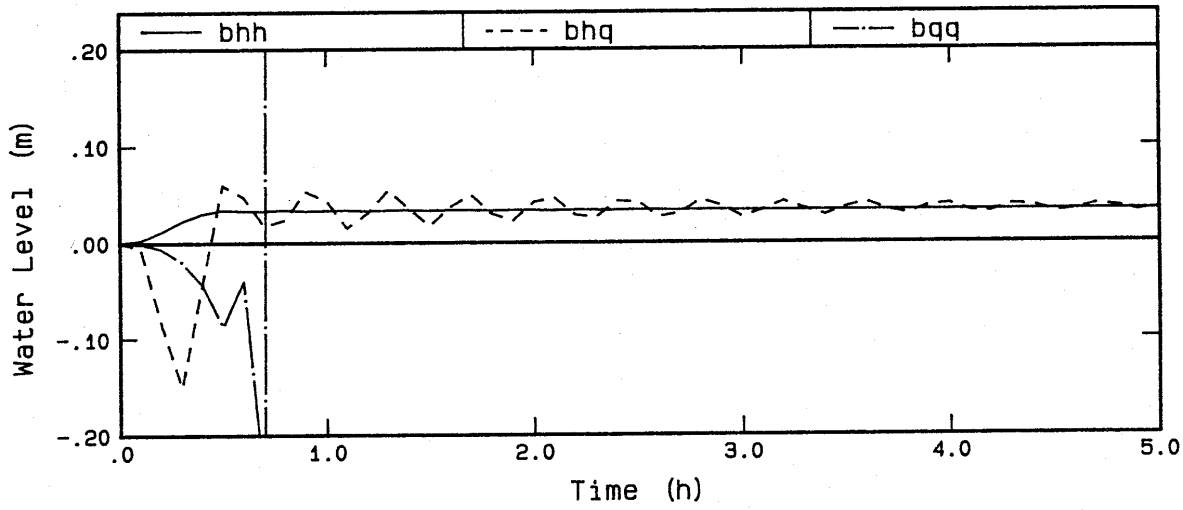


bhh, bhq & bqq Water Levels at Loc A (dt = 360 s)

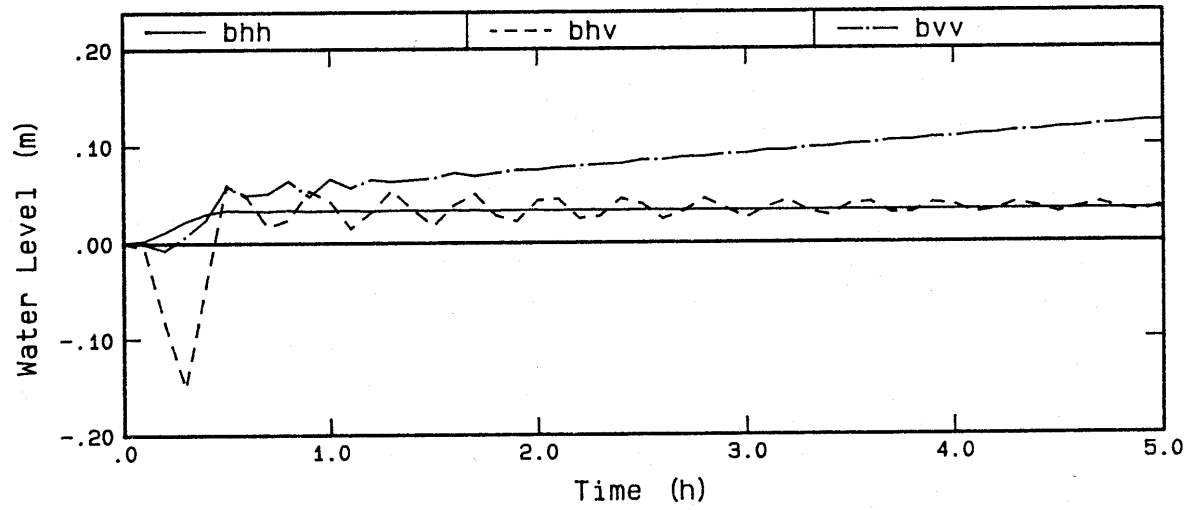


bhh, bhv & bvv Water Levels at Loc A (dt = 360 s)

**Figure 3.3b Water Level Time Histories - Uniform Flow - ?t = 360 s**

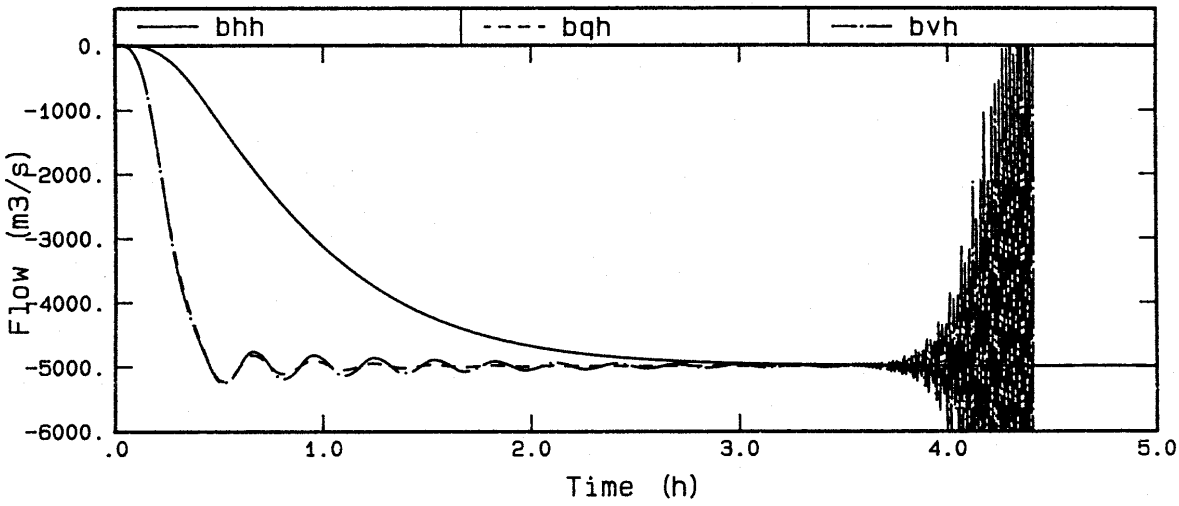


bhh, bqh & bvh Flow across Line 1 (dt = 15 s)

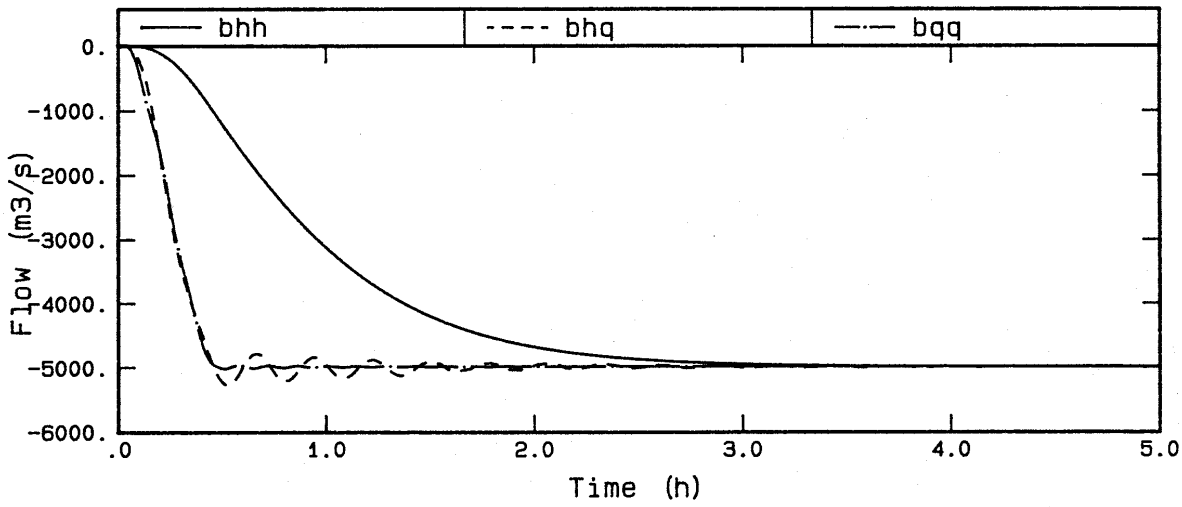


bhh, bhq & bqq Flow across Line 1 (dt = 15 s)

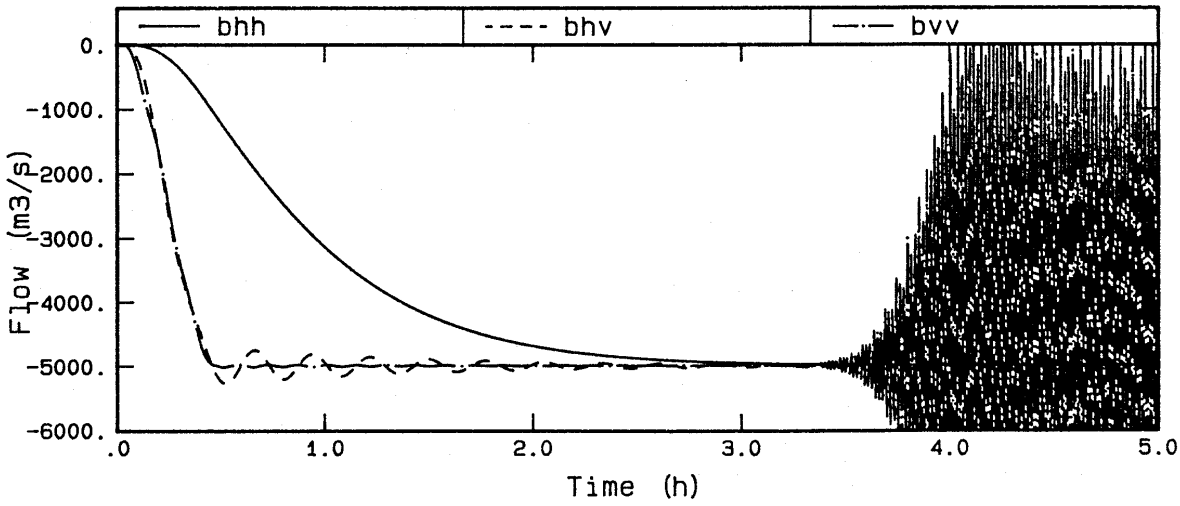


bhh, bhv & bvv Flow across Line 1 (dt = 15 s)

**Figure 3.3c Flow Time Histories - Uniform Flow - ?t = 15 s**

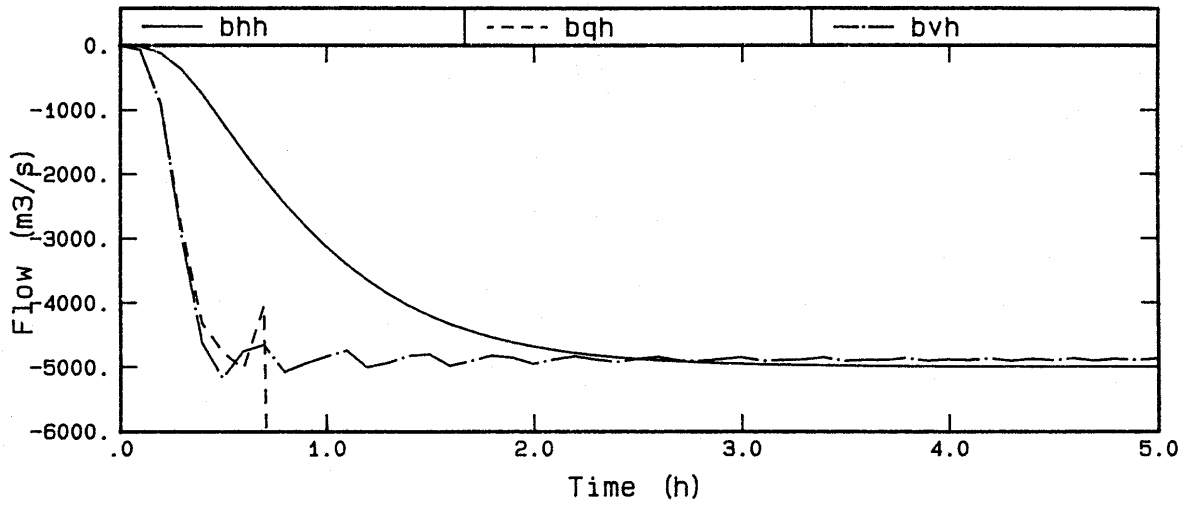


bhh, bqh & bvh Flow across Line 1 (dt = 360 s)

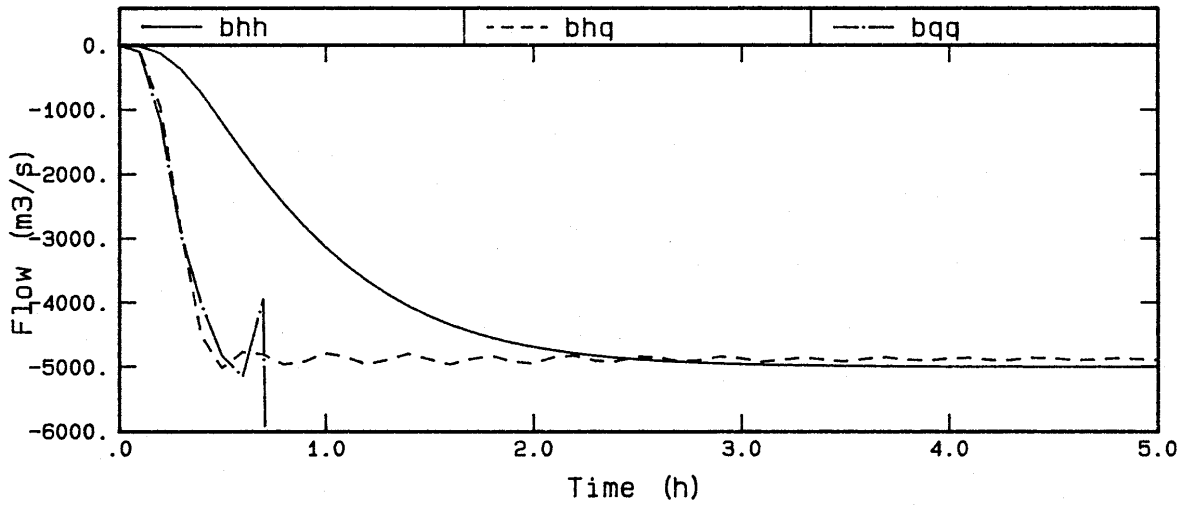


bhh, bhq & bqq Flow across Line 1 (dt = 360 s)

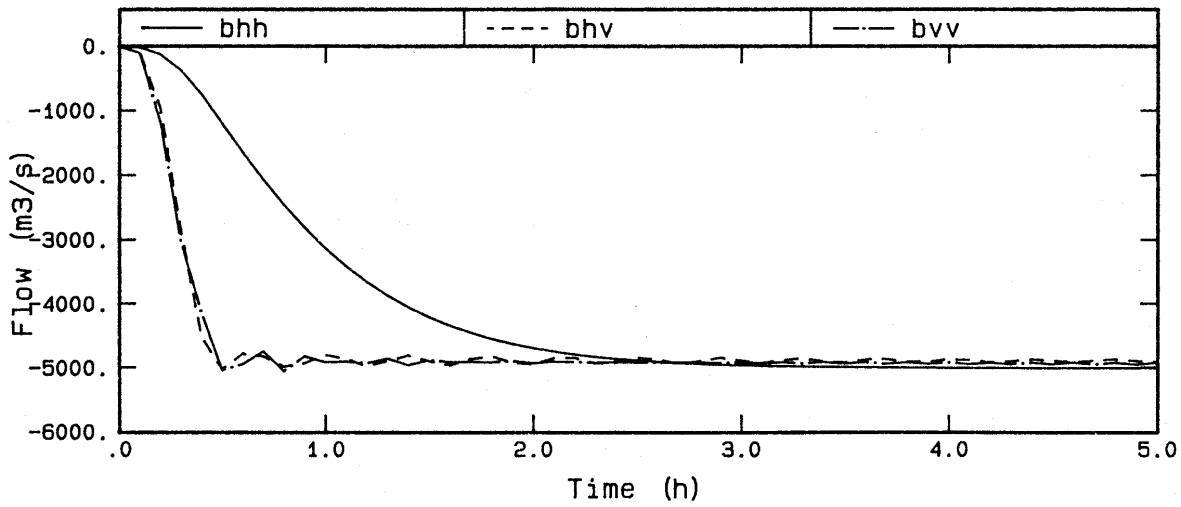


bhh, bhv & bvv Flow across Line 1 (dt = 360 s)

**Figure 3.3d Flow Time Histories - Uniform Flow - ?t = 360 s**

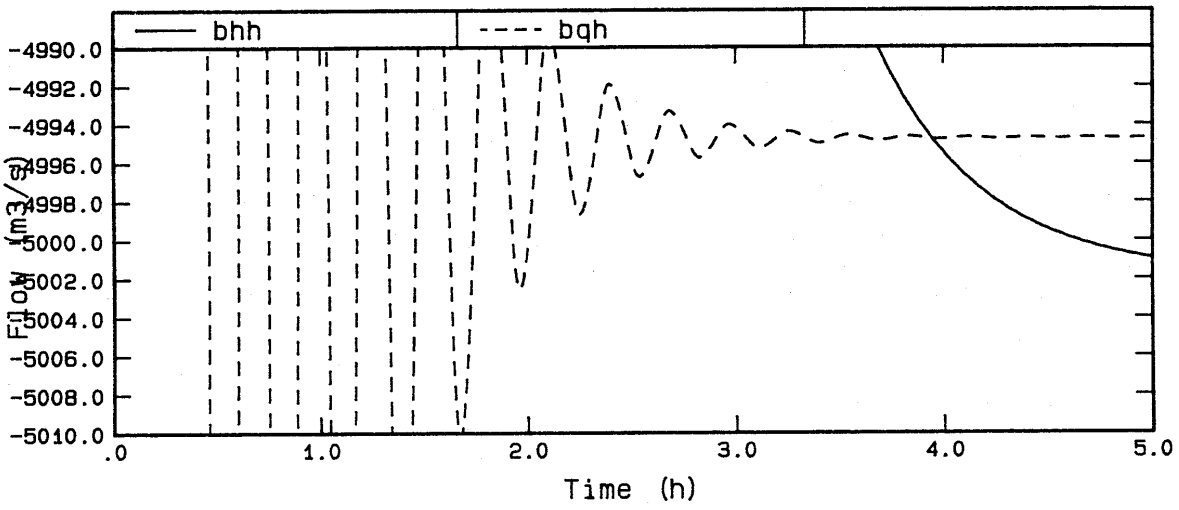


bhh & bqh Flow across Line 1 (dt = 15 s)

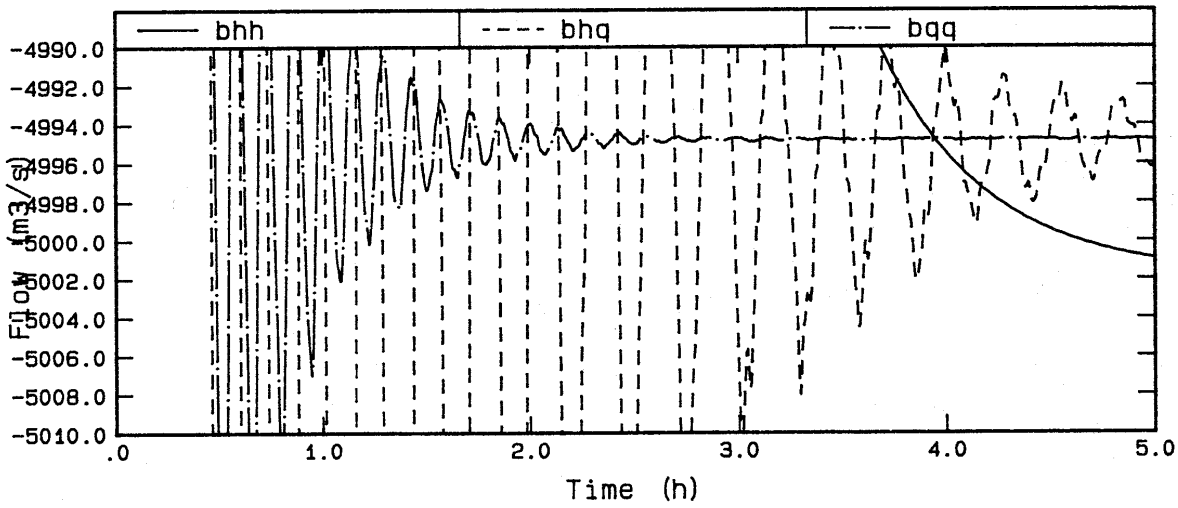


bhh, bhq & bqq Flow across Line 1 (dt = 15 s)

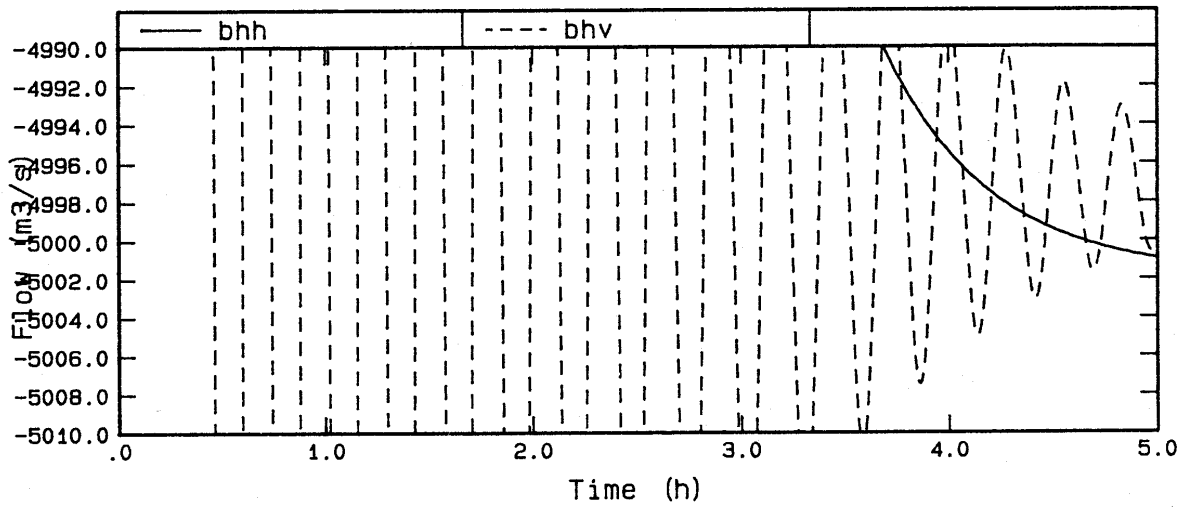


bhh & bhv Flow across Line 1 (dt = 15 s)

**Figure 3.3e Flow (Fine Scale) Time Histories - Uniform Flow - ?t = 15 s**

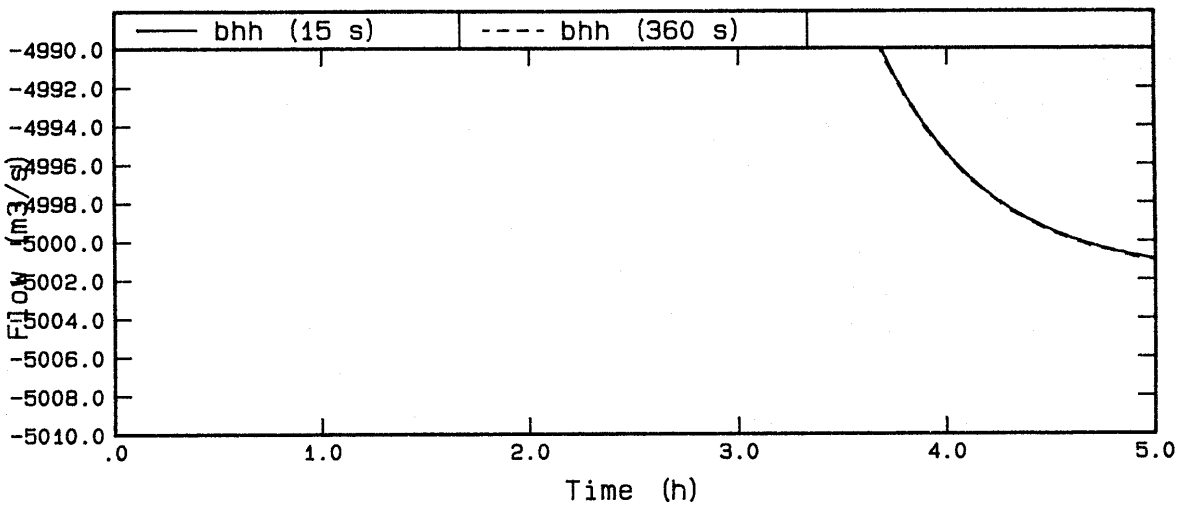


bhh Flow across Line 1 (dt = 15 s & 360 s)

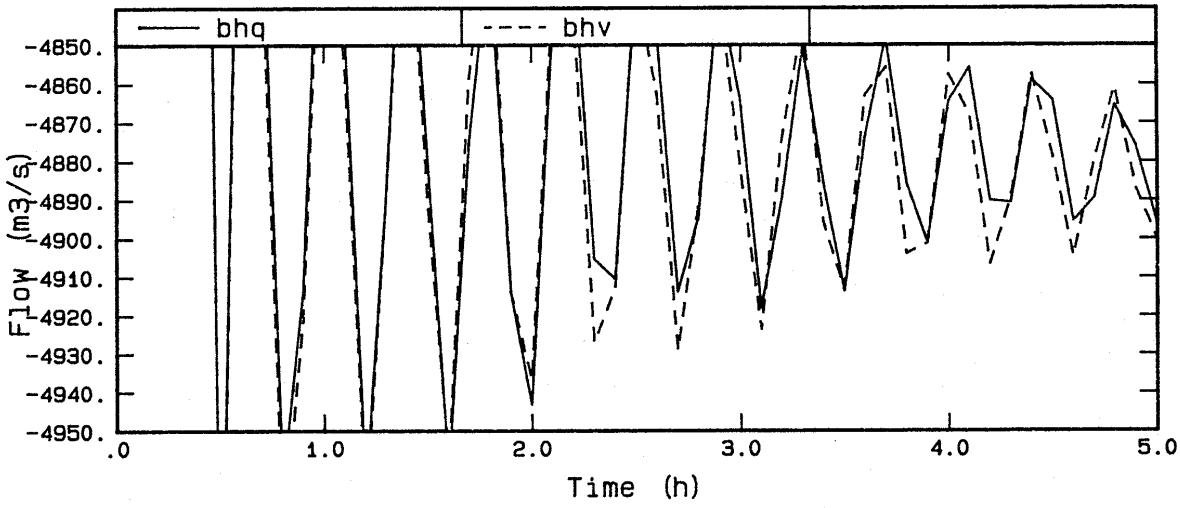


bhq & bhv Flow across Line 1 (dt = 360 s)

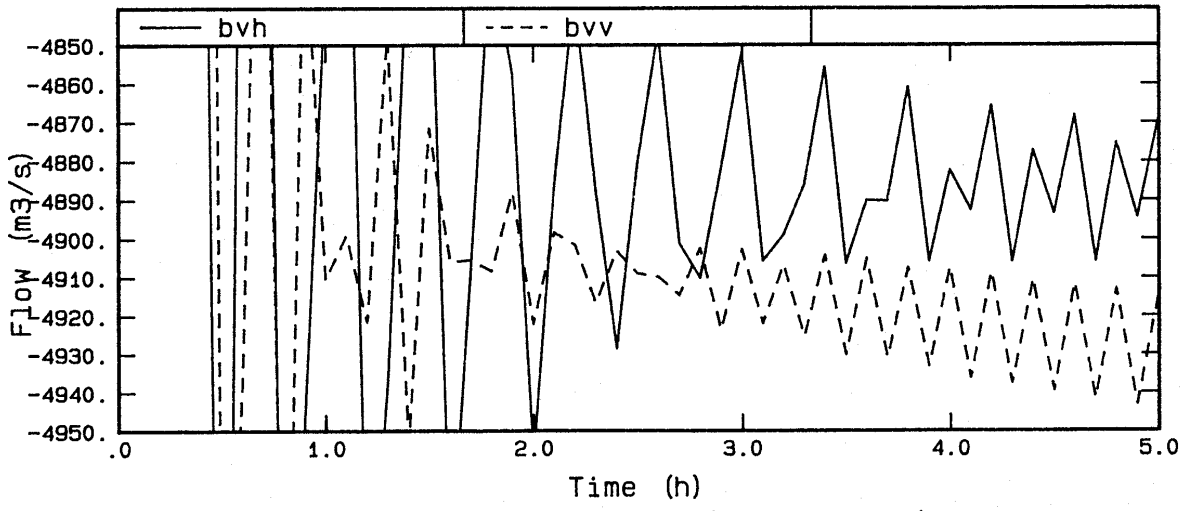


bvh & bvv Flow across Line 1 (dt = 360 s)

**Figure3.3f Flow (Fine Scale) Time Histories - Uniform Flow - ?t = 360 s**

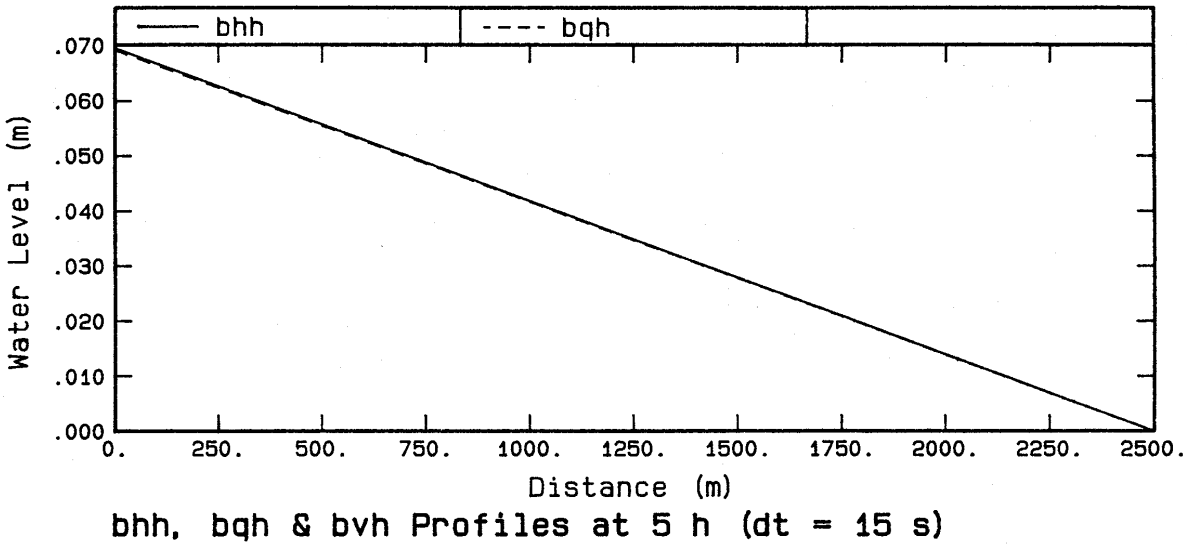


bhh, bqh & bvh Profiles at 5 h (dt = 15 s)

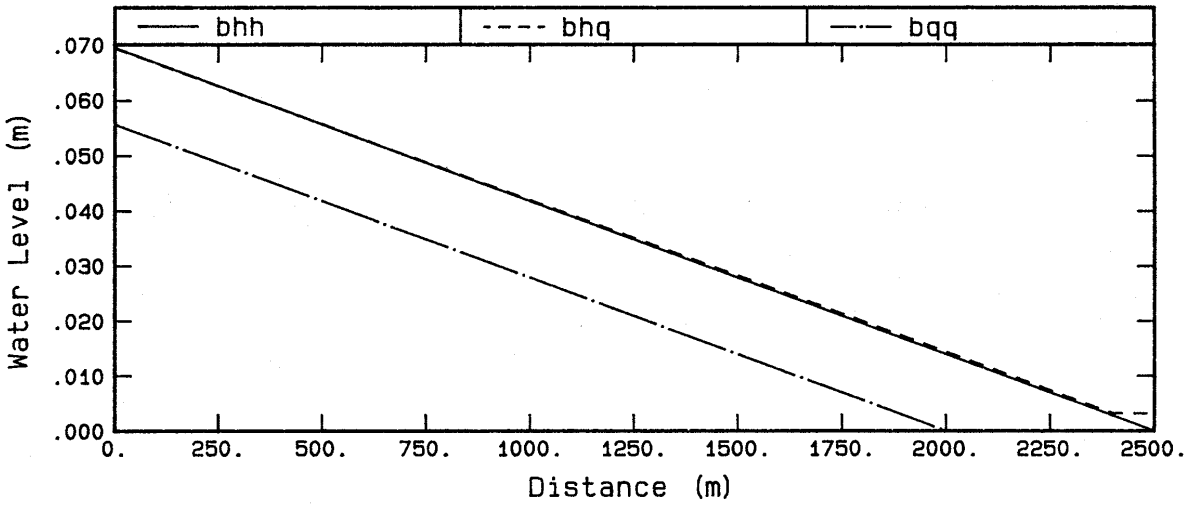


bhh, bhq & bqq Profiles at 5 h (dt = 15 s)

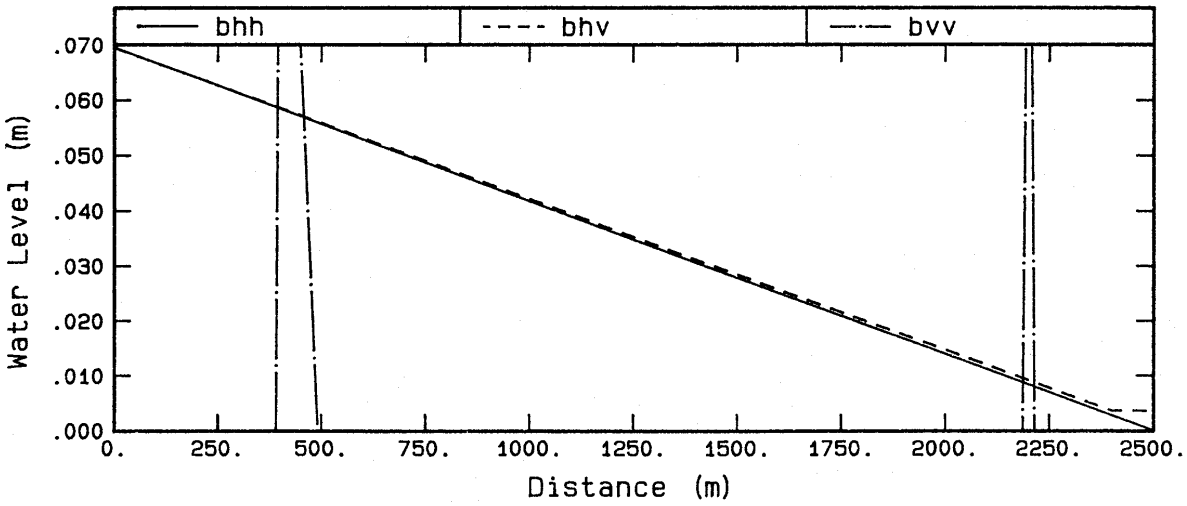


bhh, bhv & bvv Profiles at 5 h (dt = 15 s)

**Figure 3.3g Water Surface Profiles - Uniform Flow - ?t = 15 s**

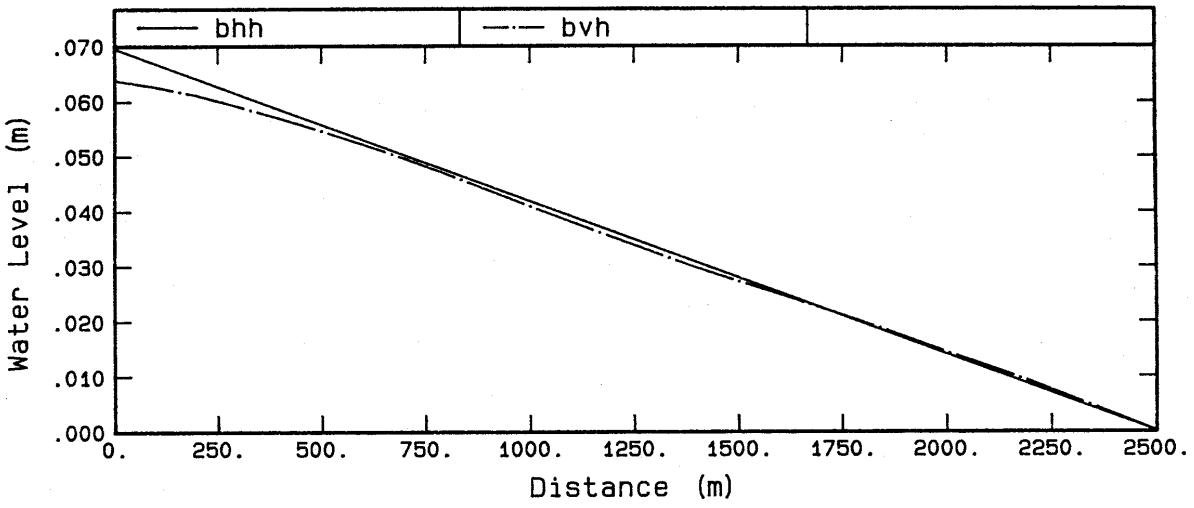


bhh, bqh & bvh Profiles at 5 h (dt = 360 s)

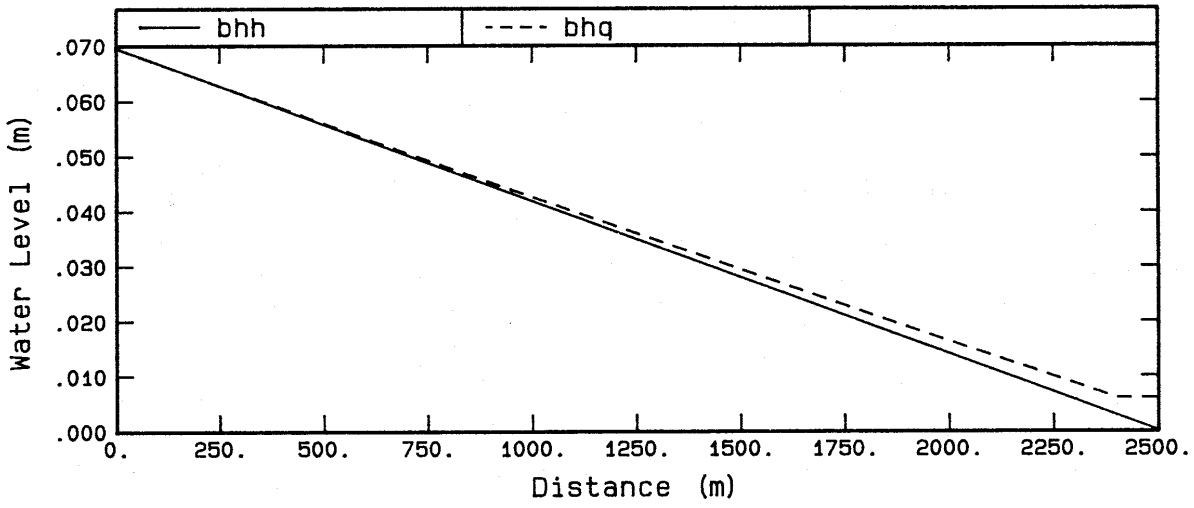


bhh, bhq & bqq Profiles at 5 h (dt = 360 s)

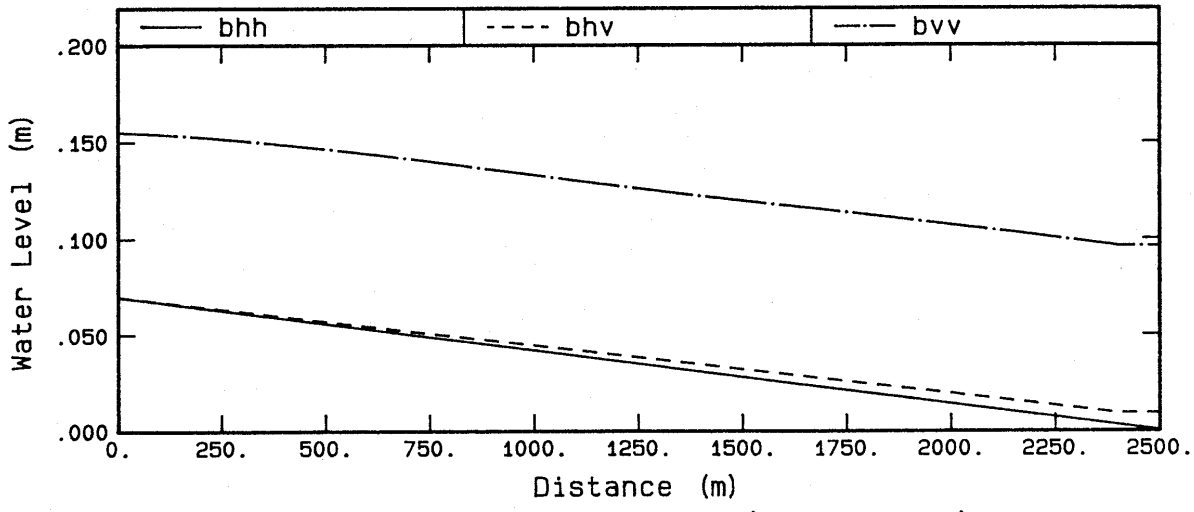


bhh, bhv & bvv Profiles at 5 h (dt = 360 s)

**Figure 3.3h Water Surface Profiles - Uniform Flow - ?t = 360 s**

### 3.4.3 Diverging Flow

As flow either expands or contracts there is a change in velocity which corresponds to a change in dynamic head and water surface level. Thus in the case of expanding flow the velocity and dynamic head reduce, and the water surface level increases where the bed friction is sufficiently low. This gives the water an appearance of flowing "uphill".

Reduction of the finite difference form of the X-momentum equation under steady state flow gives Equation 3.4.3.

$$z_1 - z_0 + \frac{u_0 u_1 - u_0 u_3}{2g} + \frac{u_0^2 \Delta x}{C^2 H} = 0 \qquad \textbf{(3.4.3)}$$

which can be re-written as

$$\Delta z + \frac{\left(\frac{u_0 + u_1}{2}\right)^2 - \left(\frac{u_0 + u_3}{2}\right)^2}{2g} + \frac{u_0^2 \Delta x}{C^2 H} = 0 \qquad \textbf{(3.4.4)}$$

giving the change in water level over one element length plus the change in dynamic head plus the friction head is equal to zero as given by Equation 3.4.5 below.

$$\Delta z + \Delta\left(\frac{u^2}{2g}\right) + \frac{\bar{u}^2 \Delta x}{C^2 H} = 0 \qquad \textbf{(3.4.5)}$$

To verify the computer code was correctly calculating the advection and friction terms, the model illustrated in Figure 3.4 was used. The depth of the model in its central portion increases in the direction of flow, causing a decrease in velocity. The element length was set to 10 m and the Chézy value to 75 $m^{1/2}/s$ to minimise the frictional losses.

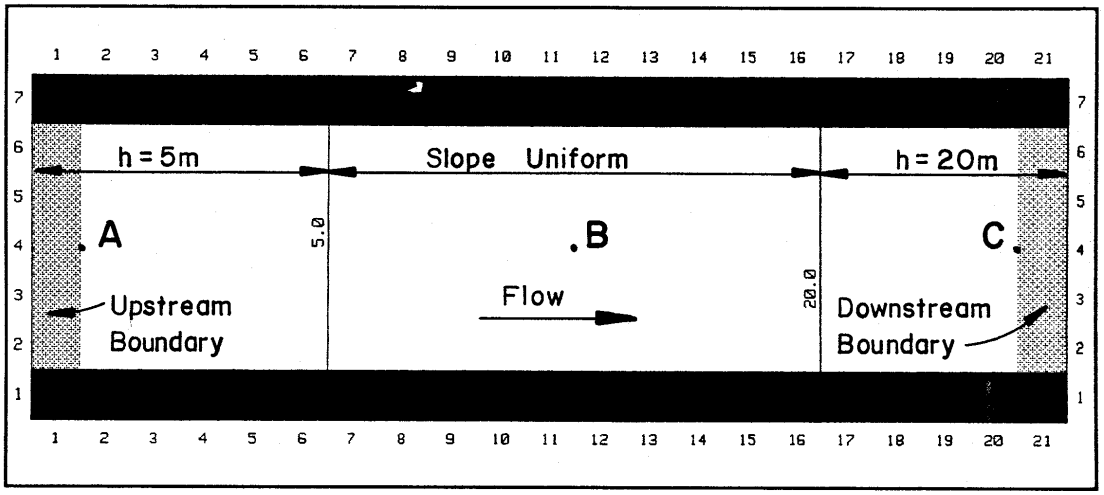


**Figure 3.4 Diverging Flow Model Layout**

Adopting a downstream boundary water level of zero and a horizontal water surface, the inflow velocity would be 1.0 m/s, and the outgoing velocity 0.25 m/s. Calculation of the frictional losses for each element in the direction of flow plus the change in dynamic head gives a calculated water level profile along the model as illustrated by the symbols in the lower graph of Figure 3.5. The total drop in water level due to friction alone was calculated to be 0.0024 m while the rise due to the change in dynamic head is 0.0478 m. This gives a net rise in water level of 0.0454 m for the length of the model. These calculations are only approximate as the water level is not horizontal, but given that the net rise is less than 0.5 % of the water depth the approximation is reasonable.

Difficulty was experienced in successfully achieving a stable simulation. All possible boundary arrangements were tried, with each one having initial oscillations and instabilities so that at no point was steady state maintained throughout the whole model.

Specifying water levels at both boundaries, ie. 0.0454 m at the upstream boundary and zero at the downstream boundary, produced a stable simulation. This arrangement is not valid as the discharge is not defined (the calculated flow for this simulation was from right to left as driven by the higher water level at the right hand boundary). Thus, for this model a flow boundary must be defined at either the upstream or downstream boundary.

The inability to stabilise this model is of some concern and certainly warrants further investigations. It was by far the most difficult to stabilise of all the models developed. This is most likely because of the combination of low bed friction ($C = 75\ m^{½}/s$), short element length (10 m), and large variation in depth, all of which are known to cause stability problems.

A dampening of the instabilities was achieved when the upstream boundary of the 2-D model was linked to a 1-D model having a single node with an inflow of 250 $m^3/s$. The details of the 2-D/1-D link are covered in Chapter Four, but for the purposes of the current discussion the results of the simulation are worth presenting. If the 1-D node is sufficiently large, in this case 11,000,000 $m^2$ in surface area, it was possible to reach a steady state condition for a sufficiently long enough period to analyse the results. Eventually the computation became unstable, even for larger nodal surface areas.

The approach to steady state is illustrated by the velocity and discharge time histories in Figure 3.5. The lower graph in Figure 3.5 compares the modelled water surface profile at time 2 h (steady state conditions) with that calculated analytically. As can be seen an excellent agreement resulted.

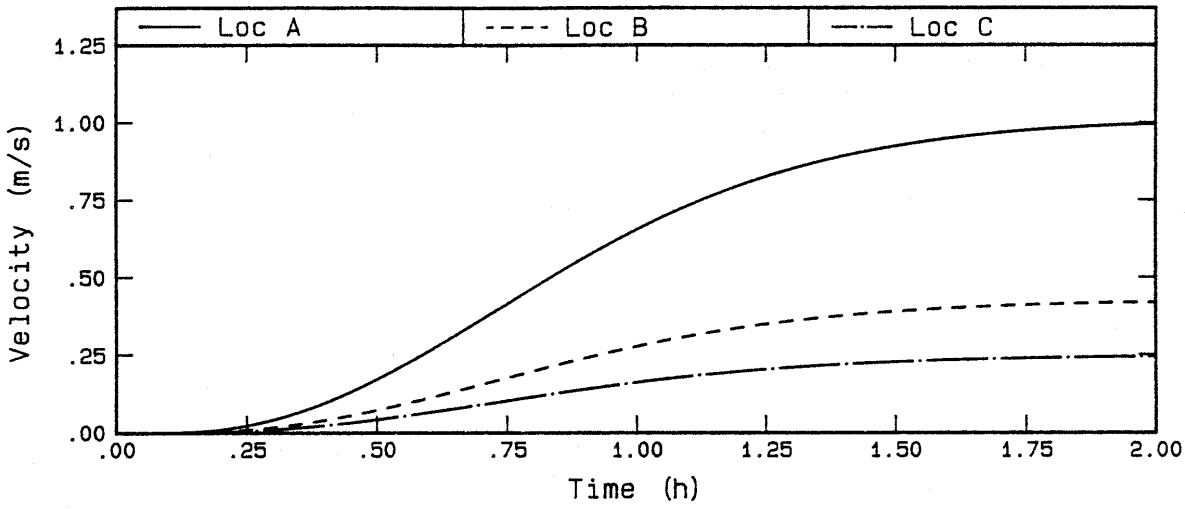


Velocities at Locs A, B and C

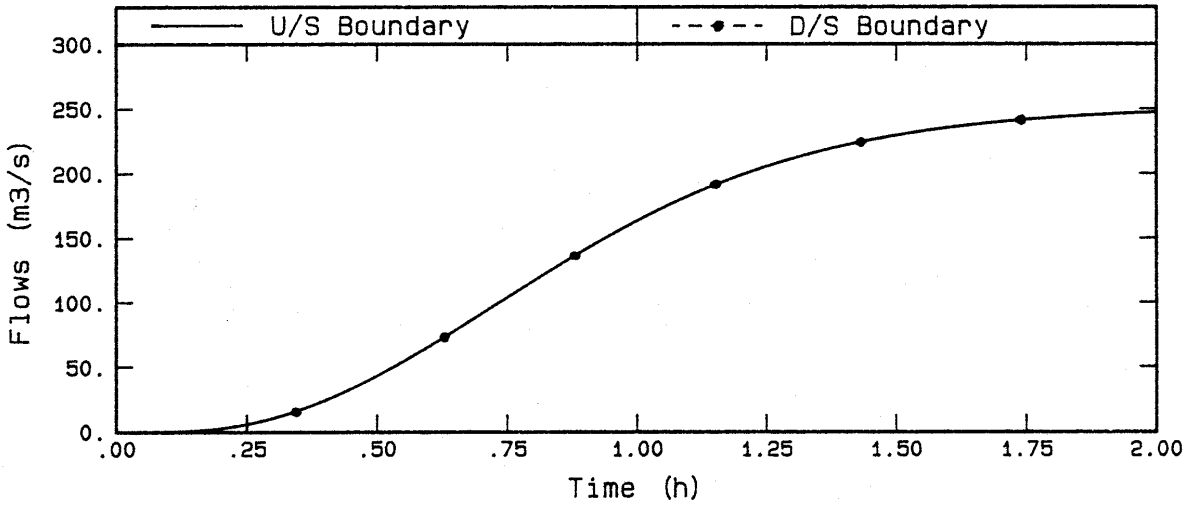


Flows across Upstream and Downstream Boundaries

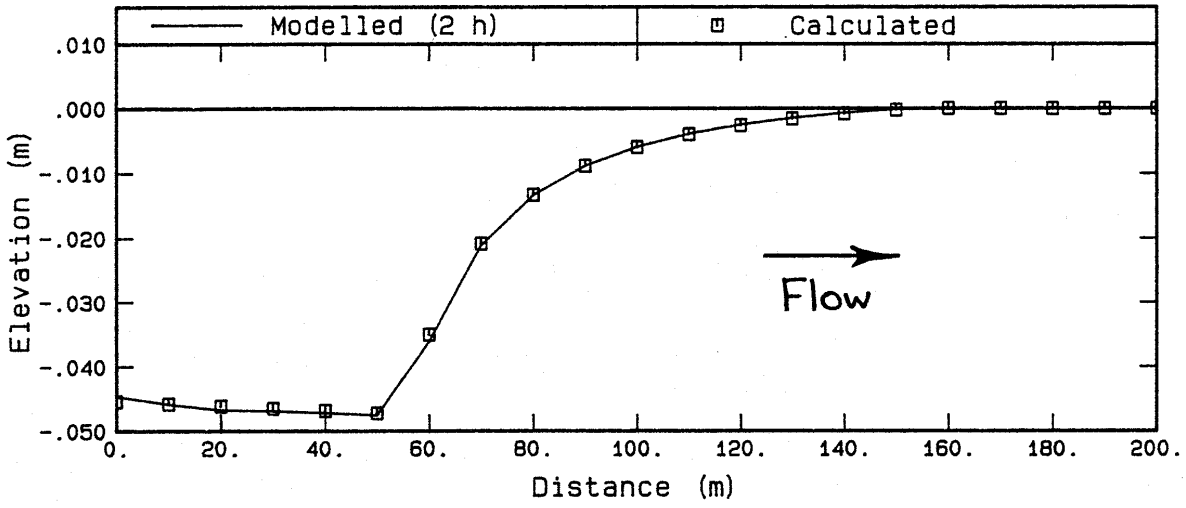


Comparison of Water Level Profiles

**Figure 3.5 Time Histories and Water Level Profiles - Diverging Flow**

### 3.4.4 Flow Past a Solid Wall

This test case is based on a model described in Stelling (1984) which aims to simulate the formation of eddies behind a solid wall.

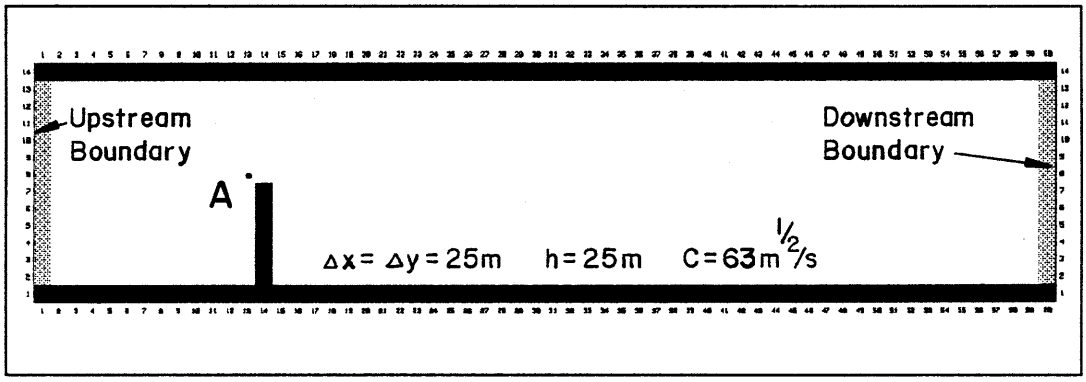


**Figure 3.6 Flow Past a Solid Wall Model Layout**

The details of the model are shown in Figure 3.6. An element length of 25 m, a constant bed level at -25 m, and a uniform Chézy coefficient of 63 $m^{1/2}/s$ were used.

The upstream boundary was defined by a constant velocity of 0.5 m/s with an entry time constant of 0.5 h (refer Equation 3.4.1), while the downstream boundary was specified as a constant water level of zero. The initial water levels and velocities were set to zero. Each simulation extended from zero to 4 h.

Numerous simulations of this model were carried out with variations of the timestep and diffusion coefficient to (a) compare the results with those reported in Stelling (1984), and (b) establish the importance of these parameters on the formation of eddies.

Difficulty was also experienced here in maintaining stability because of the upstream flow boundary. The exception was where an unrealistically high diffusion coefficient was used. For the Stelling (1984) simulations Riemann invariants were used, which implies that stability problems were encountered. No detailed discussion is presented in Stelling (1984) with regard to this, making further comparisons difficult.

The flow patterns and water level contours for a timestep of 10 s ($C_r$ = 9) and zero diffusion at 1, 2, 3 and 4 hours are shown in Figure 3.7. Note that the water level contours on each plot are based on the maximum and minimum values at that time. Clearly at time 4 h the simulation has become unstable, and the presented result is meaningless.

#### Varying the Timestep, ?t

Several simulations were carried out representing a range of timesteps. Figure 3.8a shows the water level time history at Location A (Figure 3.6) for timesteps of 1 s, 10 s and 30 s ($C_r$ = 1, 9 and 27). The water level is plotted for every timestep. Figure 3.8b illustrates the flow patterns at 2 h for timesteps of 1 s, 10 s and 30 s. Clearly the timestep has a distinct influence on the rate of formation, strength and size of an eddy. Observation of the results implies that in this case the longer the timestep the smaller, more frequent and more intense the eddy(s).

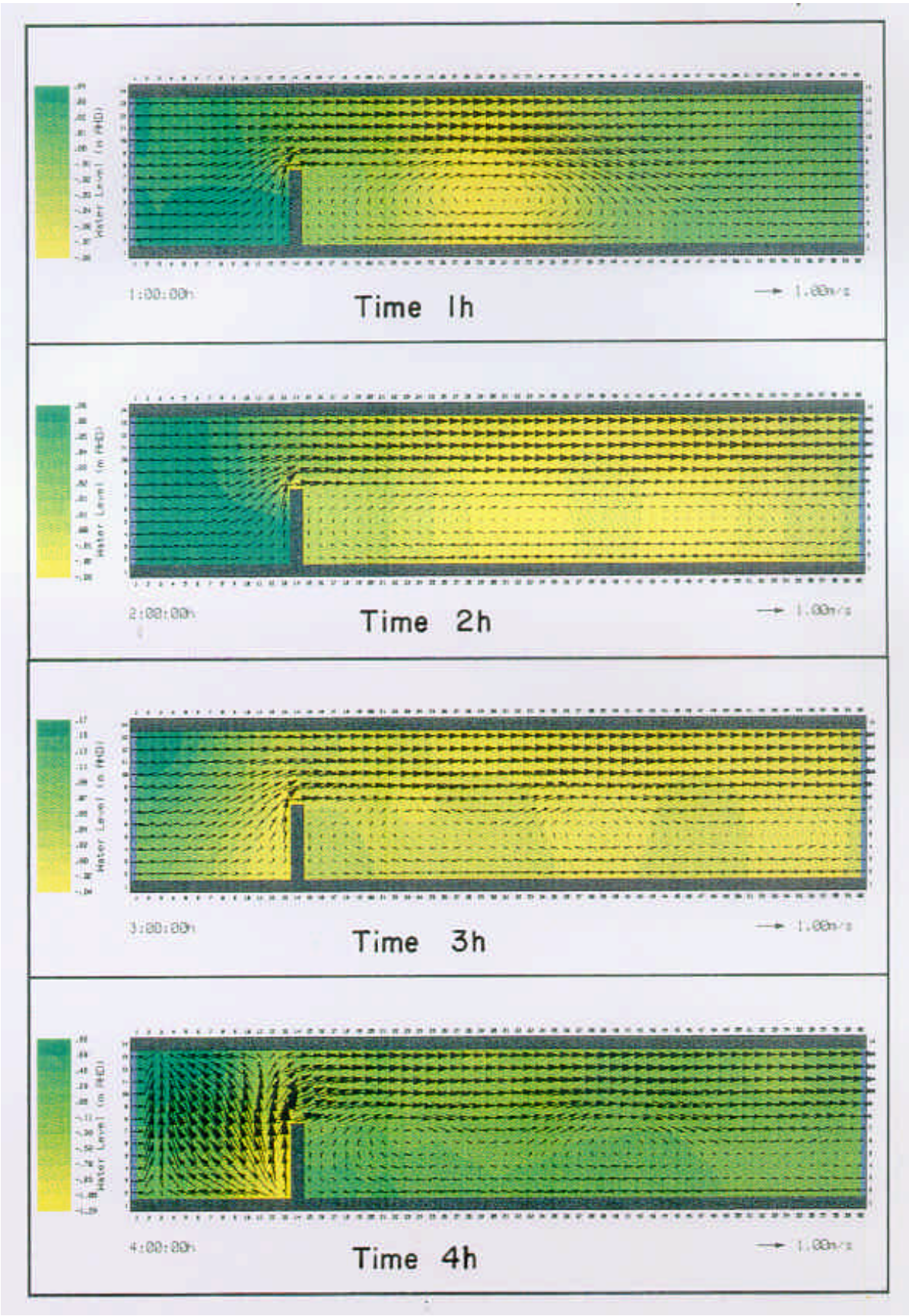


**Figure 3.7 Flow Patterns and Water Level Contours for ?t = 10 s Flow Past a Solid Wall**

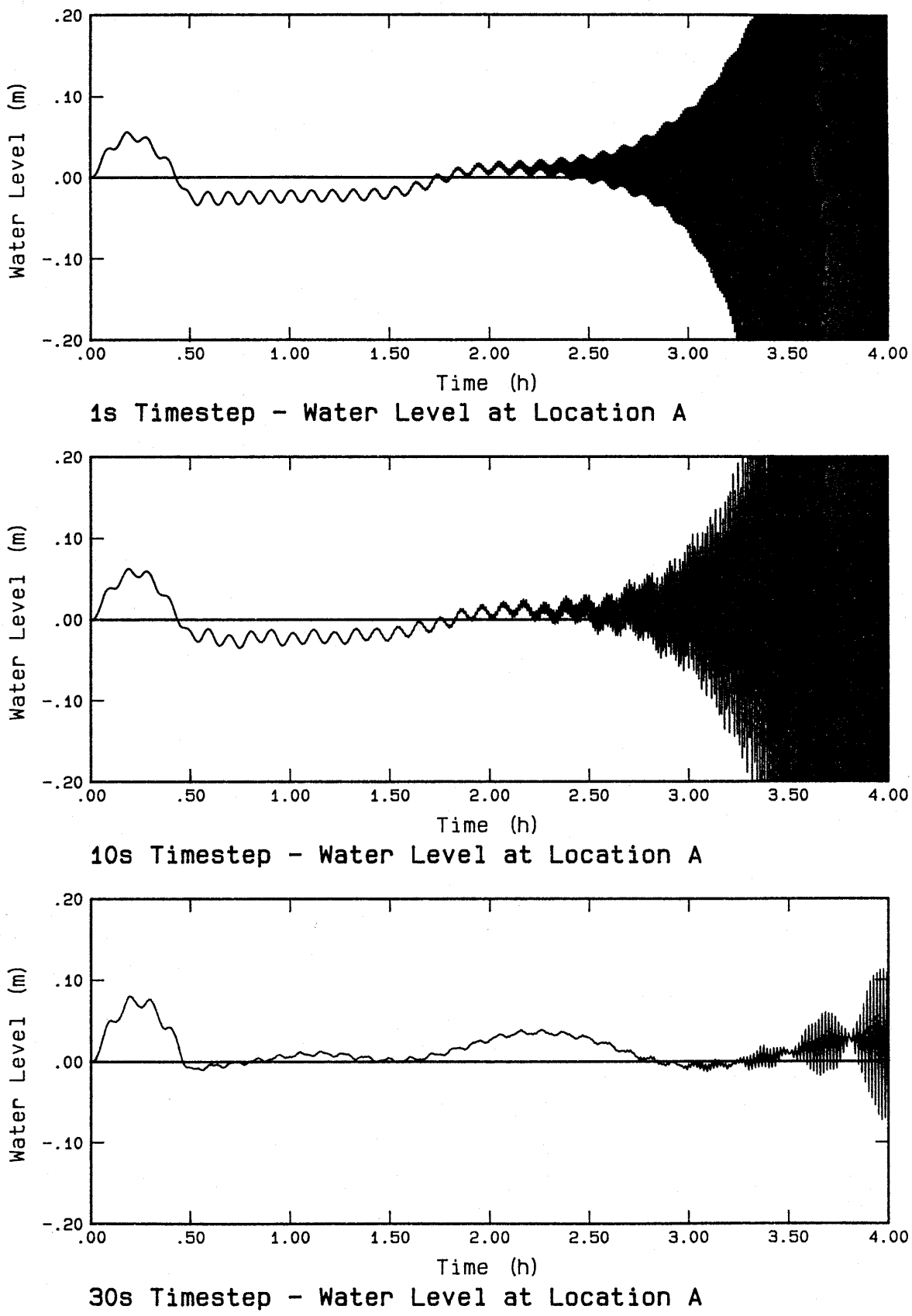


**Figure 3.8a Water Level Time Histories for ?t = 1 s, 10 s and 30 s Flow Past a Solid Wall**

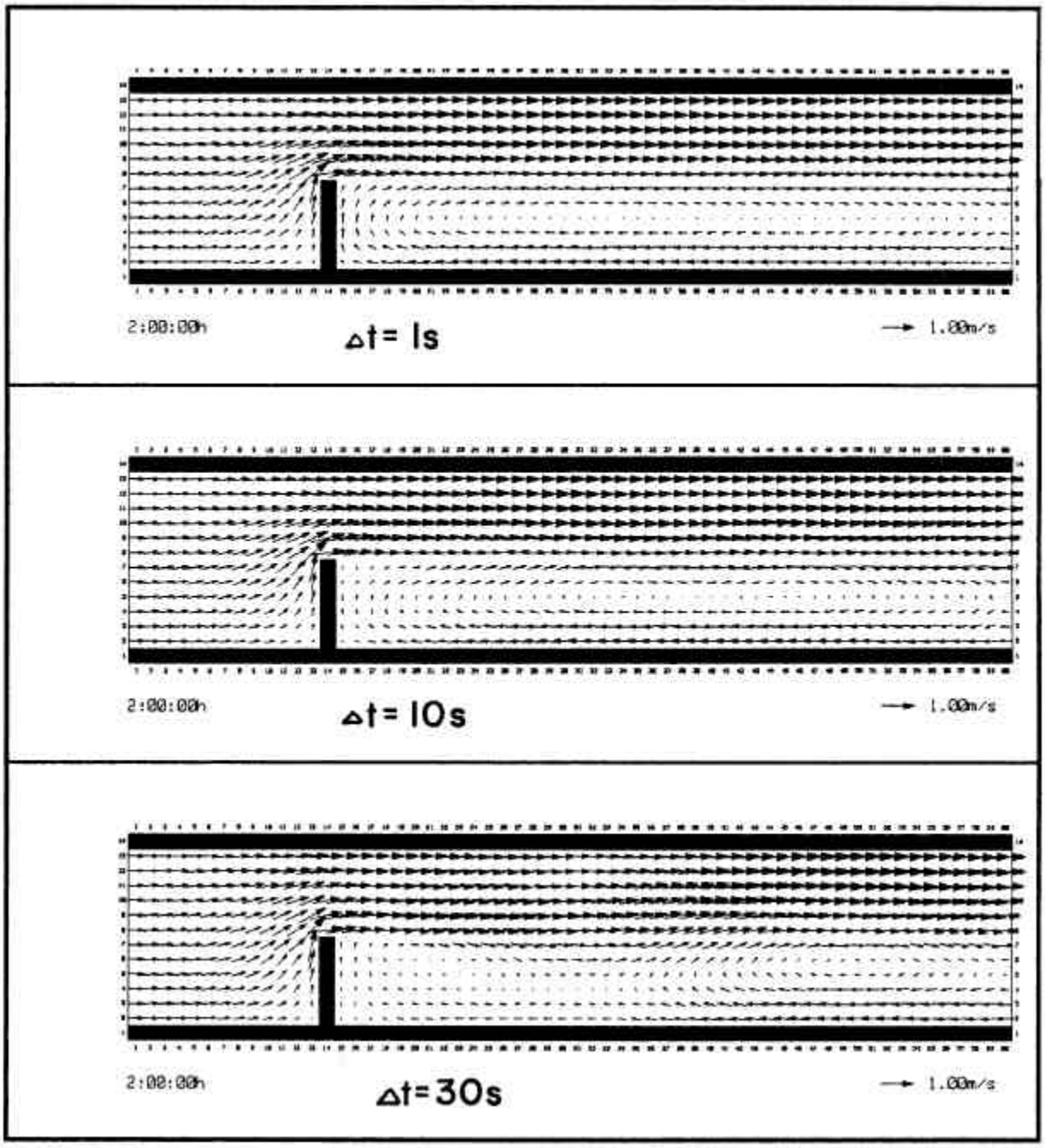


**Figure 3.8b Flow Patterns at 2 h for ?t = 1 s, 10 s and 30 s Flow Past a Solid Wall**

## Varying the Diffusion Coefficient, μ

Similar sets of simulations were carried out for different values of the diffusion coefficient, μ. Figures 3.9a and b illustrate the results from a selection of these. The 10 s timestep was used and the values of μ were 0.1, 1.0 and 10 $m^2/s$. As before, the figures show the water level time histories, and the flow patterns at 2 h. The case of zero diffusion is given at the top of each figure for comparison purposes. A dampening of the oscillations is clearly shown to occur, with the effect being only very slight for μ = 0.1, distinctly noticeable for μ = 1.0 and acute for μ = 10 to the point that the simulation has been stabilised.

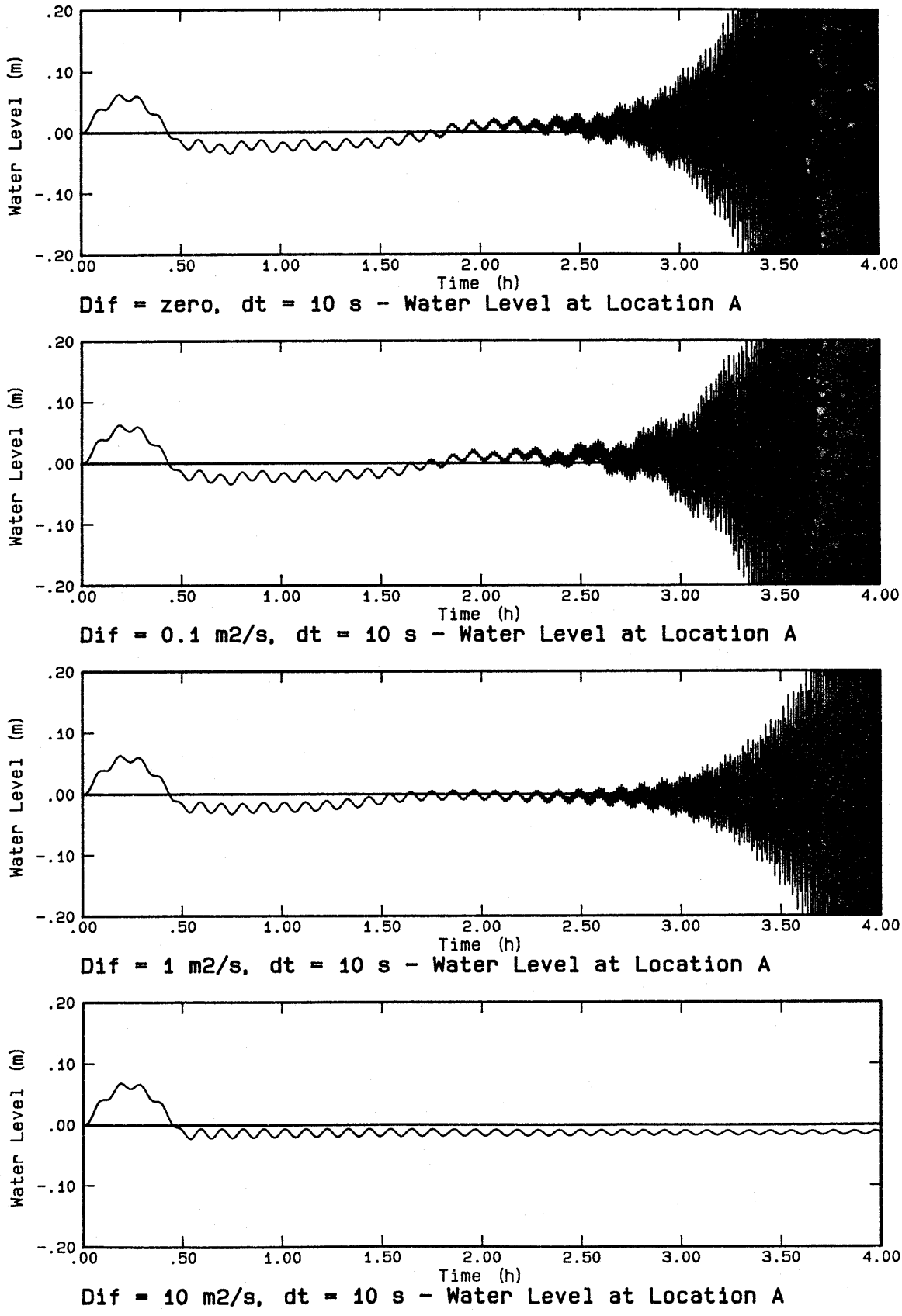


**Figure 3.9a Water Level Time Histories for μ = zero, 0.1, 1 and 10 m2/s Flow Past a Solid Wall**

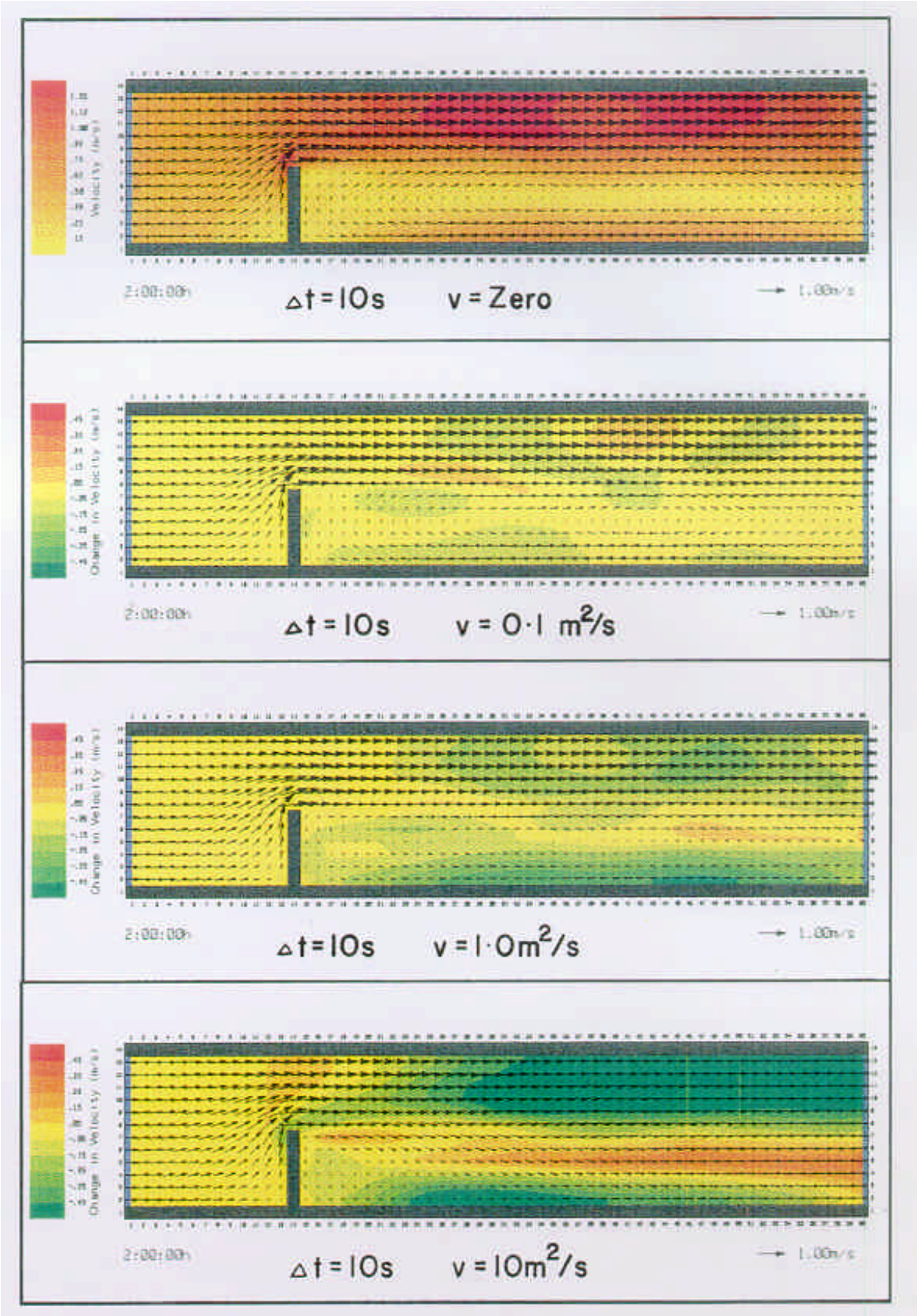


**Figure 3.9b Flow Patterns and Change in Velocity Contours at 2 h for μ = zero, 0.1, 1 and 10 m2/s - Flow Past a Solid Wall**

For Figure 3.9b, which shows the flow patterns, the case of zero diffusion is shown at the top. To visualise the effect of diffusion on the flow patterns, the velocities of the zero diffusion case have been contoured by colour shading, while for the non-zero diffusion cases the difference in velocity as compared to the zero diffusion case has been colour contoured. In the latter, a green shading represents a decrease in velocity while the red an increase, with the darker the shade the greater the change. Observation of these flow patterns and the change in velocity further shows the dampening effect of the higher diffusion coefficients. For $\mu$ = .1 only slight changes have occurred, the greatest being less than .2 m/s, while for $\mu$ = 1.0 the intensity of the eddy has been clearly reduced although the size and location are similar. In the case of $\mu$ = 10 there is a major change in velocities with significant areas having decreases in excess of 0.5 m/s. The effect is sufficiently strong to extend to regions upstream of the wall. More importantly, however, is the change in flow pattern which is characterised by the virtual elimination of the eddy.

## Different Boundary Arrangements

A number of other simulations examined the use of different open boundaries to that already described. The results of three of these simulations are presented below and their boundary arrangements are illustrated in Figure 3.11c.

The open boundary arrangement as used previously is referred to as Arr 1. Arr 2 uses the same boundary conditions as Arr 1 except in reverse causing the flow to be in the opposite direction, ie. from right to left.

Arr 3 uses a constant water level of 0.05 m for the upstream boundary in place of the 0.5 m/s velocity, and maintains the zero water level at the downstream end. The 0.05 m is a rough estimate of the average water level drop across the model.

To investigate further the cause for instabilites, a further test, codenamed Arr 4, was carried out. This involved adjusting the model to the arrangement given in Figure 3.10, where the downstream boundary of Arr 1 was moved upstream to the same distance from the wall as the upstream boundary.

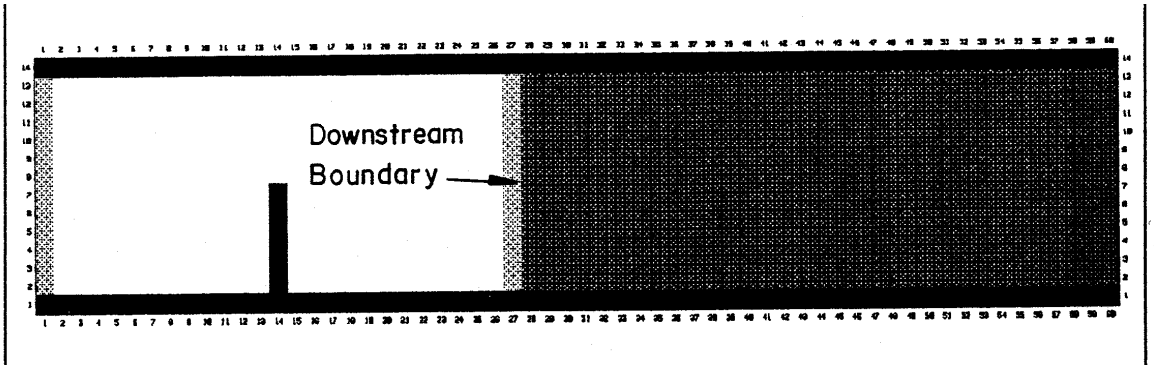


**Figure 3.10 Arr 4 Model Layout - Flow Past a Solid Wall**

Zero diffusion and a timestep of 10 s were used for the model simulations. Figures 3.11a to c illustrate the water level and flow time histories, and the flow patterns at time 2 h. Arr 1 results are reproduced at the top for easy comparison. Note that for Arr 2, Location A is located on the opposite side of the wall as the flow is in the opposite direction.

Arr 2 became unstable earlier than Arr 1 as can be seen from the time history plots. Of interest here was tracing the instability which showed its origin to be at the upstream velocity boundary. The instability was only just starting to be felt at the tip of the wall when the model became unstable, which explains why the oscillations in the time history are only small. This implies that the instabilities are not associated with the eddy formations.

Arr 3 with the water level specified for both upstream and downstream boundaries showed much improved stability properties. A very slight oscillation is evident in the time history towards the end of the simulation. The source of this oscillation was not investigated.

As discussed previously, the main problem with specifying water levels for both upstream and downstream boundaries is that the discharge is not defined. The correct change in water level across the model can therefore only be determined by a trial and error process. Even so, the discharge through the model is unlikely to stabilise (see Figure 3.11b, Arr 3) as the water level at, say, the upstream end can not be in reality constant (as is being simulated), because of the water level fluctuations caused by the eddy movements.

A solution to this problem was later found using the 2-D/1-D link, by attaching a 1-D node (area 10,000,000 $m^2$) at the upstream end of the 2-D model and specifying a constant discharge of 3,750 $m^3/s$ to the 1-D node. The simulation remained highly stable, and the water levels in the 2-D model were free to fluctuate with eddy movements, as illustrated in Figure 3.11d. The flow patterns at times 1, 2, 3 and 4 h are shown in Figure 3.11e.

The time history for Arr 4 shows that the oscillations over the first two hours are similar to Arr 2, while its stability properties are similar to Arr 1. This implies that the initial oscillations are most likely related to the length of the wall from the upstream boundary, while the instabilities are associated with the upstream velocity boundary.

Also of note is that the downstream boundary has an obvious effect on the size of the eddy as illustrated in the flow patterns.

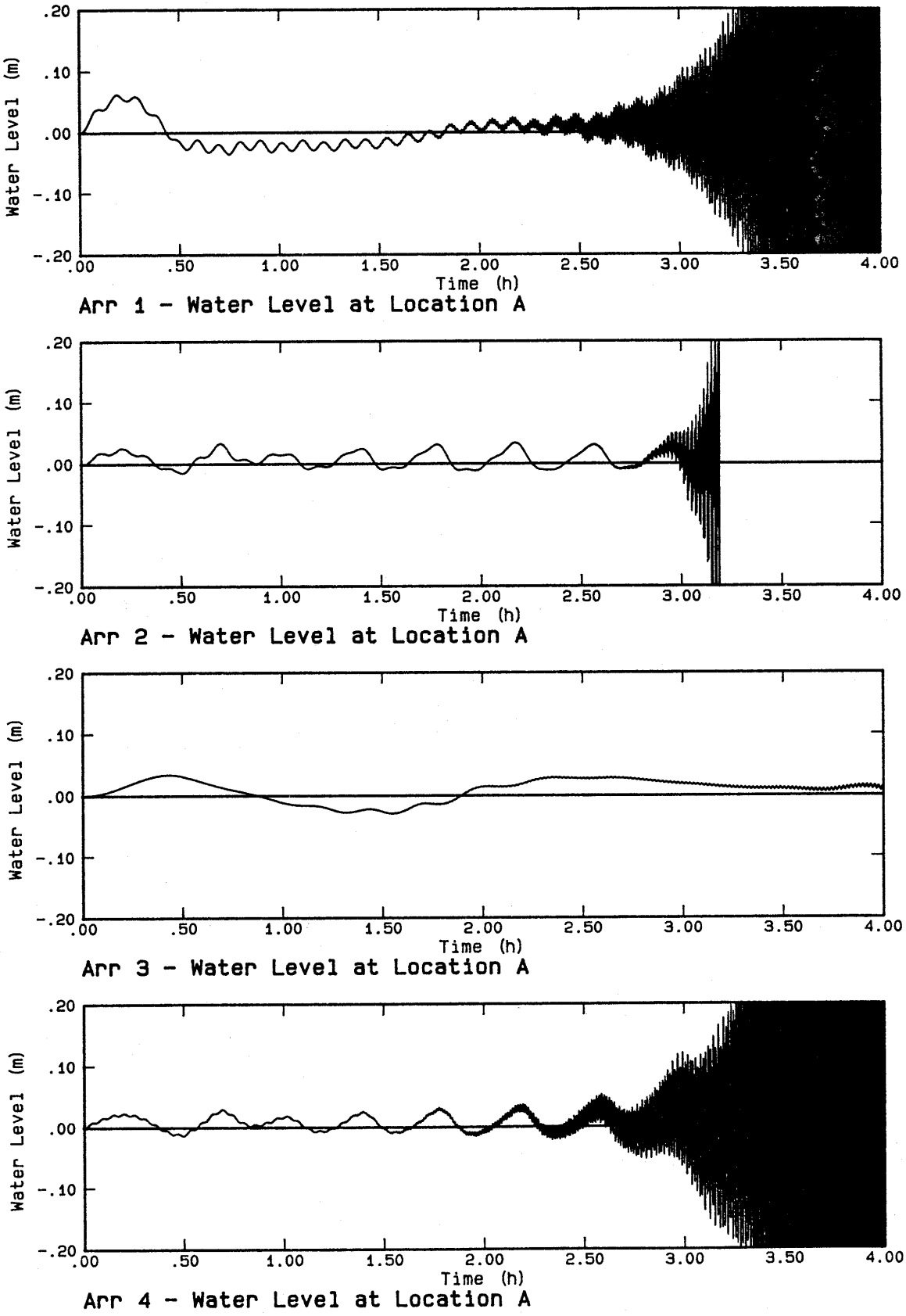


**Figure 3.11a Water Level Time Histories for Other Boundary Arrangements - Flow Past a Solid Wall**

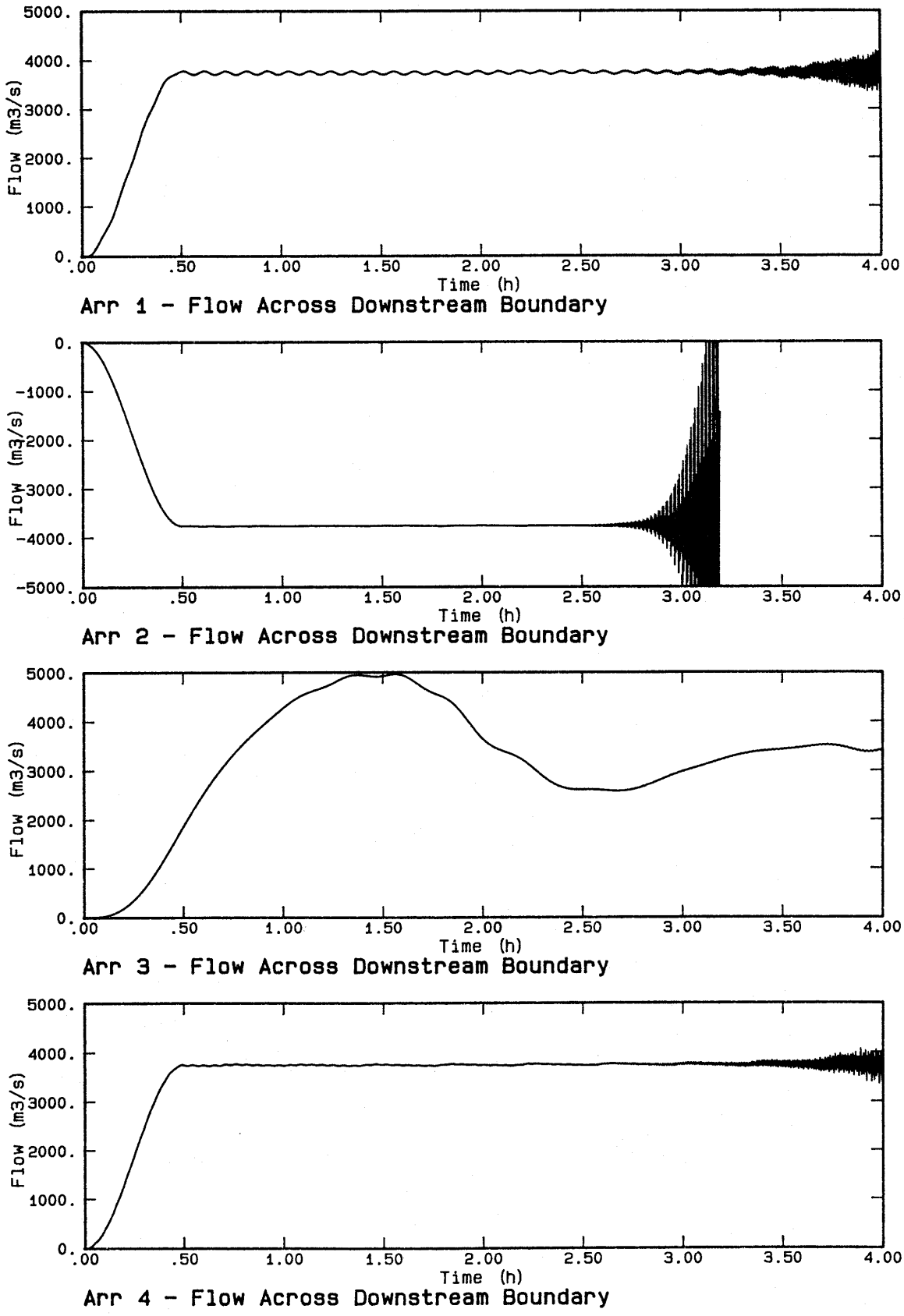


**Figure 3.11b Flow Time Histories for Other Boundary Arrangements Flow Past a Solid Wall**

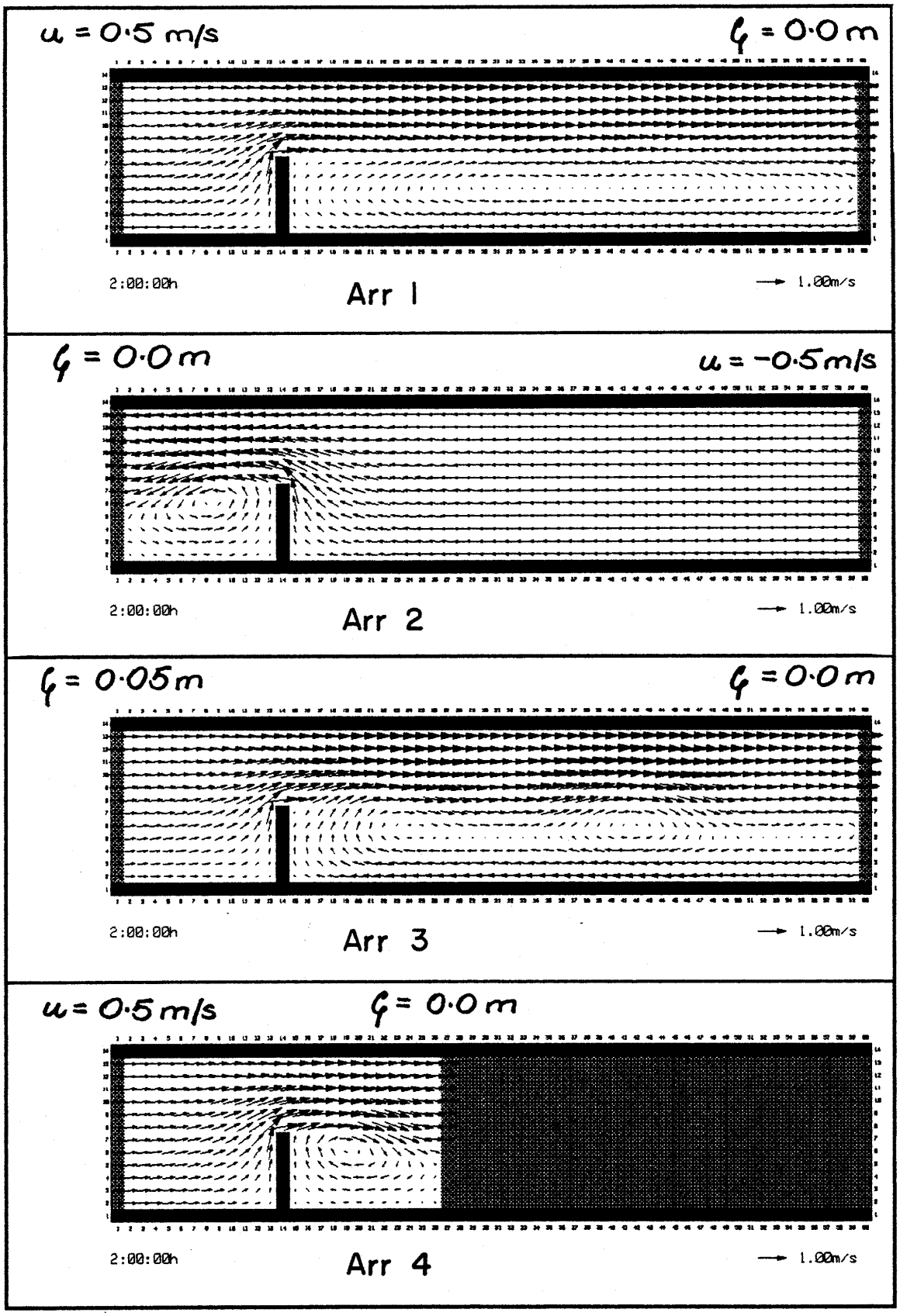


**Figure 3.11c Flow Patterns at 2 h for Other Boundary Arrangements Flow Past a Solid Wall**

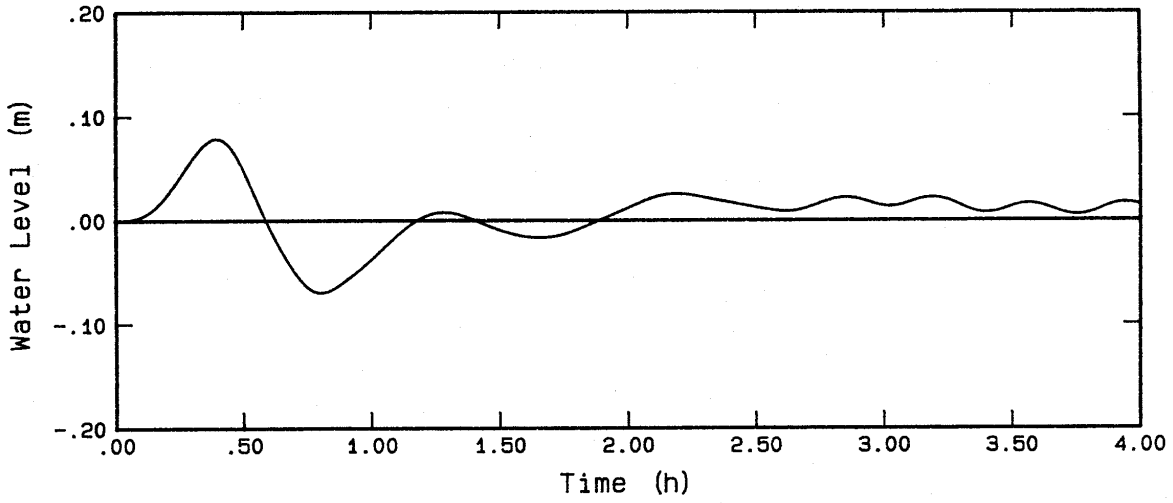


Water Level at Location A

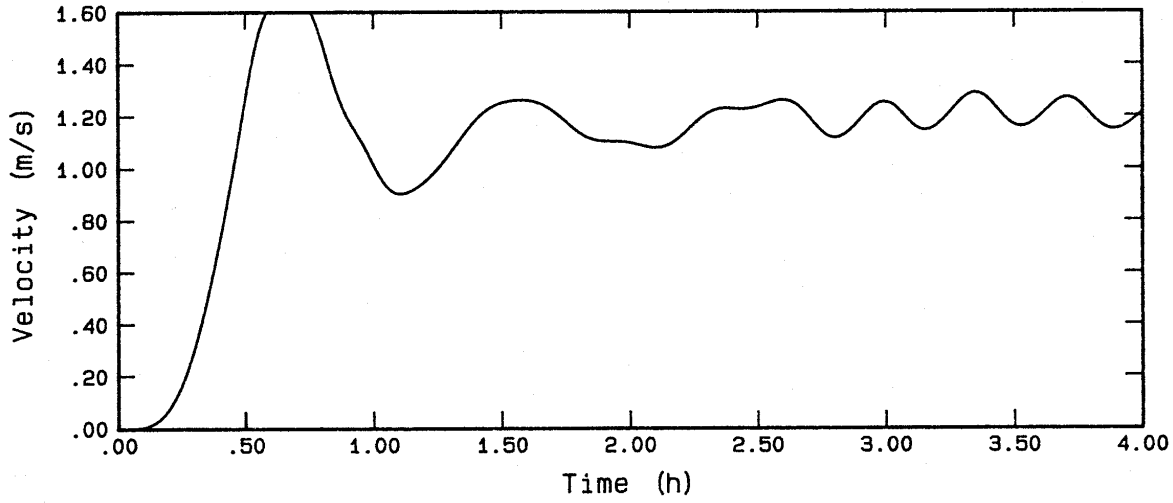


X-Velocity at Location A

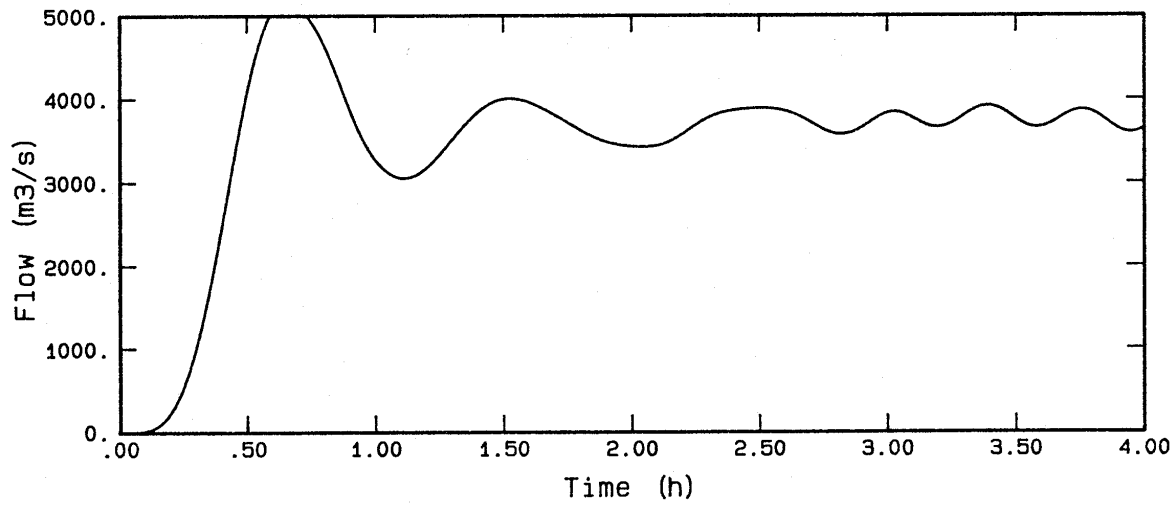


Flow Across Downstream Boundary

**Figure 3.11d Time Histories for 2-D/1-D Arrangement Flow Past a Solid Wall**

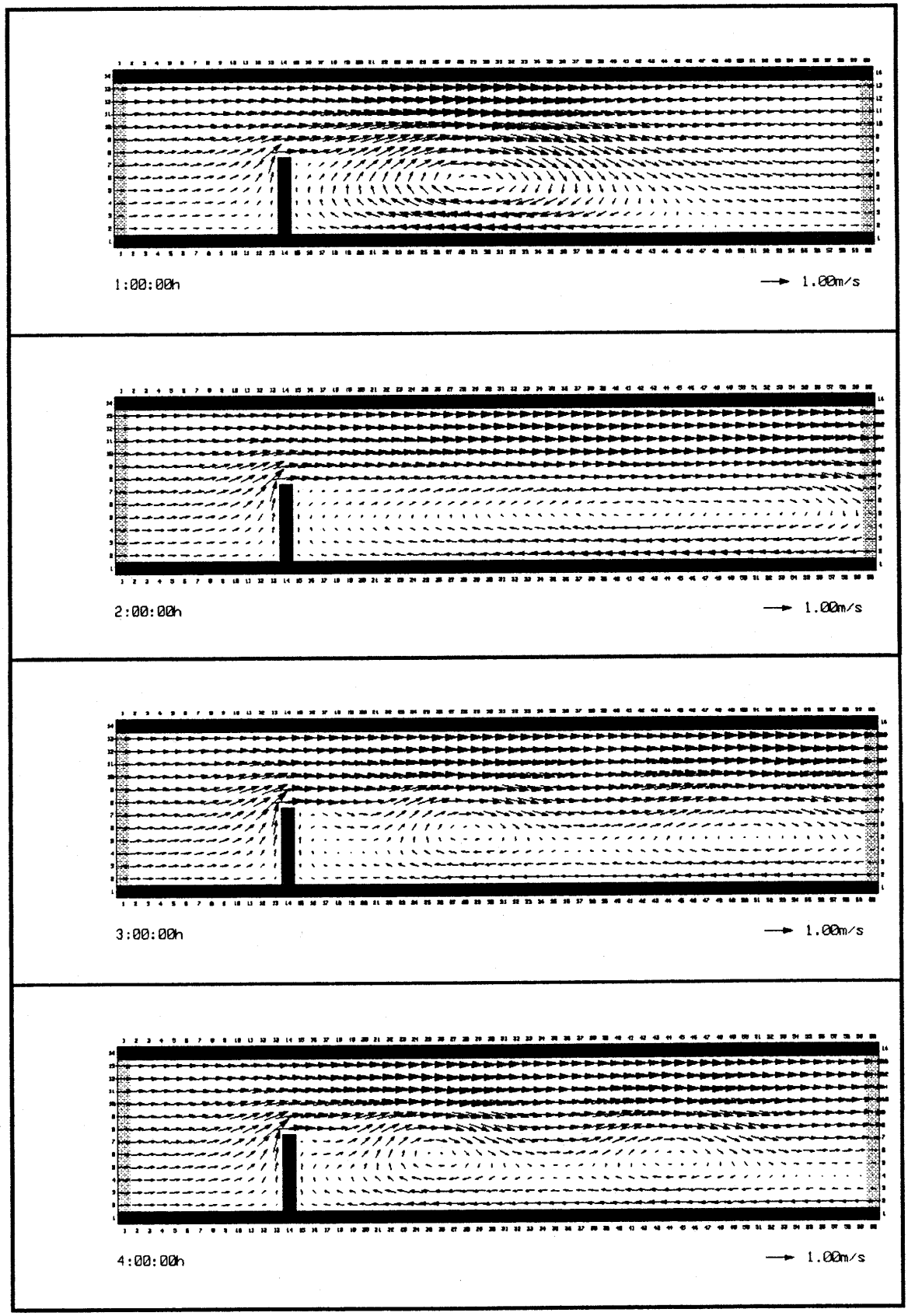


**Figure 3.11e Flow Patterns at 1, 2, 3 and 4 h for 2-D/1-D Arrangement Flow Past a Solid Wall**

## Conclusions

The conclusions which were drawn from these results are:

(i) The flow patterns were comparable with those presented in Stelling (1984), although a direct comparison can not be made because of Stelling's use of Riemann invariants. The instabilites experienced with flow boundaries also can not be confirmed for the same reason.

(ii) The length and rate of formation of an eddy was dependent on the timestep, with the larger the timestep the smaller the eddy(s).

(iii) Although steady-state boundary conditions are imposed, the simulation was a dynamic one because of the continuous process of formation and movement downstream of eddies.

(iv) Large values of the diffusion coefficient ($\mu$ > 1.0 $m^2/s$) had an acute effect on the size, intensity and rate of formation of an eddy which affected markedly the flow patterns in its vicinity.

(v) Where a velocity boundary was used, stability could only be achieved by specifying an unrealistically high diffusion coefficient ($\mu$ > 1.0 to 10 $m^2/s$).

(vi) By specifying upstream and downstream water level boundaries, much improved stability was achieved for zero diffusion, but this can be an impractical arrangement as the discharge is not defined. A solution to this problem was found by using the 2-D/1-D link, where a 1-D node with a flow boundary was attached to the upstream boundary of the 2-D model.

(vii) The location of the downstream boundary affected the size of the eddy.

### 3.4.5 S-Shaped Channel

The S-Shaped channel model described in Benque et al (1982a) was developed to illustrate the deficiencies of ADI schemes at large Courant Numbers. For this purpose alone it is an example worth reproducing here to illustrate that although a model simulation may be stable, the results can be completely erroneous.

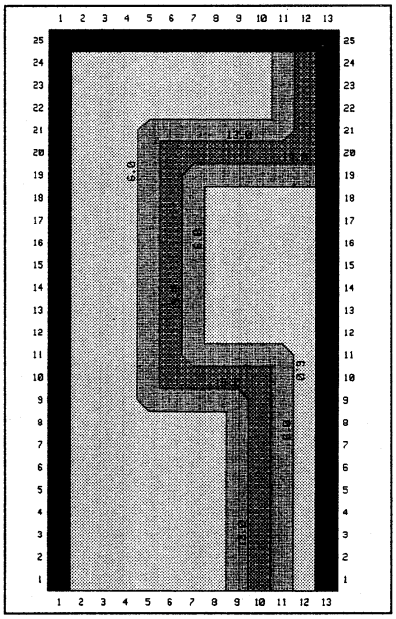

The model layout, which is detailed in Figure 3.12, depicts a 13 m deep channel passing through a 6 m deep rectangular basin. The basin is open at the bottom where a sinusoidal tide of amplitude 3 m (range 6 m) and period 12 h is defined. The element length is 300 m and diffusion was set to zero. Simulations were carried out starting at high tide for two tidal periods.

The flow patterns at mid flood tide of the second tidal period for timesteps of 300 s ($C_r$ = 16) and 1800 s ($C_r$ = 96) are presented in Figure 3.13. As can be seen, the flow patterns for the $C_r$ = 96 are clearly wrong, concluding that ADI schemes are prone to inaccuracies at high Courant Numbers.

**Figure 3.12 S-Shaped Channel Model Layout**

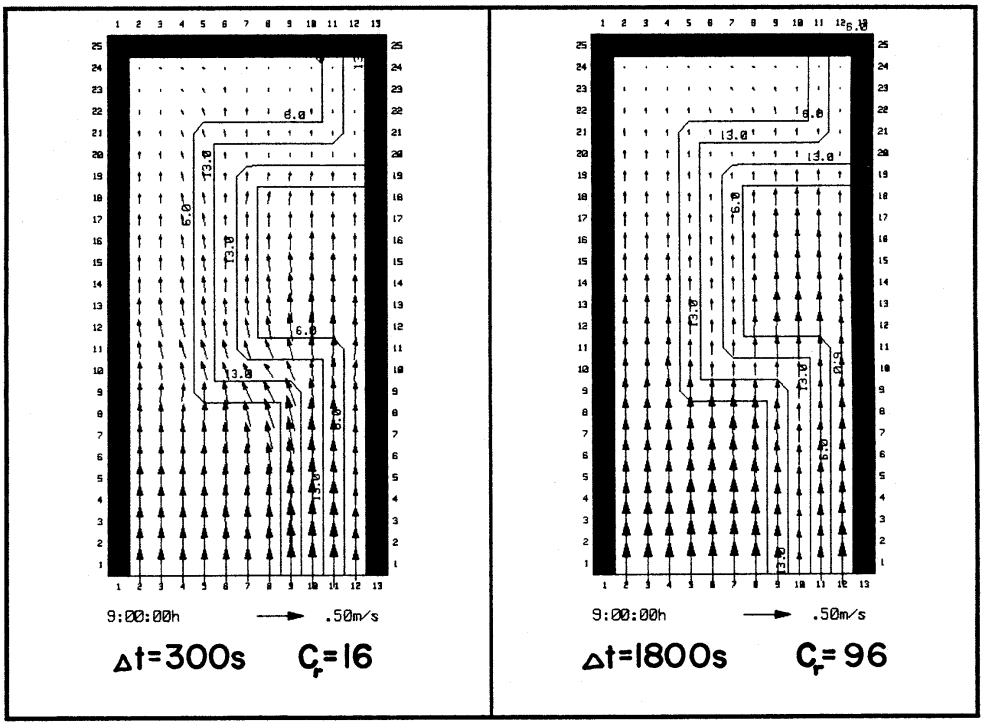


**Figure 3.13 Flow Patterns at Mid Flood Tide for $C_r$ = 16 and 96 S-Shaped Channel**

## 3.5 Wetting and Drying

### 3.5.1 General

For the practical application of the 2-D scheme which has been described, it is necessary to be able to simulate the wetting and drying of intertidal flats. The difficulties associated with this are:

(i) Spurious waves may be generated. For example, if the case of a drying tidal flat, which in reality is a relatively "smooth" process, is modelled as a series of discrete "jumps", this can cause numerical disturbances and model instabilites.

(ii) A threshold depth must be specified to indicate when an element becomes wet or dry. The lower this value can be made, the better the storage capacity of the system is modelled. This is important where a large proportion of the tidal compartment is over intertidal areas.

(iii) Checks are also required on the depth at the velocity points. This is necessary for waters draining off a perched tidal flat, otherwise negative depths at the velocity points on the edge of the flat can occur. The problem arises, however, of water becoming perched upstream of the velocity point once it has become dry.

(iv) Further to (iii), instabilities can arise where the water level gradient between the edge element and the downstream element becomes sufficiently great to cause unacceptably high velocities to be calculated.

The problems in (iii) and (iv) may be overcome by sloping artificially the bathymetry of the intertidal flats so that they drain relatively smoothly during the computations. Such practice, however, is time consuming, incorrect and sometimes not practicable.

There are numerous wetting and drying methods for ADI schemes described in the literature. Leendertse (1970), Stelling et al (1986), Falconer and Owens (1987) are examples.

In Stelling (1984), a method is proposed which incorporates a strongly dissipative solution scheme when the water depth becomes very shallow. The purpose of this was to control instabilities which occur as elements dry, thus allowing a lower threshold depth and a more correct representation of the storage capacity of the shallow areas. Stelling concludes, however, 'that for the large majority of practical applications this (the dissipative scheme) is not necessary'.

Initially a wetting and drying method similar to those discussed in the literature sources mentioned above was developed independently by the author. This is referred to as the No Free Overfall Method described below. The robustness of the method however was deficient when situations such as in Points (iii) and (iv) above were encountered. To address this the method was modified to allow for the draining of perched waters and to minimise the occurrence of high velocities. The new method, which is referred to as the Free Overfall method, originates from a similar technique used in the ESTRY program. Its implementation however was more difficult because of the implicit formulation of the 2-D scheme.

## 3.5.2 No Free Overfall Method

The No Free Overfall Method carries out a simple check on the water depth at each water level point to see if the depth has fallen below some threshold value (ie has become dry) or if the surrounding water levels have risen above the level of this threshold value (ie has become wet). Checks are also made on the water depths at the *u* and *v* points.

This method does not allow for the free overfall of perched waters to drain from one element to the next.

A grid element is flagged as wet or dry. When it is dry it is treated the same as a land element and plays no further role in the computation until it becomes wet again. The drying of elements is considered first, followed by the wetting. This order, although not important in this method, is necessary for the Free Overfall Method described next.

The procedure given below is carried out each computation step, ie. each half timestep. This causes only a minor increase in computation times as compared to checking less frequently, and gives a "smoother" wetting and drying process.

The depth at a water level point is calculated using Equation 3.5.1.

$$H_z = \frac{h_1 + h_2 + h_3 + h_4}{4} + z_0 \qquad \textbf{(3.5.1)}$$

### Drying

If the water depth at a water level point falls below the specified threshold depth (default = 0.05 m), the element is flagged as dry. Computation control flags for the surrounding four velocity points and the water level point are flagged as false or inactive. The depth of water in the element is not changed to maintain conservation of mass. This may cause the water depth to become negative in areas of rapidly changing water level, but this is not common unless a very low threshold depth is specified (< 0.001 m).

### Wetting

If an element is flagged as dry, and at least one of the four adjacent elements is both wet and has a higher water level than the sum of the element bed level plus the threshold depth, the element is re-flagged as wet.

### Velocity Points

At the completion of the above steps, an additional loop is carried out for the velocity point computation flags. The flag is set as wet if the adjoining elements are both wet and the water depth at the velocity point is greater than the specified threshold depth for velocity points (default = 0.03 m), otherwise the flag is set to dry.

### 3.5.3 Free Overfall Method

The Free Overfall Method is an extension of the No Free Overfall Method described above. It was designed to model steep water surface gradients at the edge of tidal flats where, for example, perched waters are draining into a deep channel.

The method proposes to model roughly the free overfalling effect in these situations. It is based on adjusting the water surface gradient where it exceeds a certain limit. To ensure that conservation of mass is maintained several modifications to the finite difference equations are necessary to adjust the water depth at the velocity points. The method as formulated is given below. Figure 3.14 should be referred to for part explanation of the variables.

In the equations below, a factor $f_f$, called the free overfall factor, is used. It is used to calculate the "free-overfall" depth, $H_f$, at a velocity point based on the upstream water depth, $H_{u/s}$, to determine whether to apply the modifications as described below. These variables are clearly illustrated in Figure 3.14 and defined in Equations 3.5.2 to 3.5.4.

At a velocity computation point in the Y-direction we define:

$$H_{u/s} = \max(z_0^0, z_4^0) + h_v \qquad \textbf{(3.5.2)}$$

$$H_f = f_f H_{u/s} \quad \text{where } 0 < f_f < 1 \qquad \textbf{(3.5.3)}$$

$$H_v = \frac{z_0^0 + z_4^0}{2} + h_v \qquad \textbf{(3.5.4)}$$

Prior to each stage the velocity computation flags are set true if $H_f$ is greater than the velocity point threshold depth. The following adjustments therefore only apply if the computation flag is true at the point under consideration.

For Stage 1, Step 1 of the 2-D solution scheme the water surface gradient and depth are adjusted as given in Equation 3.5.5 and illustrated in Figure 3.14.

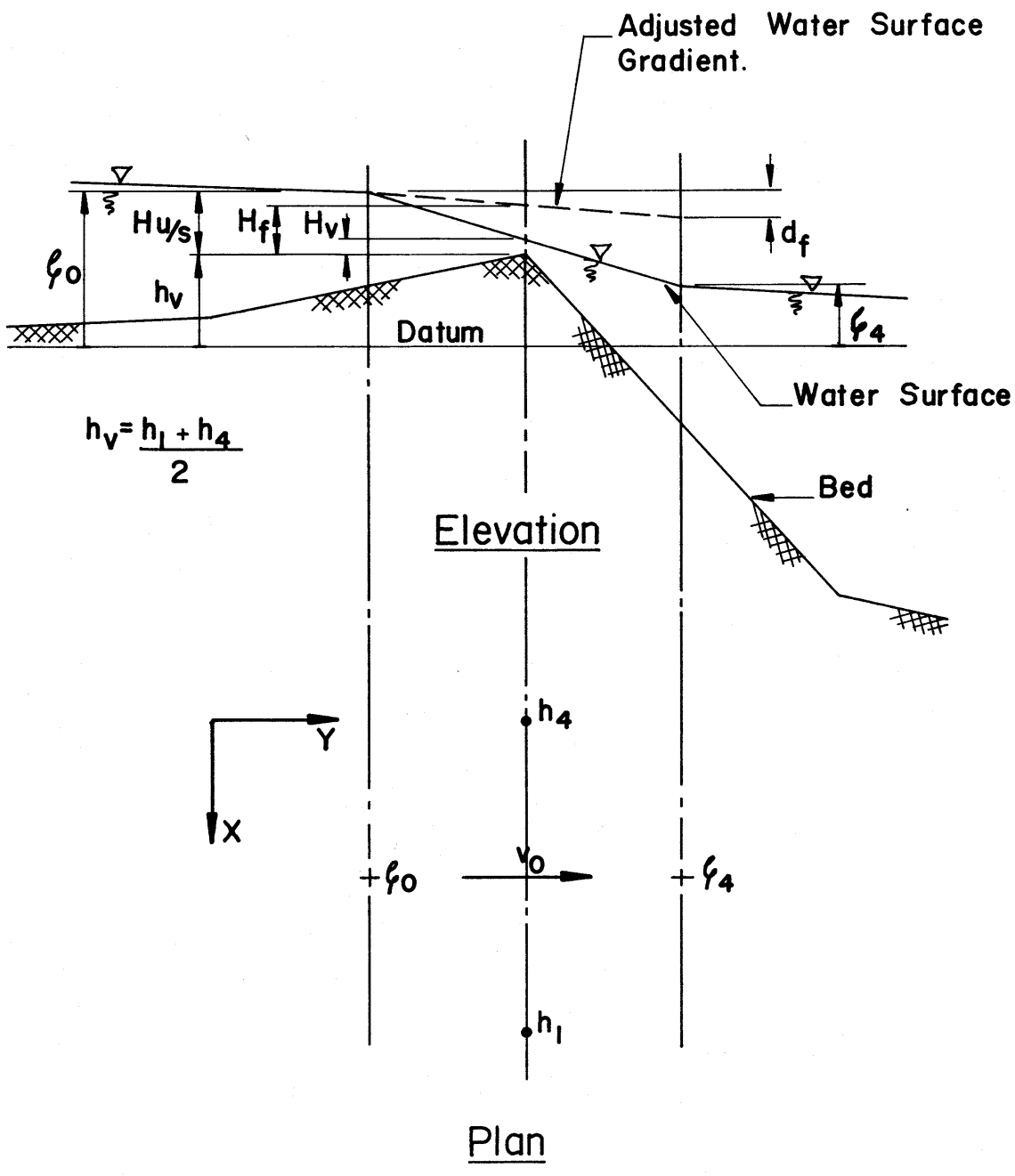


**Figure 3.14 Free Overfall Variables for a *v* Velocity Point**

$$if\ H_v < H_f \begin{cases} z_0 = z_4^0 - d_f \ \ if\ z_0^0 \le z_4^0 \\ z_4 = z_0^0 - d_f \ \ if\ z_4^0 < z_0^0 \\ where\ d_f = 2 H_{u/s} (1 - f_f) \\ and\ H_v\ is\ set\ equal\ to\ H_f \end{cases} \quad \textbf{(3.5.5)}$$

$$else \begin{cases} z_0 = z_0^0 \\ z_4 = z_4^0 \end{cases}$$

The computation continues according to Equation 3.3.2 as described in Section 3.3.2.

The modifications to Stage 1, Step 2 equations are somewhat more complex but follow a similar pattern. First the water depths used in the mass coefficient, $H_{vy}$ are checked by replacing Equation 3.3.8e with Equation 3.5.6 below.

$$H_{vy} = \frac{v_0^0 \ \max\left\{H_{v_0}, f_f \left[\max\left(z_0^0, z_4^0\right) + h_{v_0}\right]\right\} - v_2 \max\left\{H_{v_2}, f_f \left[\max\left(z_2^0, z_0^0\right) + h_{v_2}\right]\right\}}{\Delta y} \quad \textbf{(3.5.6)}$$

Secondly, prior to calculating the $E_{20}$ coefficient (Equation 3.3.9b) the upstream water depth, $H_{u/s}$, is defined by Equation 3.5.7,

$$H_{u/s} = \max(z_0, z_1) + h_u \quad \textbf{(3.5.7)}$$

and the condition given by Equation 3.5.8 is applied after computing Equation 3.3.9e.

$$H = \max(H, H_f) \quad \textbf{(3.5.8)}$$

Thirdly, the X-momentum / mass equation (Equation 3.3.7) is modified. For each water level point the following conditions at the adjacent $u_0$ point are applied.

$$if\ H < H_f \begin{cases} h_{0'} = H_f - \dfrac{z_1^{q-1} + z_0^{q-1}}{2} \\ f_0 = \dfrac{d_f}{\left| z_1^{q-1} - z_0^{q-1} \right|} \quad where\ d_f = 2 H_{u/s} (1 - f_f) \end{cases} \quad \textbf{(3.5.9)}$$

$$else \begin{cases} f_0 = 1 \ and\ h_{0'} = h_u \end{cases}$$

Values for $f_3$ and $h_3'$ at $u_3$ are determined in a similar manner.

The following modifications are then made to the $E$ coefficients in Equation 3.3.9f and to Equation 3.3.8d.

$$Define \begin{cases} E_{50} = \dfrac{h_{0'} + z_0^{q-1}}{E_{20}\Delta x} \\ \\ E_{53} = \dfrac{h_{3'} + z_0^{q-1}}{E_{23}\Delta x} \end{cases}$$

$$Re\text{-}define \begin{cases} E_{40} = f_0 E_{50} \\ \\ E_{43} = f_3 E_{53} \end{cases} \qquad \textbf{(3.5.10)}$$

$$and\ set\ \ t = \frac{2z_0^0}{\Delta t} - E_{10}E_{50} + E_{13}E_{53} - H_{vy}$$

Fourthly and finally for Stage 1, Step 2 the following conditions are applied when back substituting to calculate the $u$ values, noting that in the case of the $u$ point becoming dry on the second iteration, $u_0$ equals zero as $E_{10}$ equals zero.

$$if\ H_f \le 0 \begin{cases} z_0 = z_0^q \\ \\ z_1 = z_0 \end{cases}$$

$$else\ if\ H_u < H_f \begin{cases} z_0 = z_1^q - d_f \ and\ z_1 = z_1^q \ \ if\ z_0^q \le z_1^q \\ \\ z_1 = z_0^q - d_f \ and\ z_0 = z_0^q \ \ if\ z_0^q > z_1^q \\ \\ \qquad where\ d_f = 2H_{u/s}(1 - f_f) \end{cases}$$

$$else \begin{cases} z_0 = z_0^q \\ \\ z_1 = z_1^q \end{cases}$$

$$giving\ \ u_0^q = \frac{E_{10} - g\dfrac{(z_1 - z_0)}{\Delta x}}{E_{20}} \qquad \textbf{(3.5.11)}$$

For Stage 2 a similar approach is adopted.

The value of the free overfall factor, $f_f$, is the only parameter which needs to be specified, besides the threshold depths. The general effect of $f_f$ is the higher the value the slower the draining process. A limiting factor on the lowest value of $f_f$ can be adopted corresponding to critical flow (ie when the Froude Number is equal to unity). For general applications it is recommended that the lowest value of $f_f$ that is functional should be adopted. As a guide a value of 0.5 for element lengths greater than 200 m increasing up to 0.95 for 5 m elements is recommended.

It is important that the element where the free overfall is occurring must remain wet while the upstream element is wet, even if its own depth is below the threshold value. This allows for a cascading effect down a steep slope. Small negative depths can occasionally occur at water level points because of this, but this is acceptable as the depths at the water level points are not used for calculating the mass transfer from one element to another.

To allow negative depths at water level points was found to give better mass conservation during testing. If a negative water depth occurs a slight amount of mass is created at that time, but upon "refilling" there is an equivalent amount of mass lost. This was of particular importance in areas where the "cascading" effect occurred because some elements are constantly becoming wet and dry. If the water depth was reset to zero each time it became negative, a significant amount of mass was created.

There is always some mass created or lost because once an element became permanently dry it has a residual positive or negative water depth. Testing showed that for models with a large proportion of area which wets and drys that up to 1% of the total mass during a tidal cycle may be created or lost. Compared with the No Free Overfall Method, however, there is a greater volume of water which is active, because water can continue to drain from perched areas.

The above aspects are illustrated in the test cases described in the next section.

## 3.5.4 Test Results

### Overview

To test the method described for wetting and drying, several models were developed and tested. The main points of interest were:

(a) that the conservation of mass occurs

(b) the performance of the Free Overfall Method as compared to the No Free Overfall Method

The results of two of the most demanding models are presented below.

### Test Case 1

The model described diagrammatically in Figure 3.15 proved to be an extremely rigorous test case for the wetting and drying method. This was primarily due to the steep slope draining the waters on the higher flatter slopes.

The model represents a series of intertidal areas starting with a flat area, followed by a gently sloping section and finishing with a steeply sloping section. The area is closed along three sides and open at

the deep end to the right where a sinusoidal tide of zero mean water level, range 4 m and period 12 h was defined. An initial water level of 2.0 m was specified over the model corresponding with the top of the tide, and the initial velocities were set everywhere to zero. Each simulation was carried over several tidal cycles until periodicity was reached. The simulation results for an element length of 50 m and $f_f$ = .8 are presented below. Threshold depths for water level and velocity points were set as 0.05 m and 0.03 m.

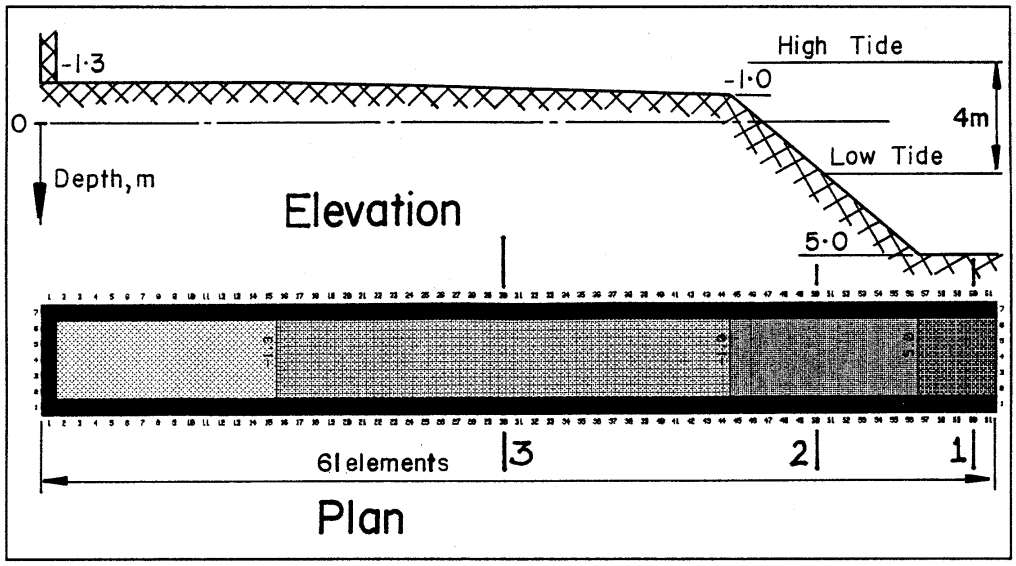


**Figure 3.15 Wetting and Drying Test Case 1 Model Layout**

The Chézy value, *C*, was re-calculated each timestep using Equation 3.5.12 with *f* equal to 0.01 m and $k_{min}$ equal to 10 ($k_{min}$ is specified to give a minimum value of *C*). Equation 3.5.12 is derived from Equations 3.5.13a to c where Equation 3.5.13a represents the average velocity along the vertical (eg. Engelund and Hansen 1972), Equation 3.5.13b is that for the friction velocity and Equation 3.5.13c is the Chézy formula. The use of Equation 3.5.12 was benefitial for models where the value of *k* varies significantly during a simulation.

$$C = 18\ \log_{10}(12\ k)\quad where\ \ k = \max\left(\frac{H}{f}, k_{\min}\right) \quad \textbf{(3.5.12)}$$

$$H = Water\ depth, m\ \ and\ \ f = Ripple\ height, m$$

$$\frac{V}{U_f} = a + 2.5\ \ln\left(\frac{H}{f}\right)\quad where\ a = 6.0\ to\ 6.4 \quad \textbf{(3.5.13a)}$$

$$U_f = \sqrt{gHI}\quad where\ I = Energy\ slope \quad \textbf{(3.5.13b)}$$

$$V = C\sqrt{H\ I} \quad \textbf{(3.5.13c)}$$

Figure 3.16a shows plots of the longitudinal water surface profiles at hourly intervals during the ebb and flood tides for the two methods, while Figure 3.16b compares the two methods at selected times. Observation of these figures shows the Free Overfall Method to provide a much better representation of the drying process

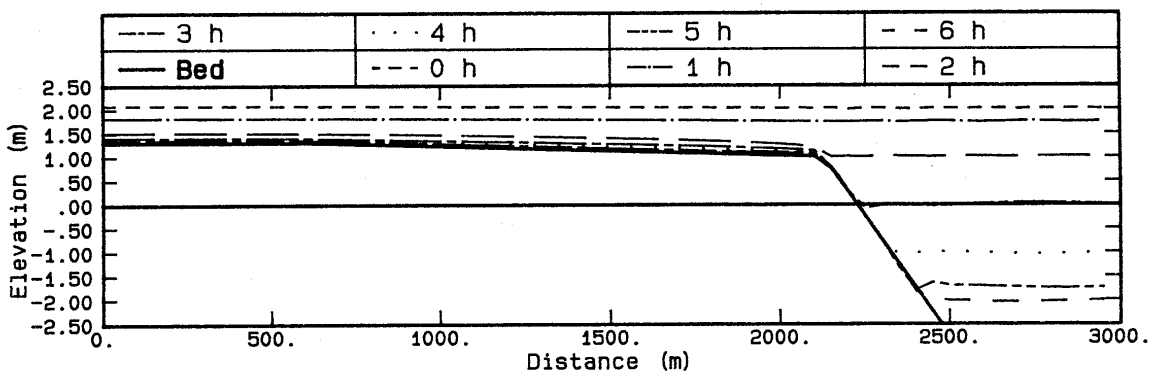


Ebb Tide Profiles - Free Overfall

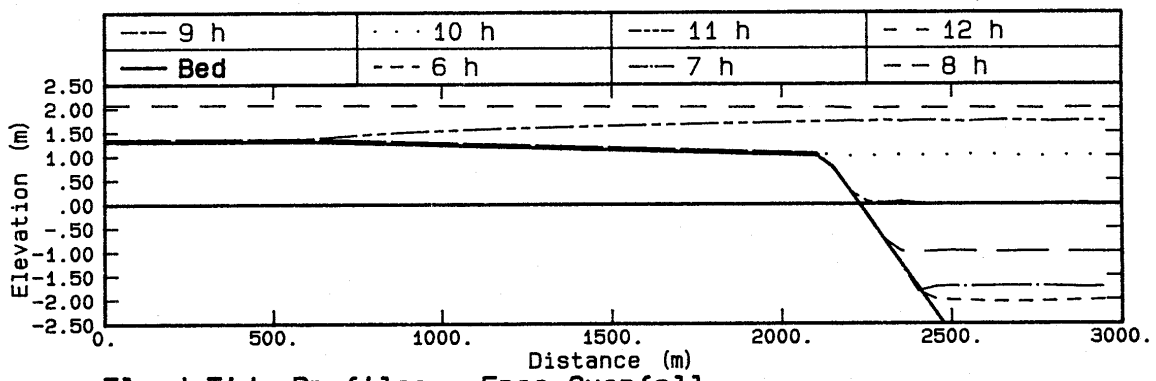


Flood Tide Profiles - Free Overfall

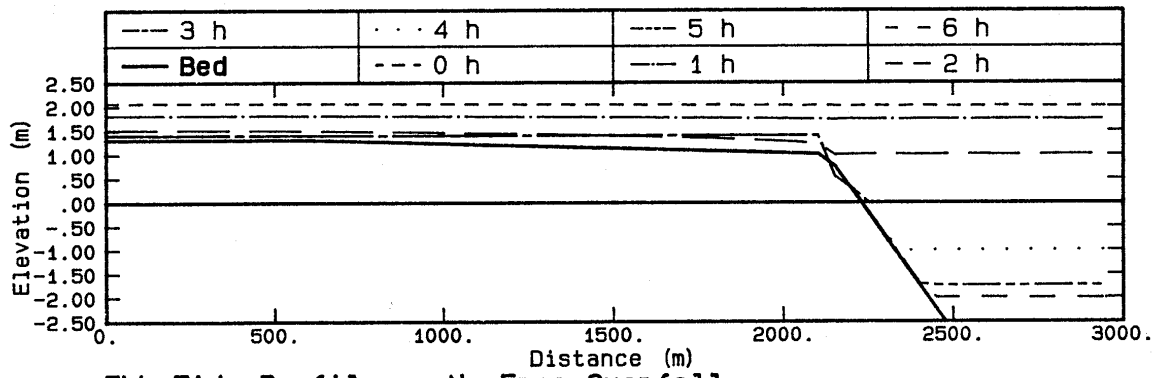


Ebb Tide Profiles - No Free Overfall

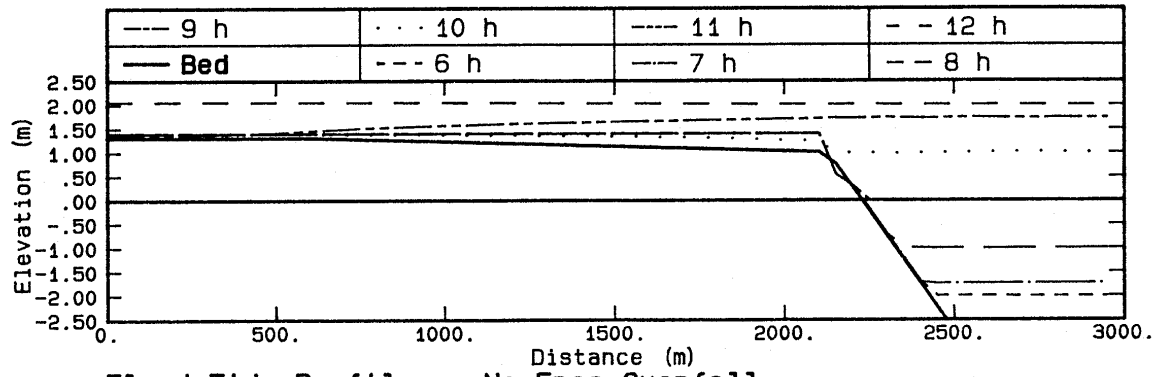


Flood Tide Profiles - No Free Overfall

**Figure 3.16a Water Level Profiles - Wetting and Drying Test Case 1**

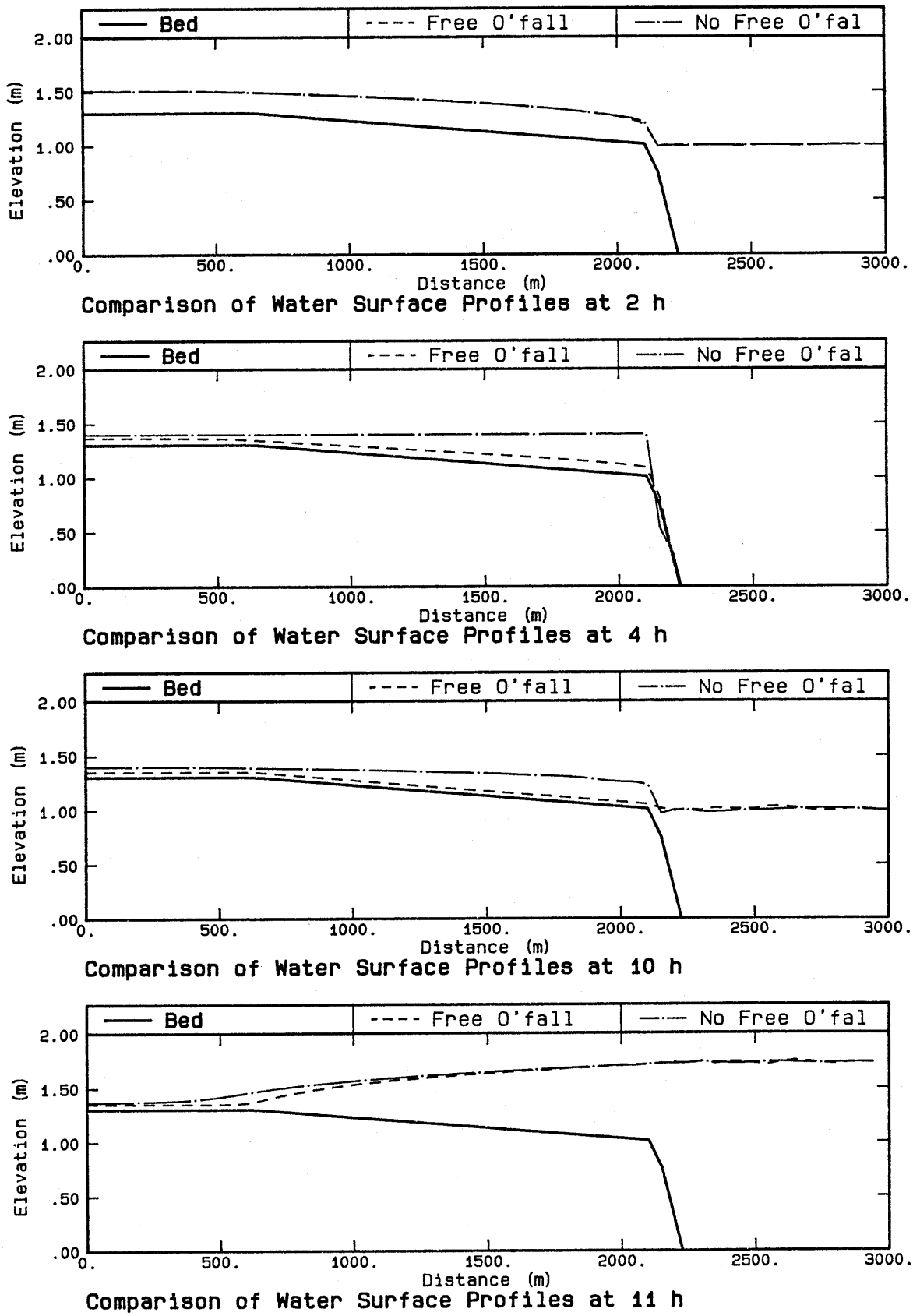


**Figure 3.16b Water Level Profiles - Comparison of Methods Wetting and Drying Test Case 1**

In the No Free Overfall case water has remained perched as the velocity point at the edge of the flatter slope has dried, preventing further draining of water. Also, the elements upstream of this point remain wet for the duration of the tidal cycle causing unnecessary computational effort. In the case of the Free Overfall Method, all of the elements on the tidal flats eventually become dry and removed from the computation until they become wet again.

During the flooding process, both methods produce similar results except at the point in the No Free Overfall simulation when the dried velocity point at the edge of the flat becomes wet and there is a surge of water against the rising tide which is clearly wrong. This is illustrated in Figure 3.16c which shows the velocity patterns for both cases at time 10 h.

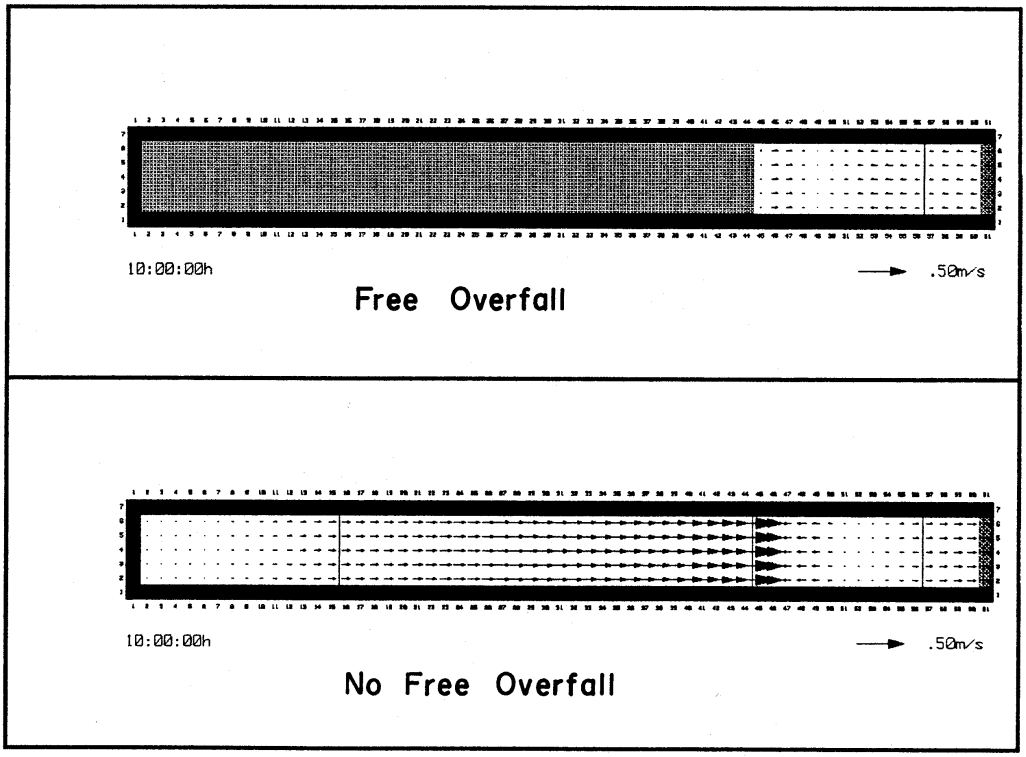


**Figure 3.16c Flow Patterns at 10 h - Comparison of Methods Wetting and Drying Test Case 1**

The conservation of mass can be seen to be maintained as shown in Figure 3.16d which shows the integral of flow over time across Lines 1, 2 and 3 (Figure 3.15) for both methods. The peaks of these plots have been reproduced on a finer scale in Figure 3.16c. Assuming pure periodicity has been reached, detailed examination of the last tidal cycle (-6 h to 6 h) showed that for across Line 1, the No Free Overflow method lost mass on the ebb tide (or gained on the flood tide) at a rate of 0.0 % of the total tidal prism per tidal cycle, while the Free Overfall method the value was 0.7 %. For Lines 2 and 3, the corresponding values were 0.0 % and -0.1 % for No Free Overfall, and 0.5 % and -0.1 % for Free Overfall. These results illustrate the high performance of both methods with regard to mass conservation, especially given the large fraction of intertidal area in the model.

Comparison of the integral flow plots (Figure 3.16d) also illustrates that a greater volume of water is being exchanged each tidal cycle for the Free Overfall case as would be expected in reality. This is an important aspect where the intertidal flats contribute significantly to the storage capacity of a model.

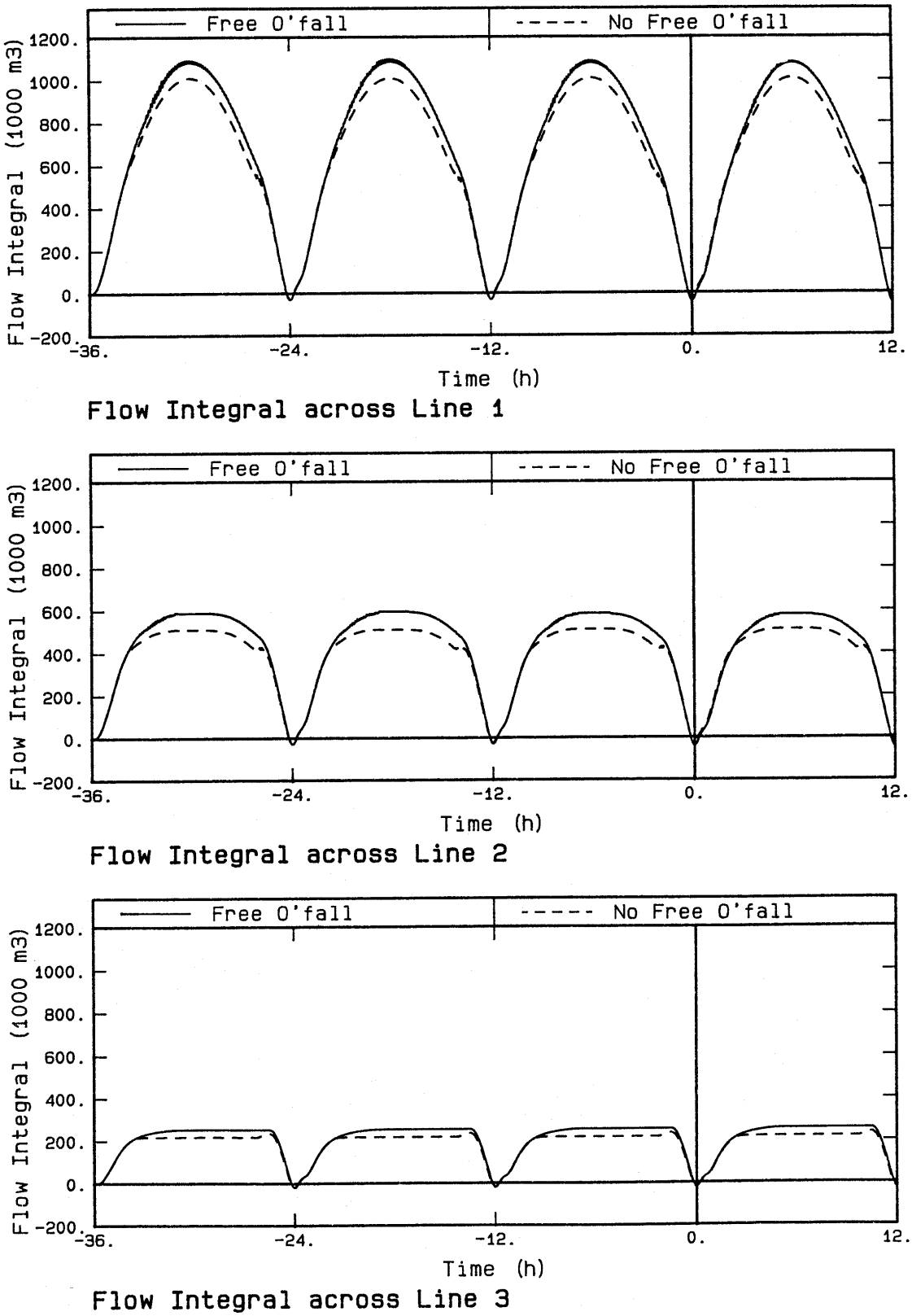


**Figure 3.16d Integral Flow Time Histories - Comparison of Methods Wetting and Drying Test Case 1**

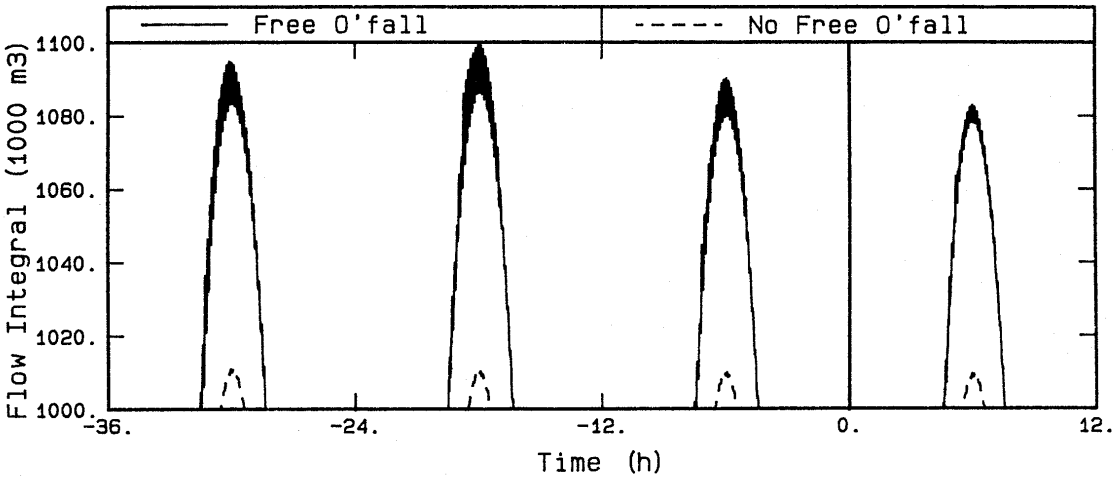


Flow Integral across Line 1

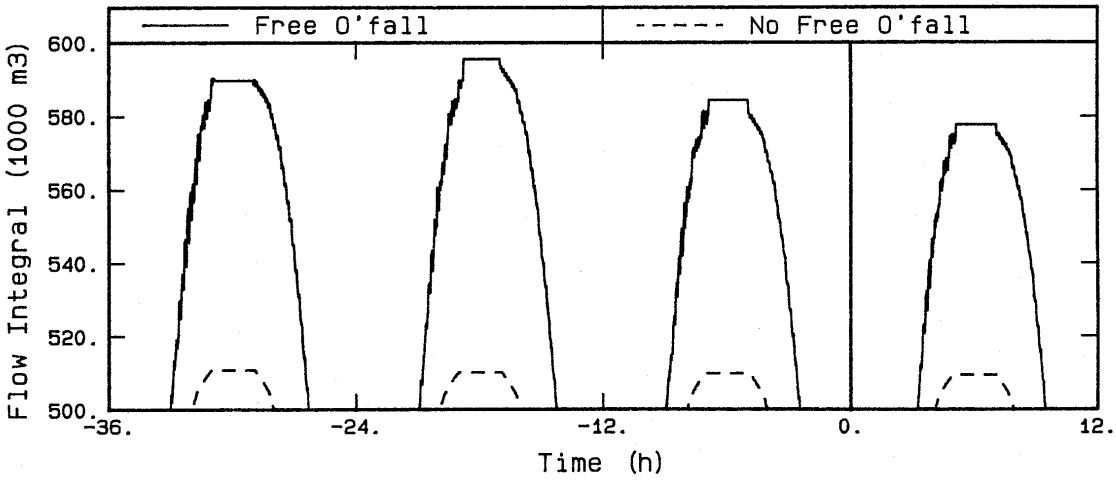


Flow Integral across Line 2

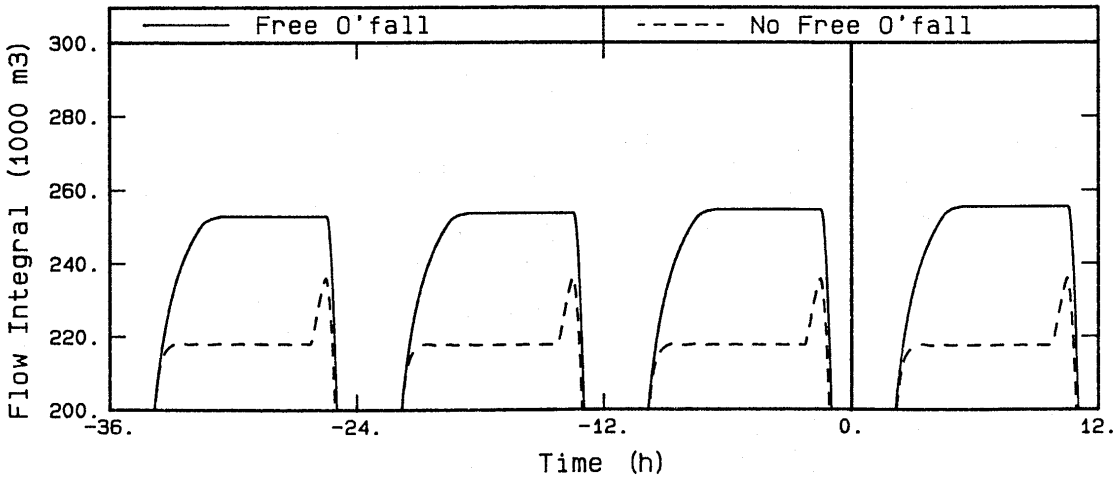


Flow Integral across Line 3

**Figure 3.16e Integral Flow (Fine Scale) Time Histories Comparison of Methods - Wetting and Drying Test Case 1**

## Test Case 2

The test model illustrated in Figure 3.17 was developed by the author to test three situations where wetting and drying can occur:

(a) a tidal flat - represented by the horizontal flat at elevation 0.0 m in the centre of the model,

(b) at velocity points - represented by the "weirs" with crest levels of 0.0 m, at the bottom centre, and connecting the tidal flat with the open boundary,

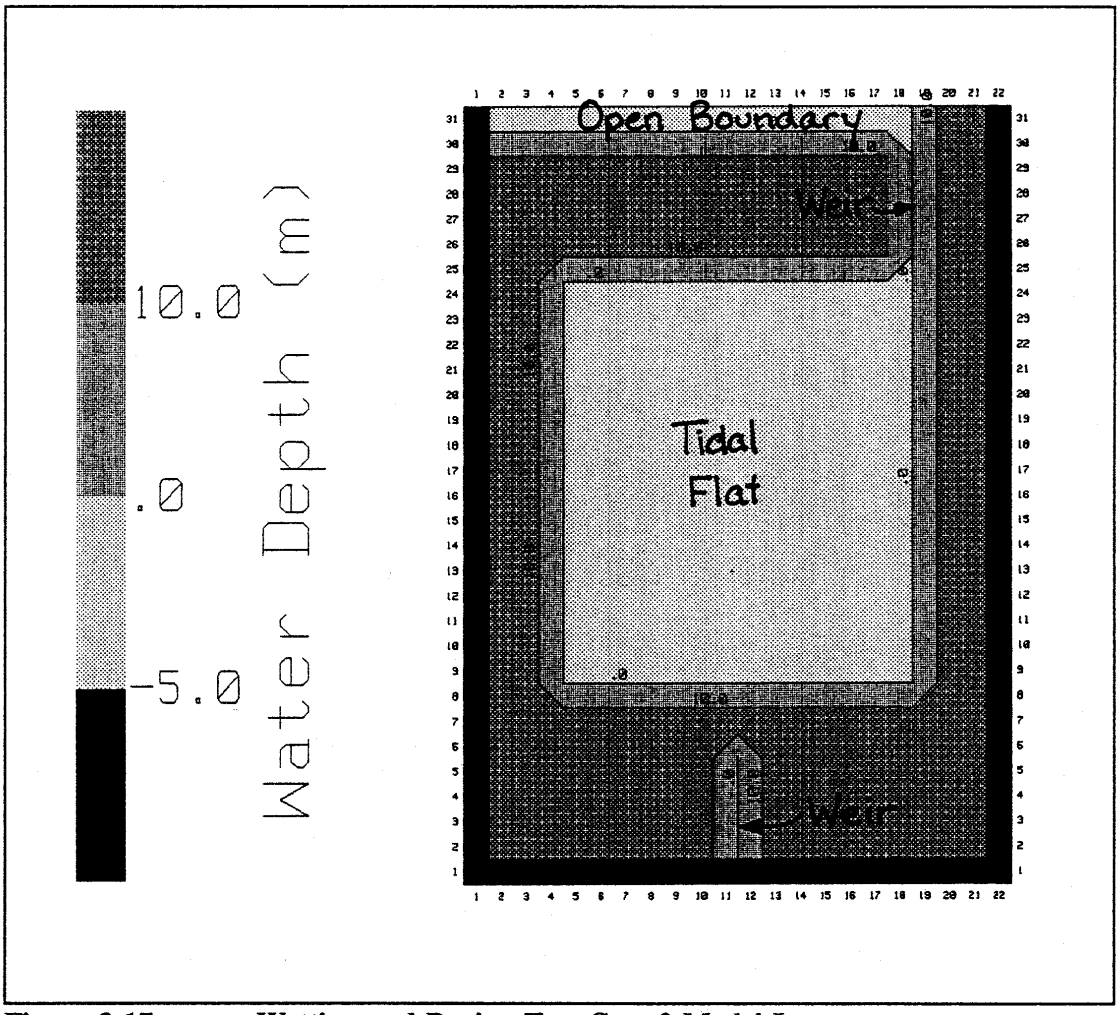


**Figure 3.17 Wetting and Drying Test Case 2 Model Layout**

(c) at an open boundary - represented by the section at level 0.0 m along the open boundary at the top of the model.

Simulations with a sinusoidal tide of range 4 m and period 12 h, were performed with using the No Free Overfall and Free Overfall methods. The simulation started at peak high tide and extended for three tidal cycles so that periodicity was achieved. The initial water levels were set equal to the open boundary high tide level, and the initial velocities to zero.

Figures 3.18a to d show the flow patterns at times 1, 3, 5, 7, 8, 8½, 9 and 10 h (0 h = high tide, 6 h = low tide). The results using the Free Overfall method are given on the left, and the No Free Overfall on the right.

As can be seen the Free Overfall method allows the tidal flat to fully dry while the No Free Overfall method keeps water perched and unable to drain. In both methods the velocity points over the "weirs" can be observed to be inactive during the lower half of the tide, and the open boundary can be seen to dry and wet with the falling and rising tide. Examination of flow integral plots at several locations showed similar mass conservation properties as described in Test Case 1.

Figure 3.19 shows colour contoured water level plots on the left at times 3½ and 10 h for the Free Overfall method and the difference in water levels between the two methods on the right (red representing a higher water level for the No Free Overfall simulation). Observation of these plots shows water levels to be higher by up to 0.1 m difference for the No Free Overfall case.

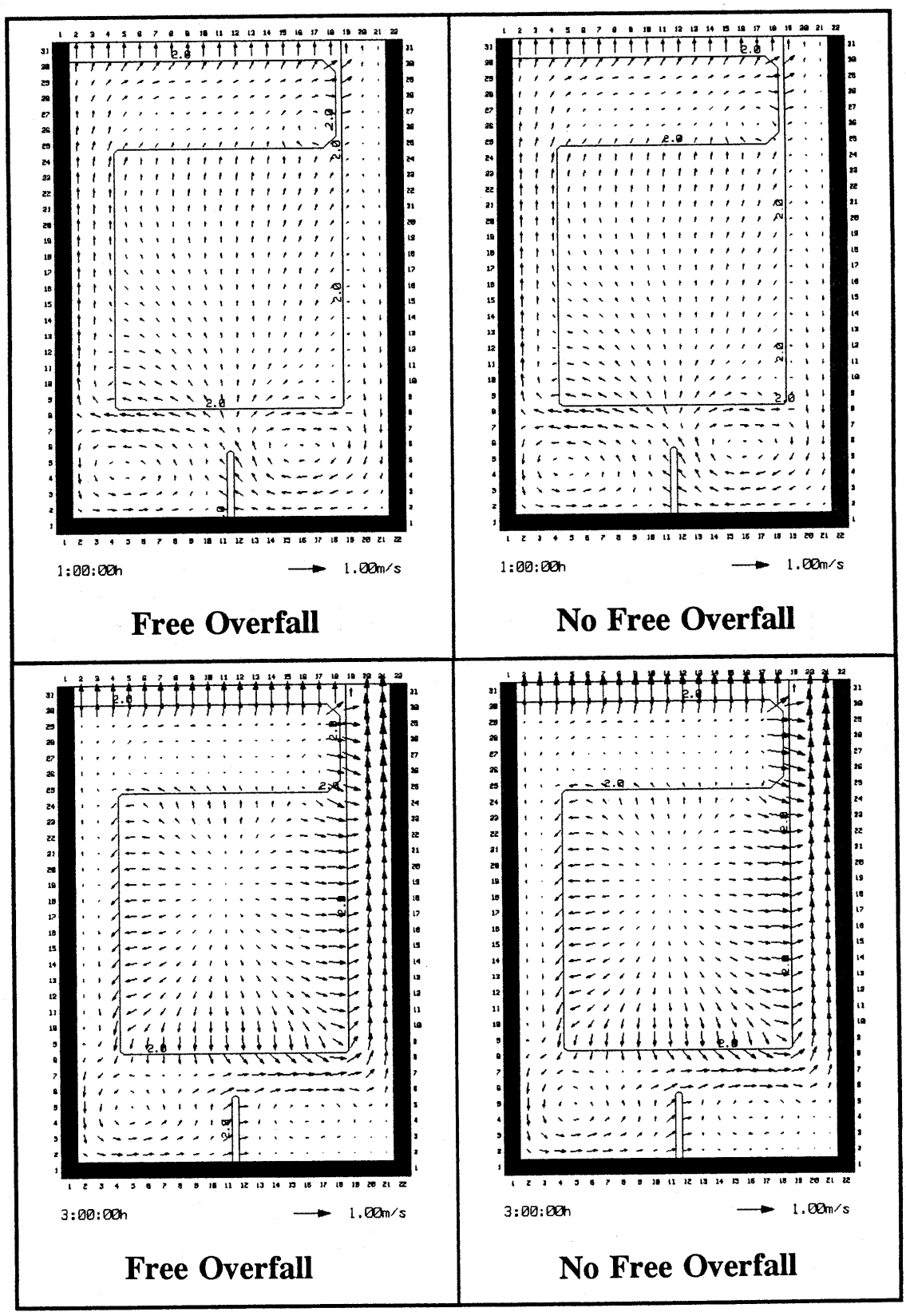


**Figure 3.18a Flow Patterns at 1 h and 3 h - Comparison of Methods Wetting and Drying Test Case 2**

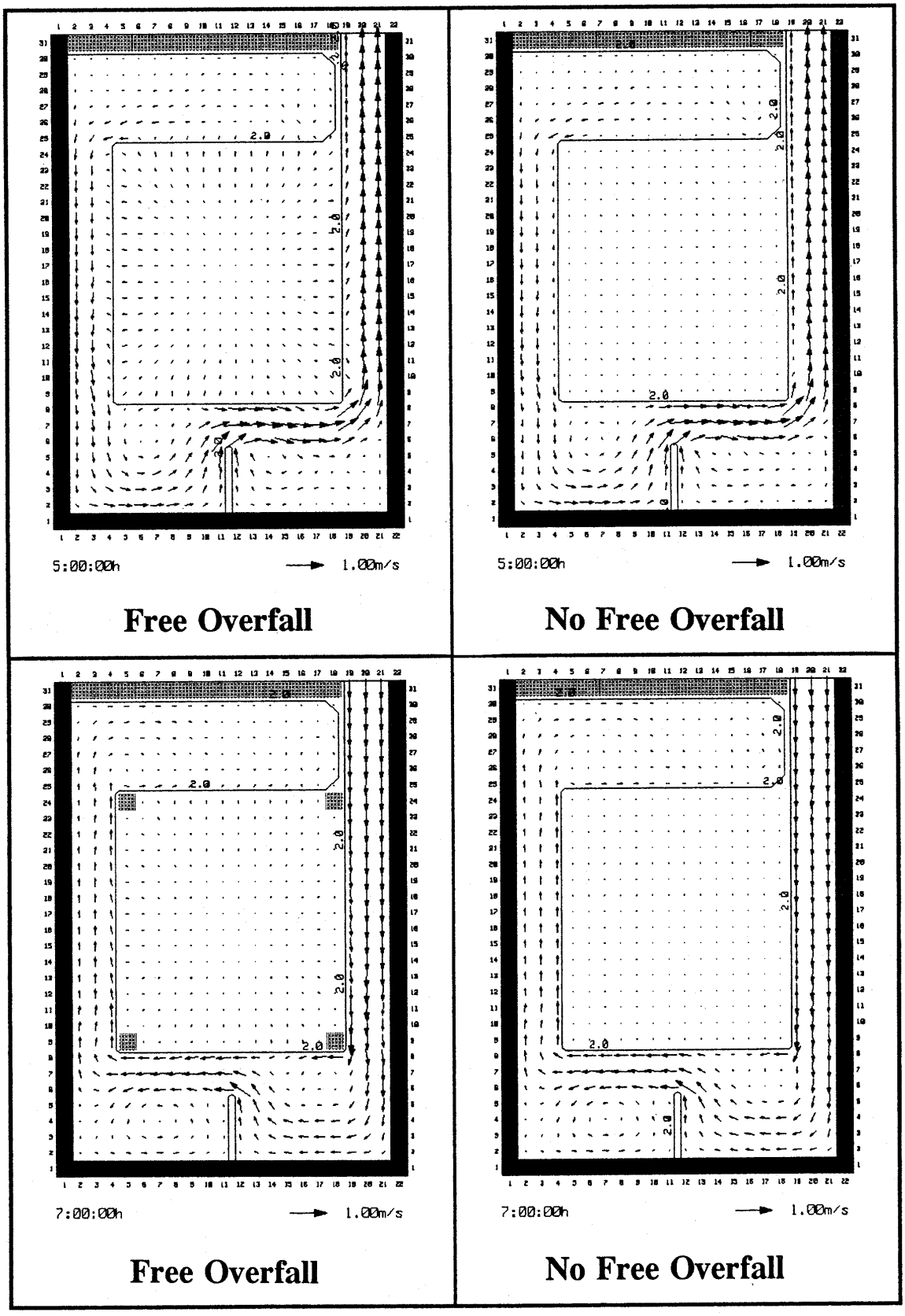


**Figure 3.18b Flow Patterns at 5 h and 7 h - Comparison of Methods Wetting and Drying Test Case 2**

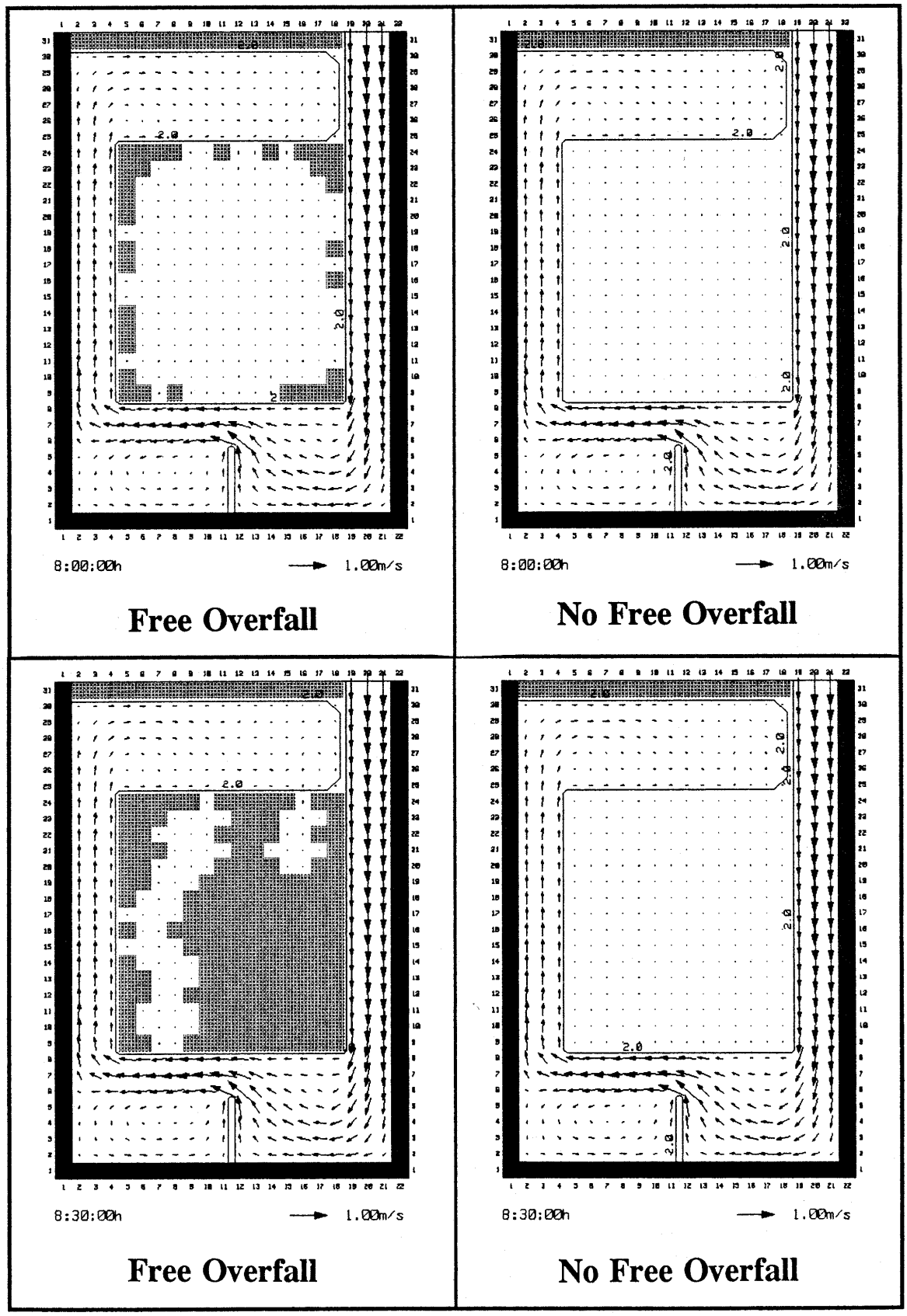


**Figure 3.18c Flow Patterns at 8 h and 8½ h - Comparison of Methods Wetting and Drying Test Case 2**

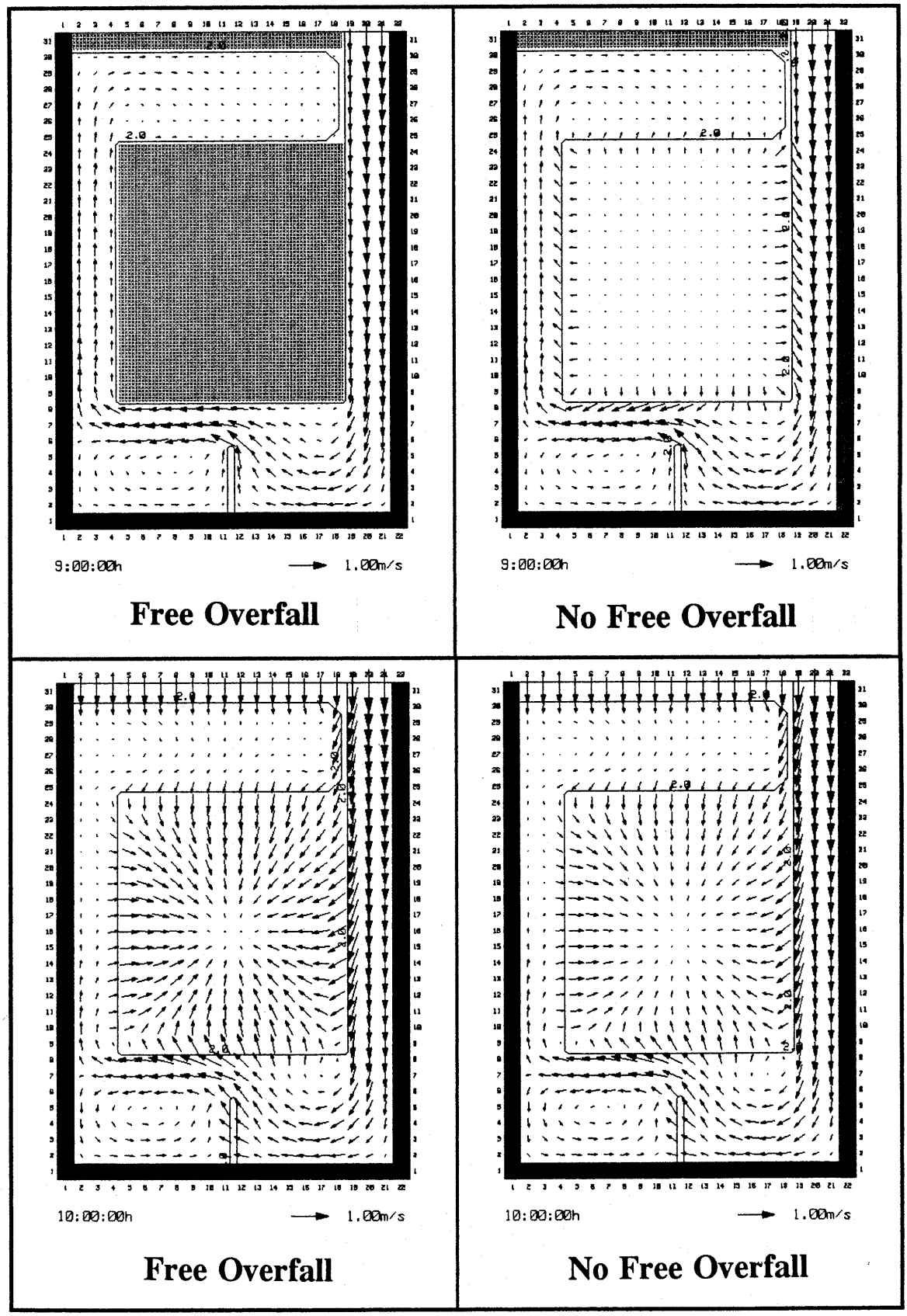


**Figure 3.18d Flow Patterns at 9 h and 10 h - Comparison of Methods Wetting and Drying Test Case 2**

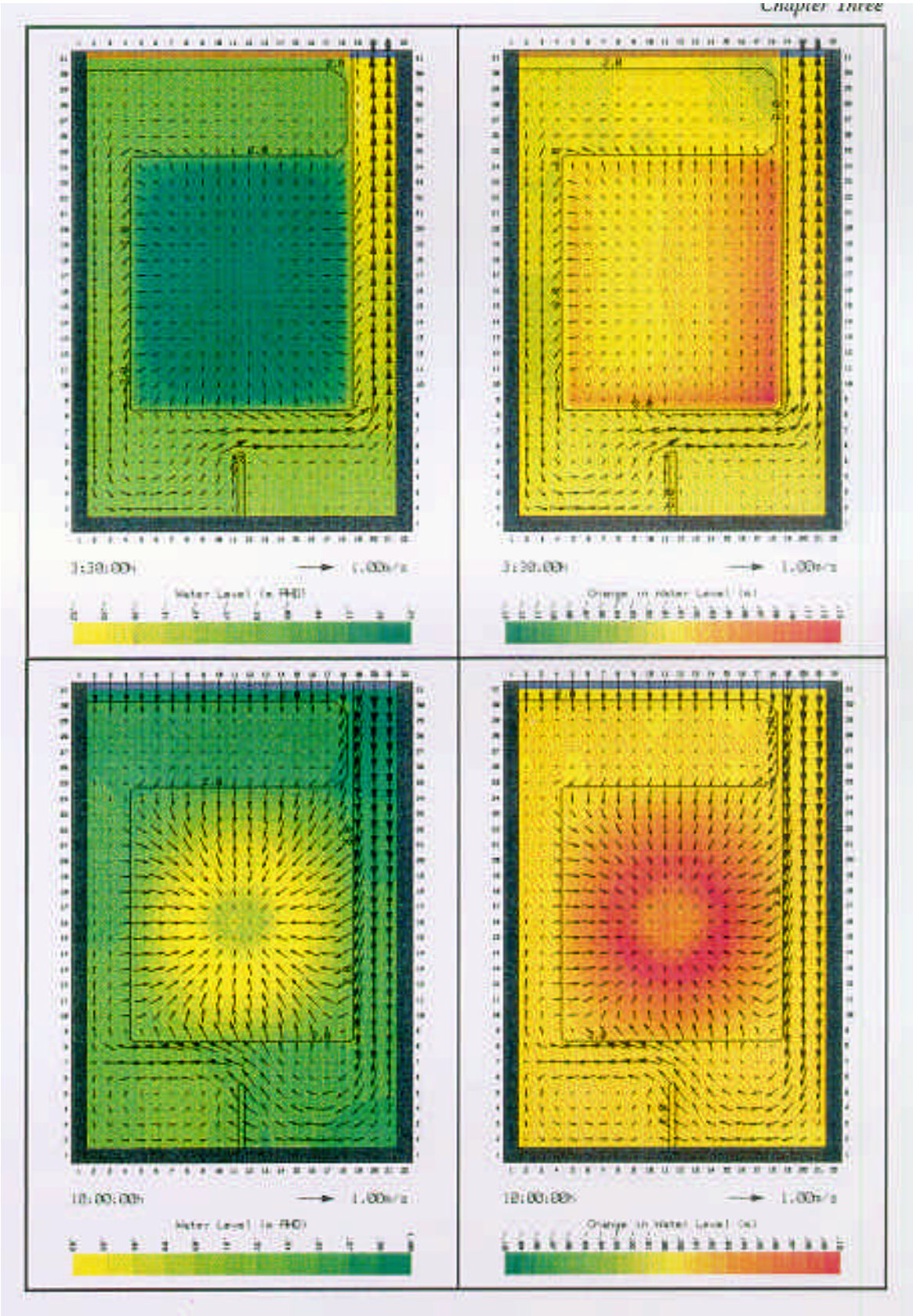

**Figure 3.19 Water Level Contours at 3½ and 10 h Comparison of Methods - Wetting and Drying Test Case 2**

# 4 TWO DIMENSIONAL/ONE DIMENSIONAL DYNAMIC LINK

## 4.1 Summary

Research and development of the 2-D/1-D dynamic interface was carried out once the 2-D scheme was operating successfully. The general objective was to develop an algorithm which was accurate, versatile and robust. With this in mind the following assumptions and guidelines were adopted.

(i) Mass must not be dissipated or created as it is transferred across the 2-D/1-D interface.

(ii) The importance of the advection terms across the interface is negligible, therefore only a mass transfer is required. This assumption is already implied in the boundary conditions of the 2-D scheme.

(iii) For use in practice it was preferred that there would be no restriction on the number of 1-D models that can be linked to a 2-D model.

(iv) Water level boundaries are preferred for the open boundaries of the 2-D scheme as discussed in Chapter Three.

The method developed for linking dynamically 1-D models onto a 2-D model is very simple, yet robust, stable and accurate. It uses a water level boundary for the 2-D model and a flow boundary for the 1-D model. Each half timestep, the 2-D model "feeds" the 1-D model a flow based on the velocity distribution across the interface, and the 1-D model "feeds" the 2-D model a water level. This arrangement makes use of the stability properties of 2-D water level boundaries and also defines the mass transfer into and out of the 2-D model.

An adjustment of the 1-D model water level by a dynamic head is necessary as the 1-D scheme calculates a static water level while the 2-D scheme computes the actual water level. The adjustment recommended is based on the average dynamic head along the 2-D model interface of the previous half timestep. Testing showed that adjustment of the 1-D model water level for each 2-D element along a boundary, is prone to instabilities, because of the non-horizontal water level distribution. It also conflicts with the 2-D scheme boundary condition of no flow between boundary elements.

Testing of the proposed method has shown mass to be conserved in all cases, excellent stability characteristics, and good results for the velocity distribution in the 2-D model at the interface. Close examination of simulation results showed mass conservation to be 100%.

The combined coding of ESTRY and the 2-D program described in Chapter 3 was codenamed TUFLOW. It is designed for both entirely 2-D models and linked 2-D/1-D models. A 2-D model can be linked to any number of 1-D models. Combining computer codes required only one common subroutine, because the two solution schemes were essentially kept autonomous.

In practice, the orientation of 2-D/1-D interfaces rarely all lie parallel to the axes of the 2-D grid. To have maximum flexibility in locating the interfaces, it was necessary to be able to (a) correctly

compute the flow in a 2-D model across an oblique line, and (b) assess the stability properties and accuracy of water level boundaries along an oblique line.

A method for the computation of the flow is detailed and shown to be theoretically correct. For oblique water level boundaries, a problem occurs in that the water level boundary values are offset from the oblique line because they are located at fixed points on the 2-D grid. This gives localised variations in water surface gradients which cause instabilities and flow concentrations. This problem did not arise where the boundary line lies at 45° to the grid axes as the water surface points lie directly on the line.

To overcome this problem two methods are proposed. They both use a weighting factor to adjust the water level boundary value. The weighting factor is calculated using the length of the offset of the boundary point from the oblique line. The first method developed does this implicitly by modification of the finite difference equations of Section 3.3. The second method explicitly adjusts the boundary water levels prior to the next computation step based on the water surface gradient of the previous half timestep. The results of a test case are presented to illustrate their performances. The first method has produced the best results both in testing and practical application, and is that which is recommended.

## 4.2 Description of Method

### 4.2.1 Boundary Definition

The types of open boundaries of a hydrodynamic model are either (a) a water level boundary, or (b) a flow boundary. A flow being either a velocity or a discharge. The boundaries, which are represented numerically as time histories of water levels and/or flows, are normally defined prior to the simulation.

In the case of the 2-D/1-D interface, the type of open boundaries for both the 2-D and 1-D models must be specified and must be dynamic as they cannot be defined prior to the simulation. Regarding the type of boundaries, clearly there are four possible combinations of which two can be eliminated.

The four combinations are:

(i) 2-D Water Level / 1-D Water Level

(ii) 2-D Flow / 1-D Flow

(iii) 2-D Water Level / 1-D Flow

(iv) 2-D Flow / 1-D Water Level

Combination (i) can be rejected as the water level at the interface would remain fixed at its initial value. For example, the 2-D model feeds the 1-D model a water level at the interface. The 1-D computations are completed, and the 1-D model feeds the 2-D model the same water level. The calculations would continue with no change in water level, and no definition of the mass transfer across the interface.

Combination (ii) can also be rejected based on a similar argument to that of Combination (i) above.

Both Combinations (iii) and (iv) define both the water level and the flow at the interface. In either case, the water levels at the boundaries would be free to adjust dynamically, and the mass transfer across the interface would be defined.

Combination (iii) has two advantages over (iv), namely:

(a) The flow distribution across the interface in the 2-D model does not have to be defined.

(b) For the adopted 2-D scheme (refer to Chapter Three), water level boundaries were far superior in performance compared to flow boundaries.

The 2-D water level / 1-D flow combination was therefore selected as the preferred option.

### 4.2.2 Methodology

During each computation timestep, it is necessary for both the 1-D and 2-D models to provide the other with boundary values at the interface. For the adopted 2-D water level / 1-D flow combination, this requires that the 1-D model provides the 2-D model with a water level prior to each computation step of the 2-D scheme. Similarly, the flow across the interface based on the velocities calculated in the 2-D model needs to be transferred to the 1-D model before each computation step of the 1-D scheme.

Conveniently, both the 1-D and 2-D schemes use computational schemes which have two (2) stages, each being one half of a timestep in duration. Thus, both models can be run using the same timestep with boundary values at the dynamic interface being transferred every half timestep.

If the schemes differred in the number of computation stages each timestep, this would not be a restriction on the 2-D/1-D dynamic interface. In such a situation the 1-D and 2-D models would use different timesteps, rather than extrapolate boundary values. For example, if the 2-D scheme has two half timestep stages and the 1-D model has one, then the timestep for the 1-D model would be equal to half the timestep of the 2-D model.

For each timestep there are eight consecutive steps (Figure 4.0):

Step 1: Compute Stage 1 of the 2-D scheme. The water level boundary values at the 2-D/1-D interface are based on that from Step 8 of the previous timestep.

Step 2: Calculate the discharge leaving / entering the 2-D model across the 2-D/1-D interface (see Section 4.4.2) and transfer to 1-D scheme.

Step 3: Compute Stage 1 of the 1-D scheme. The flow boundary value at the 2-D/1-D interface is set equal to the discharge calculated in Step 2.

Step 4: Transfer the water level at the 2-D/1-D interface computed in the previous step to the 2-D scheme. An adjustment of the water level by a dynamic head is made as discussed in Section 4.2.3.

Step 5: As for Step 1 but for Stage 2 of the 2-D scheme.

Step 6: As for Step 2.

Step 7: As for Step 3 but for Stage 2 of the 1-D scheme.

Step 8: As for Step 4.

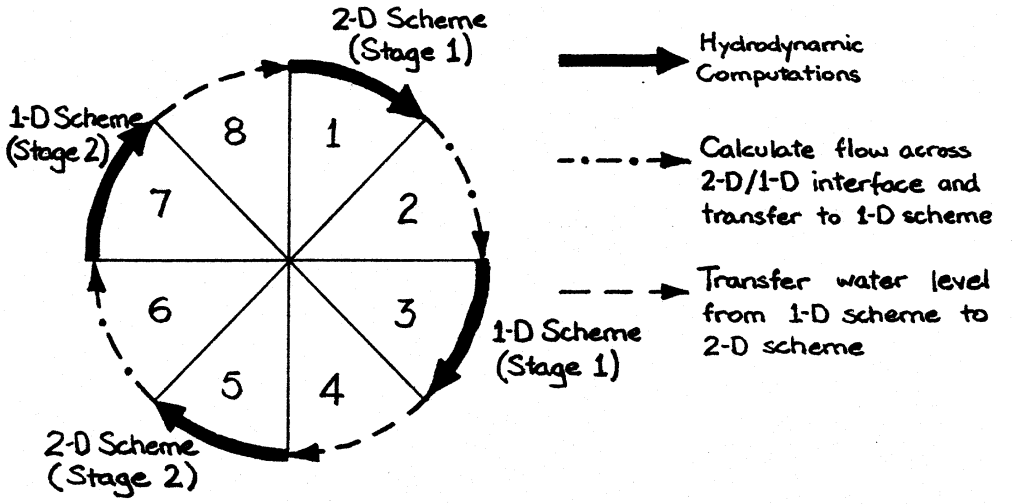


**Figure 4.0 Computation Cycle for 2-D/1-D Link over One Timestep**

### 4.2.3 Water Levels of 1-D & 2-D Models

An adjustment of the water level which is computed in the 1-D model and passed as a boundary value to the 2-D model is required. This is necessary as the 1-D scheme calculates static water levels, while the 2-D scheme computes actual water levels. The static water level is equal to the actual water level plus the dynamic head as given by Equation 4.2.1.

$$z_s = z_a + \frac{V^2}{2g} \qquad \textbf{(4.2.4)}$$

*where*

$z_s$ *is the static water level*

$z_a$ *is the actual water level*

This incompatibility was accounted for by adjusting the water level of the 1-D model by the dynamic head calculated using the velocities in the 2-D model of the previous half-timestep. Initially, the water level was adjusted at each 2-D grid element across the interface. Testing showed that where the velocity distribution varied significantly across the interface, the differences in water level (due to the variation in dynamic head) was prone to cause instabilities.

This problem was found to be overcome best by averaging the dynamic head of the 2-D elements across the interface and adjusting the 1-D water level by this average. Testing showed that this procedure has no stability problems. This also complies with the 2-D water level boundary conditions which specifies no flow between adjoining boundary elements, ie. a horizontal water surface is assumed along the boundary.

## 4.3 Validation and Testing

### 4.3.1 Summary

The 2-D/1-D dynamic link was subjected to validation testing using a similar approach to that for the 2-D scheme (Section 3.4). The primary objectives of the tests were to establish the performance of the 2-D/1-D link to transfer and conserve mass, and to establish stability characteristics.

A variety of both steady state and dynamic flow test models was developed. In each test scenario, a fully 1-D or a fully 2-D model was developed first. A section of this model was then replaced by a 2-D or a 1-D model to give a linked 2-D/1-D model. The linked model was simulated and the results were compared with and assessed against those for the fully 1-D or 2-D model.

The results of both a uniform flow and a dynamic flow test case are presented and discussed in the following two sections.

The results from the testing demonstrated that the 2-D/1-D link was accurate, conserved mass 100% (based on calculations) and imposed no stability constraints.

### 4.3.2 Uniform Flow

Two models were developed to represent a rectangular channel of 2000 m in length, bed slope 0.05 m/km, and Manning's n friction coefficient of 0.03. The first model was fully 1-D, while the second model was a 2-D/1-D linked model. In the 2-D/1-D model, the 2-D section replaces Channels 3, 4, 5, and 6 of the fully 1-D model as illustrated in Figure 4.1.

The fully 1-D model consists of 10 channels all of length 200 m, and 11 storage nodes. The channel beds were sloped from 9.9 m below datum at Node 1 to 10.0 m below at Node 11. The 2-D section of the 2-D/1-D model has an element length of 10 m and a bed sloping from 9.92 m to 9.96 m below datum from its upstream to downstream end.

To maintain compatibility between the two models, the wetted perimeters of the 1-D channels were set equal to the flow width, and a Chézy coefficient of 48.927 was specified for the 2-D section of the 2-D/1-D model.

A constant inflow of 1094 $m^3/s$ was defined at Node 1 based on a 10 m deep uniform flow, and a constant water surface elevation of zero was specified for Node 11. The initial water levels and velocities were everywhere set to zero. The drop in water level over the length of each model should therefore be 0.1 m, while the velocity should be constant at 1.094 m/s. Each simulation was warmed-up using an entry time constant of 0.5 h for the upstream boundary inflow. The simulations were run using a timestep of 5 s ($C_r$ = 7).

The results of the two simulations are presented in Figures 4.2a to c. Figure 4.2a shows the flow time histories calculated across Lines 1, 2, 3 and 4 for both models, while Figure 4.2b depicts the velocity time histories. The Y-axis scale of the plots in these figures has been enlarged to more clearly show the steady state values. As can be seen, the flow of 1094 $m^3/s$ is maintained throughout each model clearly showing that mass is being conserved 100% across the 2-D/1-D interface.

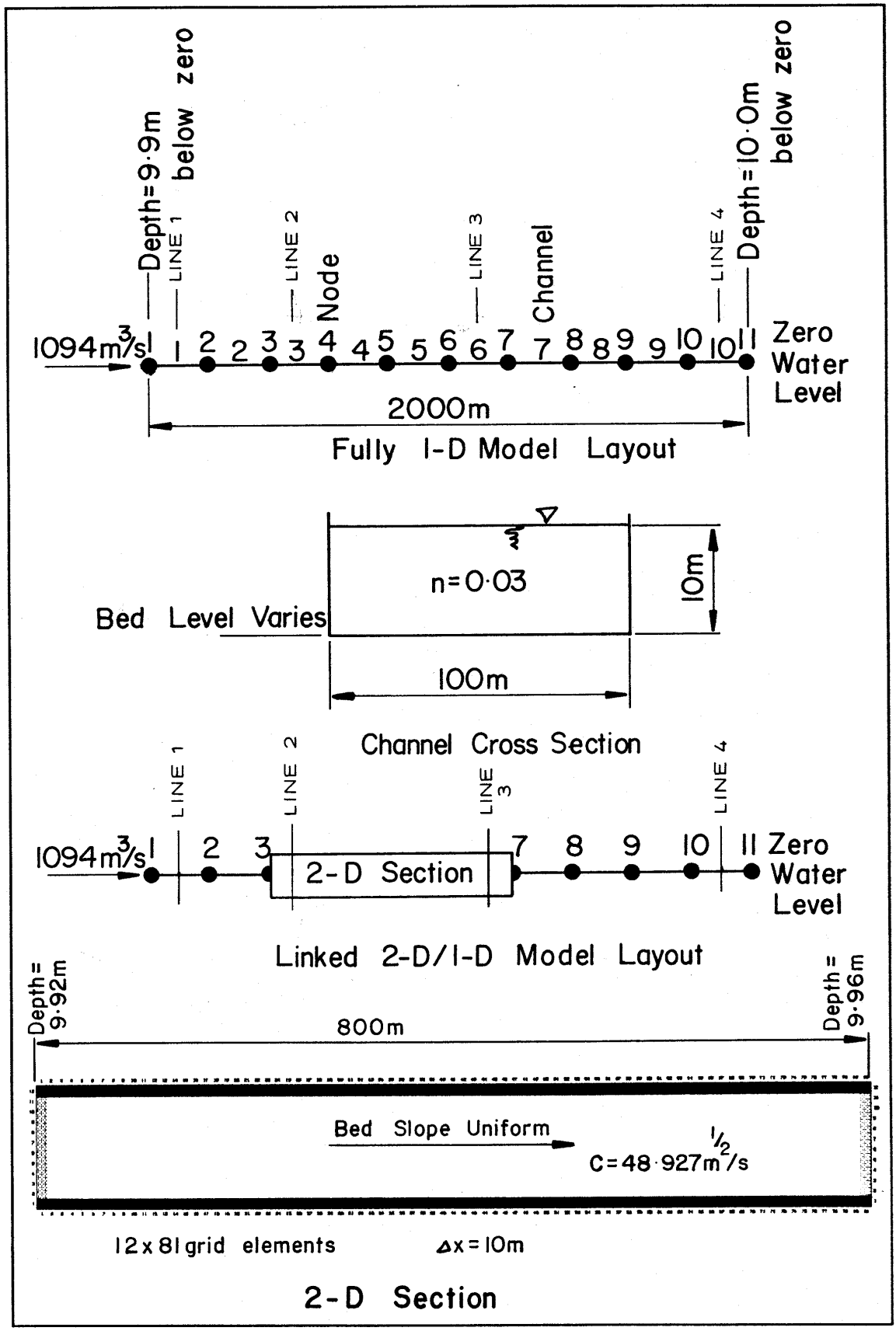


**Figure 4.1 Uniform Flow Test Model Layouts for 2-D/1-D Link**

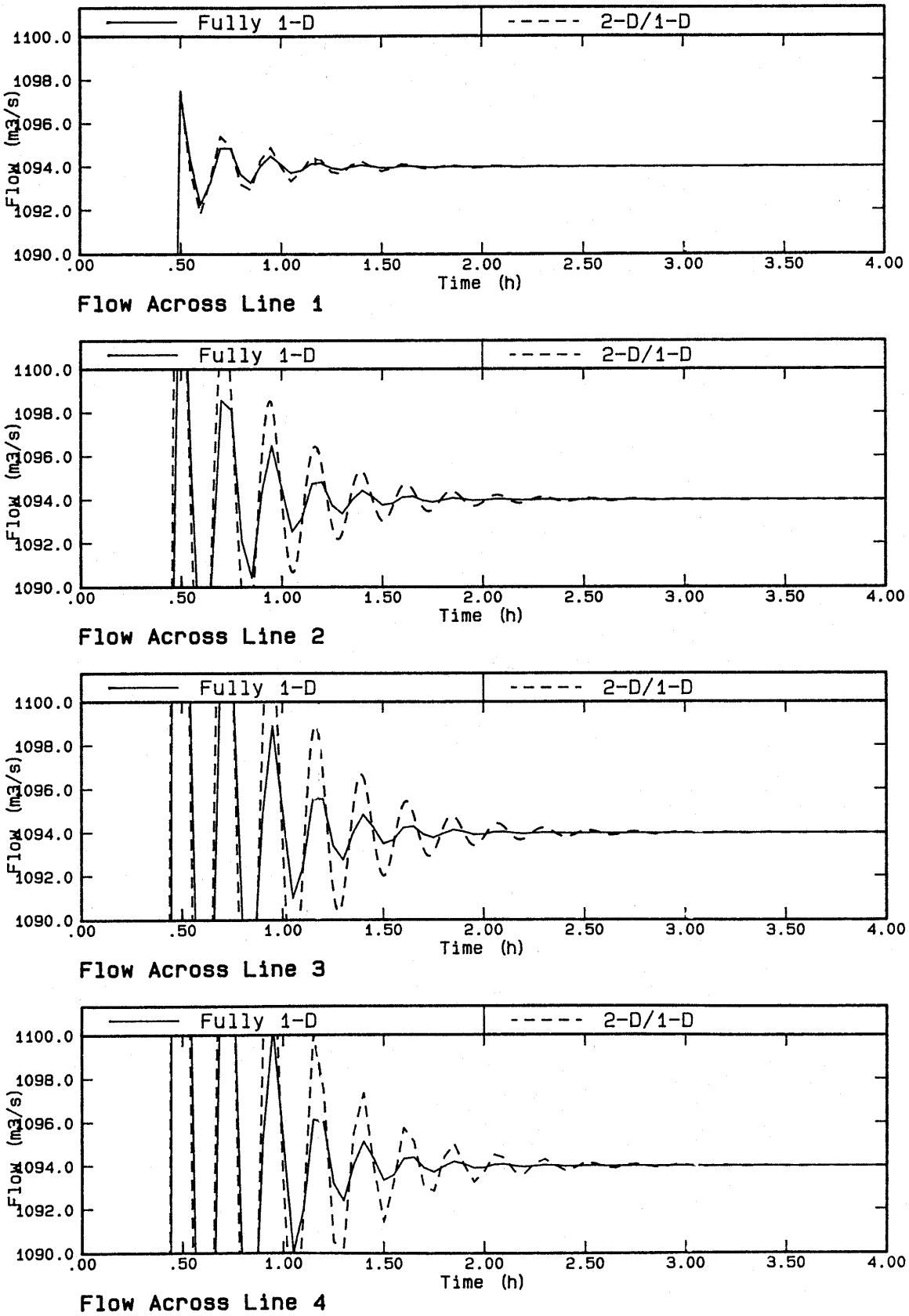


**Figure 4.2a Flow Time Histories - 2-D/1-D Uniform Flow**

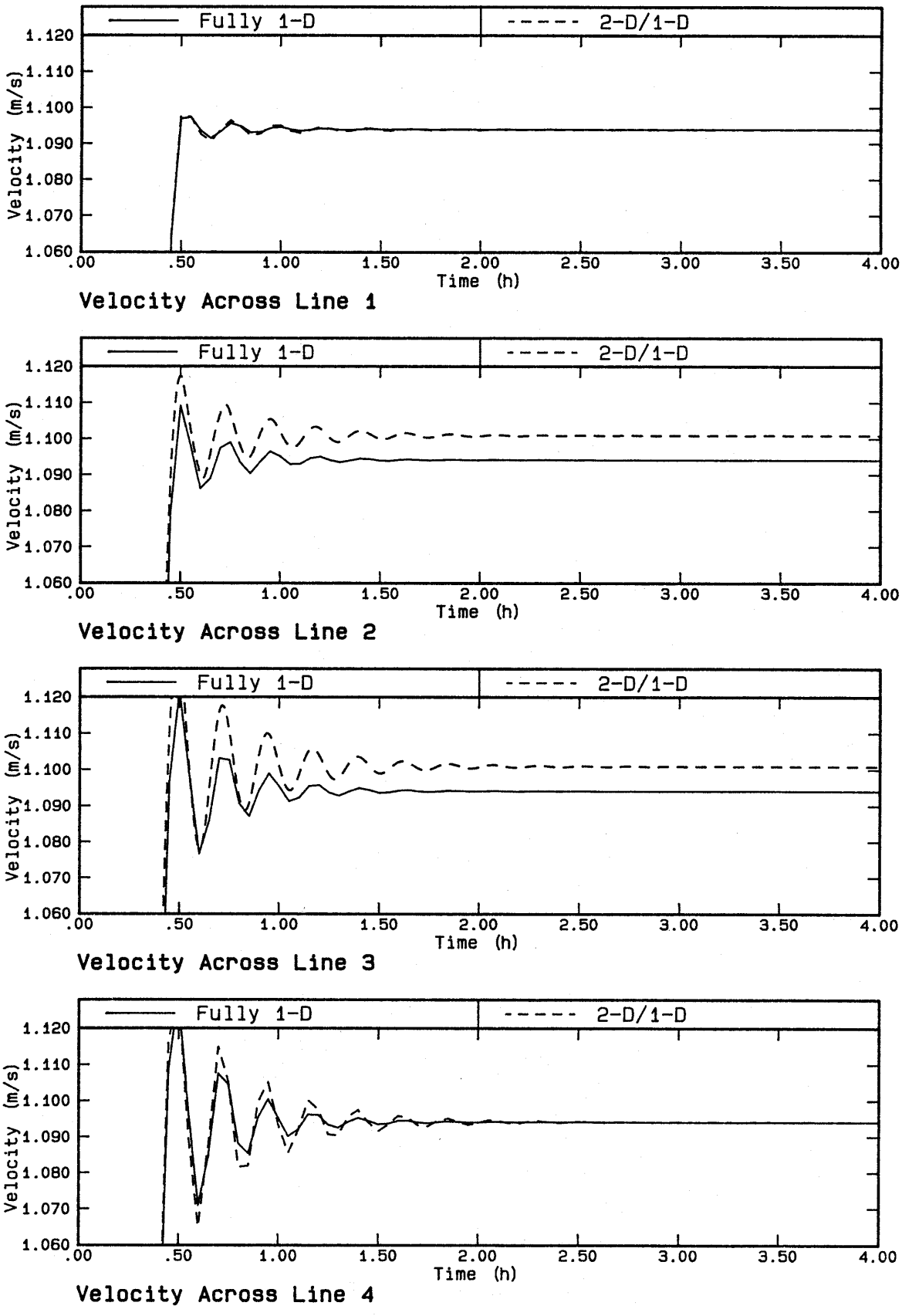


**Figure 4.2b Velocity Time Histories - 2-D/1-D Uniform Flow**

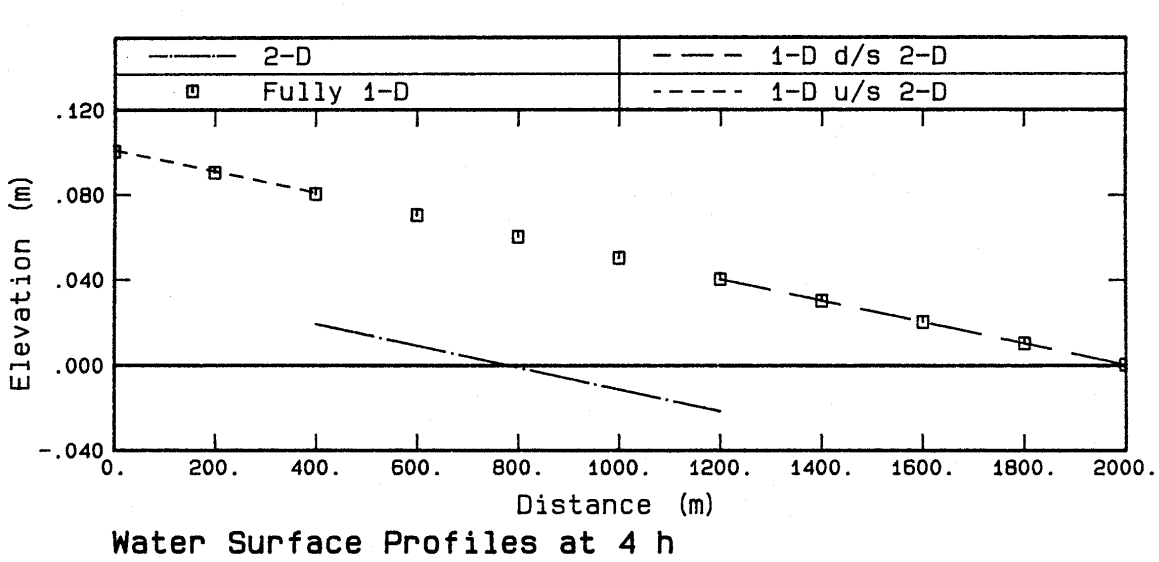


**Figure 4.2c Water Surface Profiles - 2-D/1-D Uniform Flow**

The correct velocity of 1.094 m/s was calculated for the fully 1-D model and the 1-D section of the 2-D/1-D model downstream of the 2-D section. For the 2-D section, slightly higher velocities were computed. This occurs because the water surface profile in the 2-D section is lower than that for the fully 1-D model because of the adjustment of the 1-D water level at the interface by a dynamic head (Section 4.2.3). This is illustrated by the water surface profiles at time 4.0 h in Figure 4.2c.

It is important to note here that when analytically calculating the "correct" velocities, etc., that the bed friction term in the 1-D scheme is computed using the static water levels, while the 2-D scheme uses actual water levels, so a slight difference in values will occur, especially for high velocities. However, as shown below the differences are very minimal. In this case the boundary inflow has been based on the 1-D scheme approach.

The velocity in the 2-D section was calculated analytically by iteration to be 1.1008 m/s. Further calculations for the velocity in the 1-D section upstream of the 2-D section gives a value there of 1.0939 m/s. As can be seen in the figures the model results are in accordance with these values.

Further to the above, the water surface gradient across the 2-D section would be steeper because of the higher velocity (ie. greater frictional losses). Calculations gave the corresponding decrease in water level along the length of the 2-D section to be 0.04075 m. The corresponding value calculated in the 2-D/1-D simulation was found to be the same after detailed examination of the model results.

In conclusion, the results of all the steady state simulations demonstrated the 2-D/1-D link to transfer and conserve mass correctly (with zero loss or gain of mass calculated from the results), and to have no stability constraints.

### 4.3.3 Dynamic Flow

The fully 2-D model illustrated to the left in Figure 4.3 represents a rectangular basin 3000 m by 5000 m by 20 m deep at mid tide. Waters enter and leave the basin via a long straight channel of 4000 m in length as shown in the figure. A uniform Chézy bed friction coefficient of 65 $m^{1/2}/s$ was specified

over the entire basin and the element length was set to 100 m. A sinusoidal tide of zero mean water level, 6 m range and 12 h period was defined at the entrance to the channel.

The fully 2-D model was modified to form a 2-D/1-D link model as schematised to the right in Figure 4.3. The central 2000 m of the entrance channel was replaced by two 1-D channels, and the two areas either side of the entrance channel were substituted by two 1-D storage nodes. For the 1-D channels the Manning's n value was varied with depth to comply with the Chézy formula used by the 2-D scheme. The same boundary conditions were applied to the 2-D/1-D model as for the fully 2-D model.

The simulations extended for three tidal cycles, with periodicity being achieved after the first cycle. A computation timestep of 30 s ($C_r$ = 6) and a zero diffusion coefficient was used. The timestep here was restricted by the short channels and small storage nodes in the 1-D section.

Figure 4.4a shows the flow integral time histories across Lines 1 and 2C, 2L and 2R, and Figure 4.4b presents the water surface profiles along Line 3 at the peaks of the ebb tide (3 h) and the flood tide (9 h). Comparison of each of the model simulations shows the results to be very close (in Figure 4.4a they are indiscernible). Mass can be seen to be conserved for both simulations by observation of the flow integral time histories. These plots ascertain the volume of water entering the basin during the flood tide is equal to that leaving the basin during the ebb tide. The maximum difference in water levels between the two simulations along the entrance channel (Figure 4.4b) was less than 0.005 m.

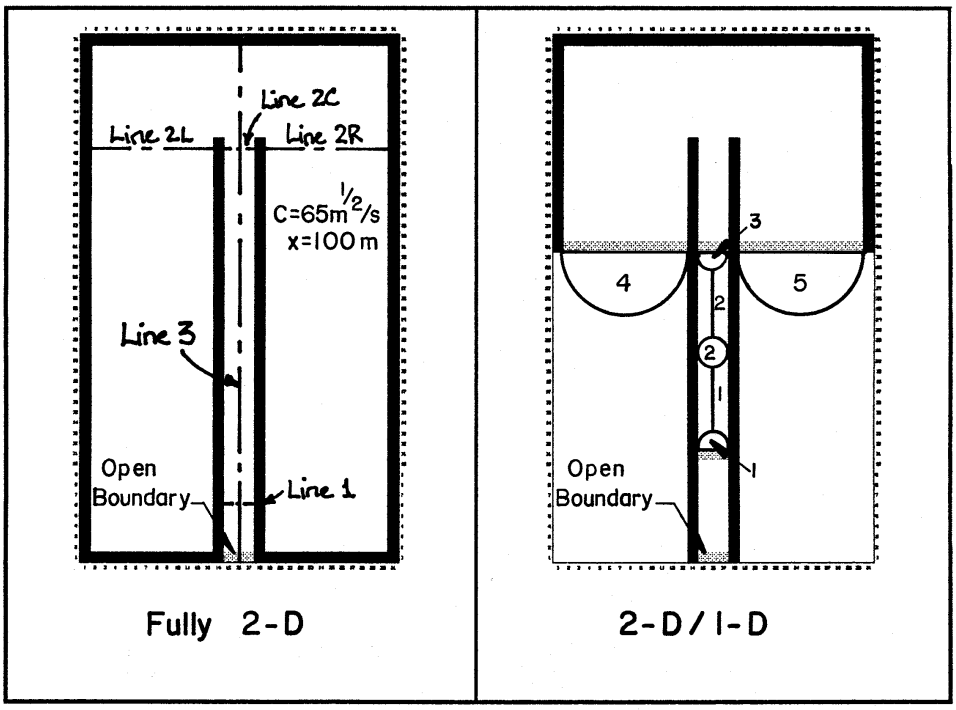


**Figure 4.3 Dynamic Flow Model Layouts for 2-D/1-D Link**

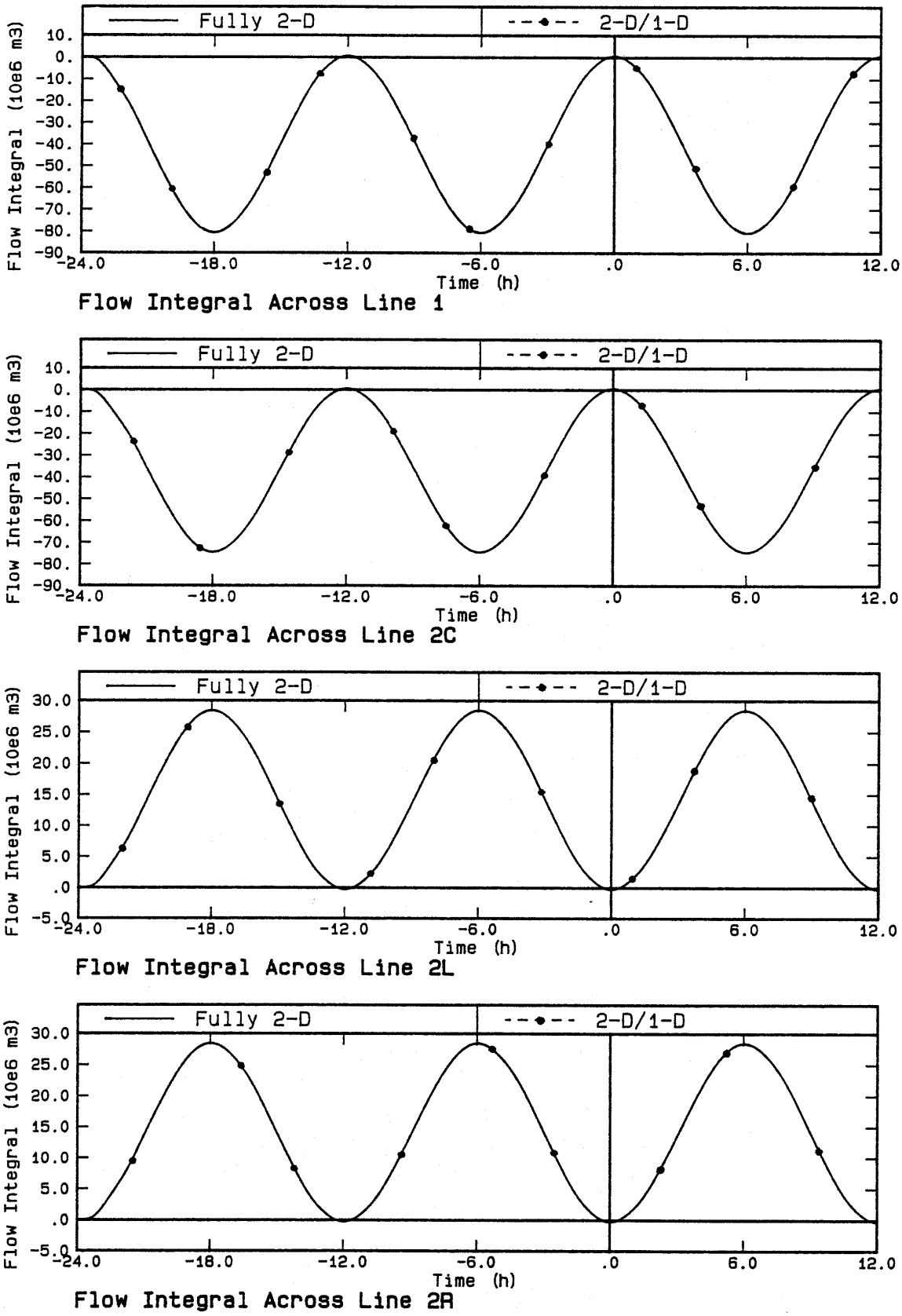


**Figure 4.4a Flow Integral Time Histories - 2-D/1-D Dynamic Flow**

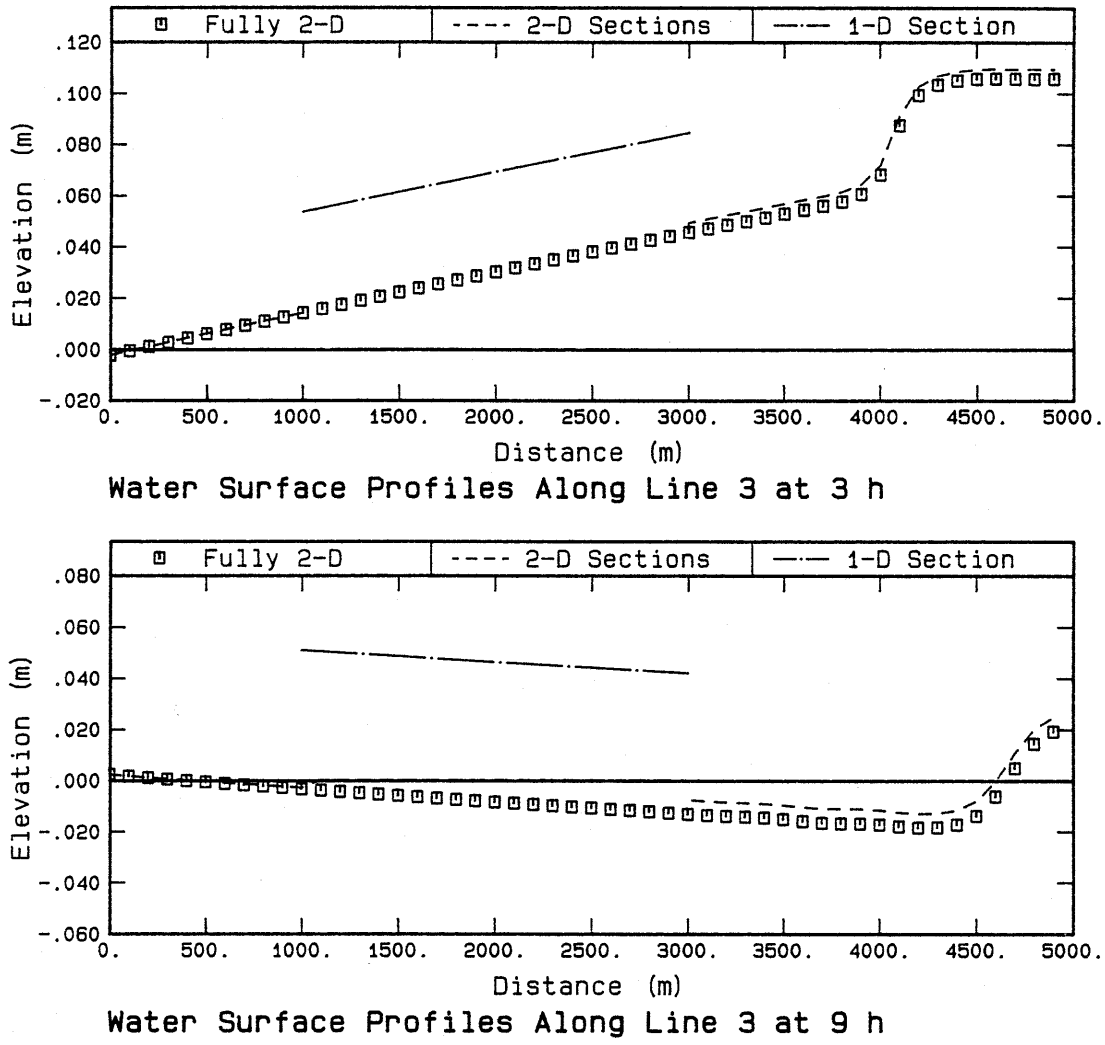


**Figure 4.4b Water Surface Profiles - 2-D/1-D Dynamic Flow**

The influence of the 1-D sections on the 2-D flow patterns can be visualised by examination of Figure 4.4c. The diagrams on the left of the figure show the flow patterns and water level contours at the peak of the flood and ebb tides for the fully 2-D model. On the right the flow patterns and the change in the velocity magnitudes for the 2-D/1-D model as compared to the fully 2-D model are shown. A green shade indicates a decrease in velocity while the red shade represents an increase in accordance with the scale shown. As can be seen, the effect of inserting the 1-D sections into the fully 2-D model was minor during the ebb tide and negligible during the flood tide with the greatest changes in velocity being 0.1 m/s and 0.04 m/s respectively.

In conclusion, the testing carried out using dynamic flow models clearly showed the 2-D/1-D link to be accurate, versatile and extremely useful for replacing sections of 2-D models by more computationally efficient 1-D models.

The selection of the areas in a 2-D model which can be replaced by 1-D models must be made so that there is no significant impact on the flow patterns in the remaining 2-D section. For example, as the 1-D sections in this test case are extended up into the flow circulations (see Flood Tide, Figure 4.19) there will be a greater influence on the flow patterns of these circulations.

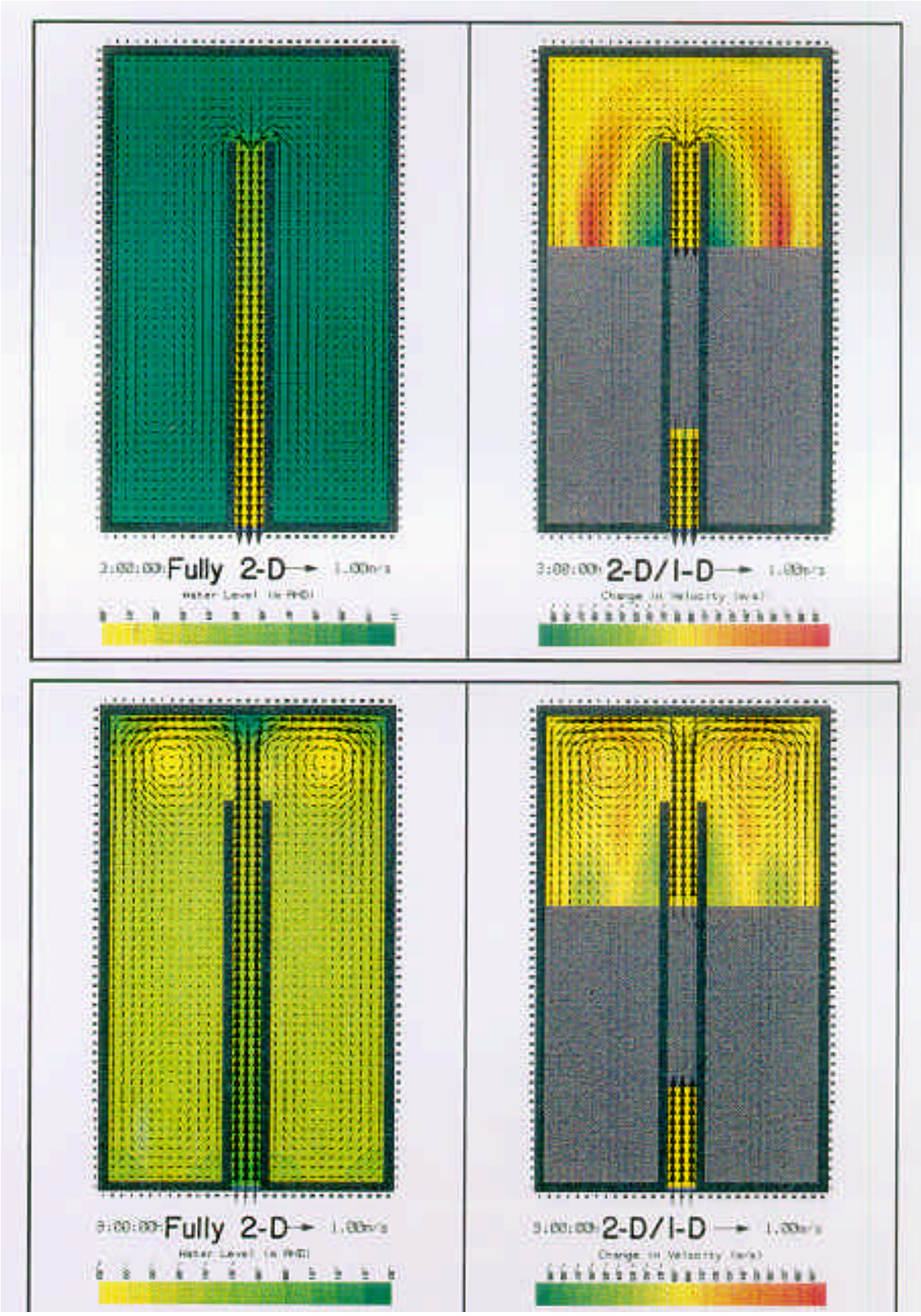


**Figure 4.4c Change in Flow Patterns at Peak Ebb (top) & Flood Tide 2-D/1-D Dynamic Flow**

## 4.4 Treatment of Oblique Boundaries

### 4.4.1 General

For practical application, it is essential to have total flexibility in locating the 2-D/1-D interface because of the irregularity of natural watercourses. This necessitates that open water level boundaries of a 2-D orthogonal grid can be specified obliquely to the grid axes, and that the flow across this boundary can be calculated accurately.

Investigations were carried out to establish whether the above requirements are practicable. Initially, several models were developed and run under steady state conditions with oblique water level boundaries. The results of these simulations were unsatisfactory because of incorrect flow distributions and instabilities (except in the case where the boundary line was at 45 degrees).

The problem arises because the water level boundary values can only be defined at fixed locations, namely the grid points where the water levels are computed.

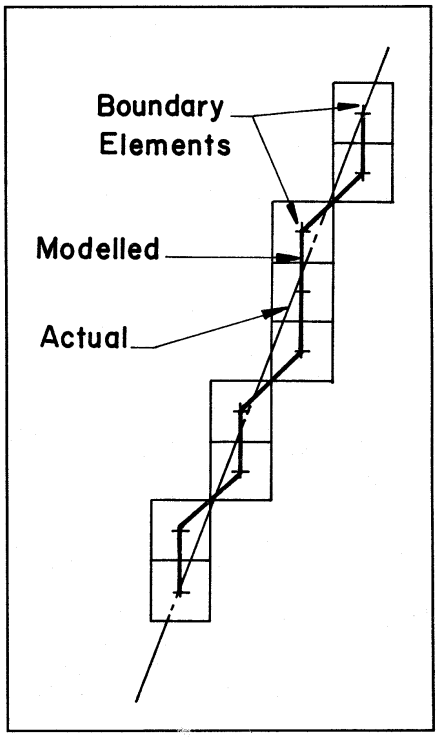


**Figure 4.5 Modelled and Actual Water Level Boundary Lines**

Thus, if an open water level boundary does not lie parallel to or at 45 degrees to the axes of the orthogonal grid, it follows an irregular path as illustrated in Figure 4.5, which tended to cause concentrations of flow where the water surface gradient was greatest.

Investigations were carried out to establish methods which would give a more accurate representation of the flow patterns and reduce the occurence of instabilities. Firstly, a method, which is presented in the next section, was established for calculating the flow across an oblique boundary. Secondly, two methods which were developed for handling oblique water level boundaries, are presented in the following sections.

### 4.4.2 Discharge Across an Oblique Boundary

It can be shown easily that the flow per unit depth across a line at 45 degrees is equal to the sum of the X and Y flow components ($u$ and $v$ velocities) multiplied by the X and Y element lengths. For lines which lie at other angles the proof of this method is somewhat more detailed.

For the arrangement shown in Figure 4.6, the discharge per unit depth, $q$, across the oblique line is given by Equation 4.4.1, while $q$ calculated by summation of the $u$ and $v$ components of the boundary elements is given by Equation 4.4.2. Both these equations can be reduced to the same form as given

in Equation 4.4.3 justifying the use of the *u* and *v* velocity components to calculate the flow across an oblique line.

$$q = \left| \sqrt{(M-1)^2 + (N-1)^2} + \cos(f) + \sin(f) \right| \Delta x \; V \quad \textbf{(4.4.1)}$$

$$q = M \; \Delta x \; V \; \cos f + N \; \Delta x \; V \; \sin f \quad \textbf{(4.4.2)}$$

Equation 4.4.4 gives the general form of the formula which can be used to calculate the discharge, *Q*, between any two elements $n_1,m_1$ and $n_2,m_2$. For the coding developed, flow was defined as positive if the X-component was positive, therefore, to be consistent with this the sign of *v* must be changed in certain situations. Also note that the element side from which the value of *v* is taken from is the lower one where the Y-component is negative. This is illustrated in Figure 4.7.

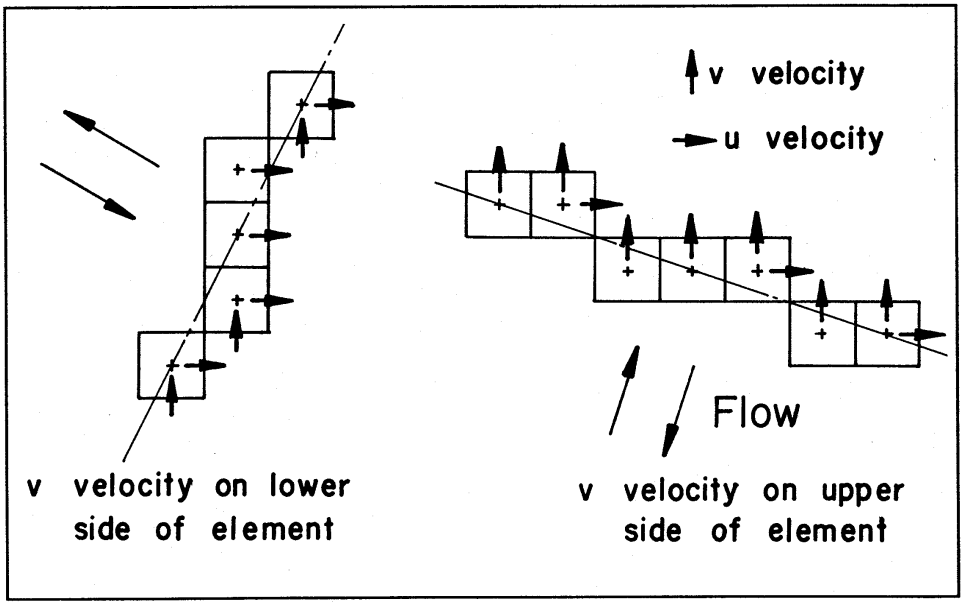


**Figure 4.6 Flow Across an Oblique Line**

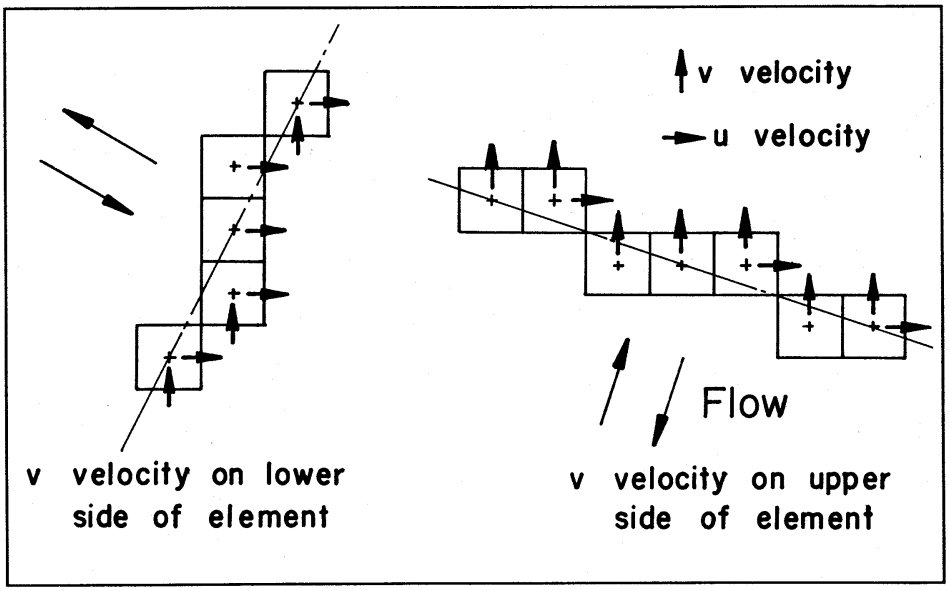


**Figure 4.7 Location of Velocity Components for Different Angles of Flow**

$$q = \frac{M^2 - M + N^2 - N}{\sqrt{(M-1)^2 + (N-1)^2}} \Delta x \; V$$

*where*

$$M = |m_2 - m_1| + 1 \qquad \textbf{(4.4.3)}$$

$$N = |n_2 - n_1| + 1$$

$$\tan f = \frac{N-1}{M-1}$$

$$Q = \sum_{i=1}^{\max(M,N)} \left[ u \, \Delta y \, H_u + v \, \Delta x \, H_v \right]$$

*where for u (v being similar) we have*

$$u = \begin{cases} 0 & \text{if } n(i) = n(i+1) \\ u_0 & \text{if } n(i) \neq n(i+1) \end{cases} \qquad \textbf{(4.4.4)}$$

*where for the case of* $n_2 > n_1$

$$n(i) = n_1 + int[d_n(i)]$$

$$d_n(i) = .5 + \frac{(i-1)(n_2 - n_1)}{\max[(n_2 - n_1), |m_2 - m_1|, 1]}$$

### 4.4.3 Stabilising Oblique Water Level Boundaries

Investigations were carried out to establish methods which would provide a more accurate simulation of the flow patterns and prevent instabilities at oblique water level boundaries.

Two methods, which are detailed below, were developed. They both make use of weighting functions which are given by Equations 4.4.5 and 4.4.6, and are illustrated in Figure 4.8. An upper X-bound is a boundary where, if the flow is leaving the model, it is flowing in the positive X-direction. Similar definitions apply to the other bounds.

$$f_x = \frac{n - b}{a} - m$$

$$f_y = a\,m + b - n$$

*where*

$$a = \frac{n_2 - n_1}{m_2 - m_1} \qquad \textbf{(4.4.5)}$$

$$b = n_1 - a\,m_1$$

*n, m are the element coordinates*

$n_1, m_1$ *and* $n_2, m_2$ *are the coordinates of the end elements*

$$f_{ob} = \begin{cases} \dfrac{1}{1 - f_x} & \text{at a lower } X\text{-bound} \\ \dfrac{1}{1 + f_x} & \text{at an upper } X\text{-bound} \\ \dfrac{1}{1 - f_y} & \text{at a lower } Y\text{-bound} \\ \dfrac{1}{1 + f_y} & \text{at an upper } Y\text{-bound} \end{cases} \qquad \textbf{(4.4.6)}$$

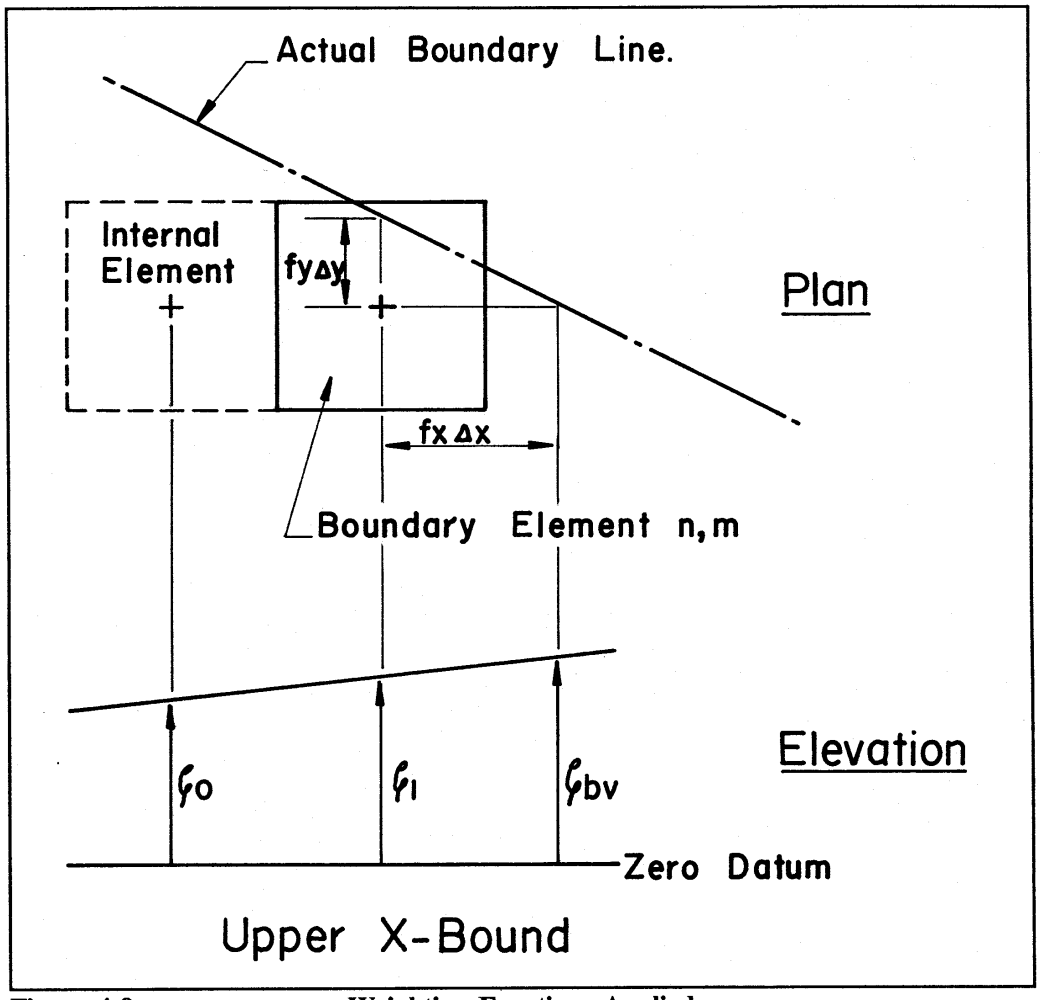


**Figure 4.8 Weighting Functions Applied at Oblique Water Level Boundaries**

## Method 1

Method 1 incorporates the weighting factor, $f_{ob}$, by adjusting implicitly the water level boundary value based on the gradient between the boundary line and the first internal grid point.

For Stage 1, Step 1 of the 2-D SWE scheme the boundary water levels are adjusted using Equation 4.4.7 and as illustrated by the Elevation in Figure 4.8.

$$z_0 = (1 - f_{ob})\, z_4^0 + f_{ob}\, z_{bv}^0 \quad \textit{at a lower bound}$$

$$z_4 = (1 - f_{ob})\, z_0^0 + f_{ob}\, z_{bv}^0 \quad \textit{at an upper bound} \qquad \textbf{(4.4.7)}$$

*where*

$z_{bv}$ = *boundary value*

Stage 1, Step 2 involves three adjustments. Firstly, the boundary water levels are adjusted when calculating the mass equation coefficients in the Y-direction in a similar manner to that given by Equation 4.4.7.

Secondly, when applying water level boundary values, the water level at the boundary element of a lower bound can be approximated by Equation 4.4.8.

$$z_3^q = z_0^q + f_{ob}(z_{bv}^1 - z_0^q) \quad \textbf{(4.4.8)}$$

Substitution of Equation 4.4.8 into Equation 3.3.7 gives Equation 4.4.9 at the first element inside the boundary.

$$q\left[f_{ob} z_{bv}^1 + (1 - f_{ob}) z_0^q\right] + r z_0^q + s z_1^q = t$$

*giving* **(4.4.9)**

$$\left[q(1 - f_{ob}) + r\right] z_0^q + s z_1^q = t - f_{ob} q z_{bv}^1$$

The modification for an upper bound is carried out in a similar manner.

Lastly, when back substituting to calculate the *u* velocities the water level boundary value is modified implicitly in accordance with the procedure for the *v* velocities of Stage 1, Step 1.

The procedure for Stage 2 is similar to that described above for Stage 1.

## Method 2

Method 2 uses the same principles as Method 1, but uses the water surface gradient at the boundary of the previous computation step to adjust explicitly the water level boundary values prior to the next computation step.

The adjustment is made using the average gradient, *S*, in the direction of the greater X or Y component of the perpendicular to the boundary line. This direction referred to as the dominant direction, is in the X-direction for the left hand diagram of Figure 4.8 and in the Y-direction for the right hand diagram. Where the dominant direction is in the X-direction, the adjusted boundary water level is given by Equation 4.4.10.

$$z_3 = z_{bv} - f_x S \quad \textit{at a lower bound}$$
$$z_1 = z_{bv} + f_x S \quad \textit{at an upper bound} \qquad \textbf{(4.4.10)}$$

*where*

$S$ = *water surface gradient*

## Test Case

To illustrate the capabilities of the above two methods the results from one of the test cases developed are presented below. The model, which is detailed in Figure 4.9, consists of a uniform channel lying obliquely to the 2-D grid axes. The channel cross-section varies uniformly from zero to 15 m deep between the banks.

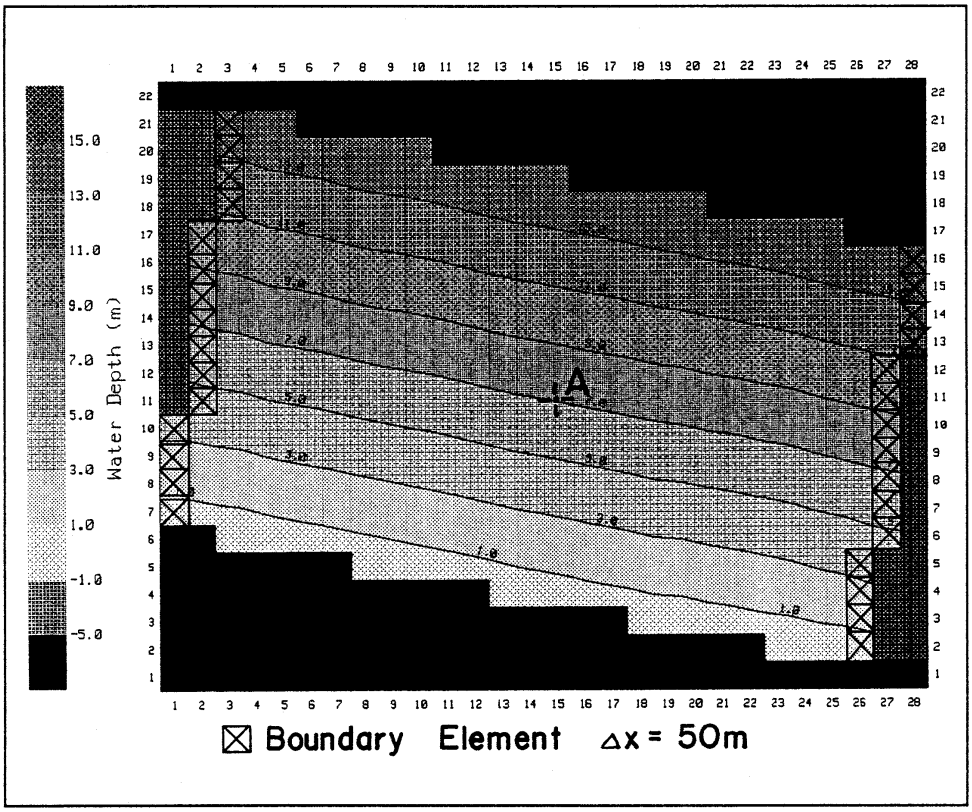


**Figure 4.9 Oblique Boundary Test Model Layout - 2-D Section**

The downstream (left hand side) boundary was defined as a constant water level of zero. For the upstream boundary a 1-D node of surface area 1,000,000 $m^2$ was linked onto the 2-D model and an inflow of 6000 $m^3/s$ was specified. The element length was 50 m and a ripple height of 0.01 m was defined for the bed friction. The Chézy value for each element was calculated according to Equation 3.5.12 in Section 3.5.4. A 45 s timestep and a simulation period of 6 h were specified.

For the case of not using either of the methods described above, ie. no adjustment of the boundary water level values, the simulation becomes unstable at around 1 h as shown by the series of flow patterns at times 35, 40, 45, 50, 55 and 60 minutes in Figure 4.10a. The instability occurs because of the variations in water surface gradients along the upstream boundary which generate localised areas of flow concentrations as can be seen by observing the flow patterns.

Application of Methods 1 and 2 both produced stable simulations with much improved flow patterns. Figure 4.10b presents the flow patterns for each method at time 6 h. Steady state conditions and mass conservation were established as shown by the time history plots in Figure 4.10c. The two methods both produce slightly different flow patterns along the upstream boundary because of their different formulation.

Practical application has shown Method 1 to be preferable to Method 2, especially in dynamic flow situations, and where there is a significant variation in depth across the boundary.

In conclusion, Method 1 is preferred, and based on the excellent results from its use in practical problems, has become a key attribute for allowing maximum flexibility in locating a 2-D/1-D interface.

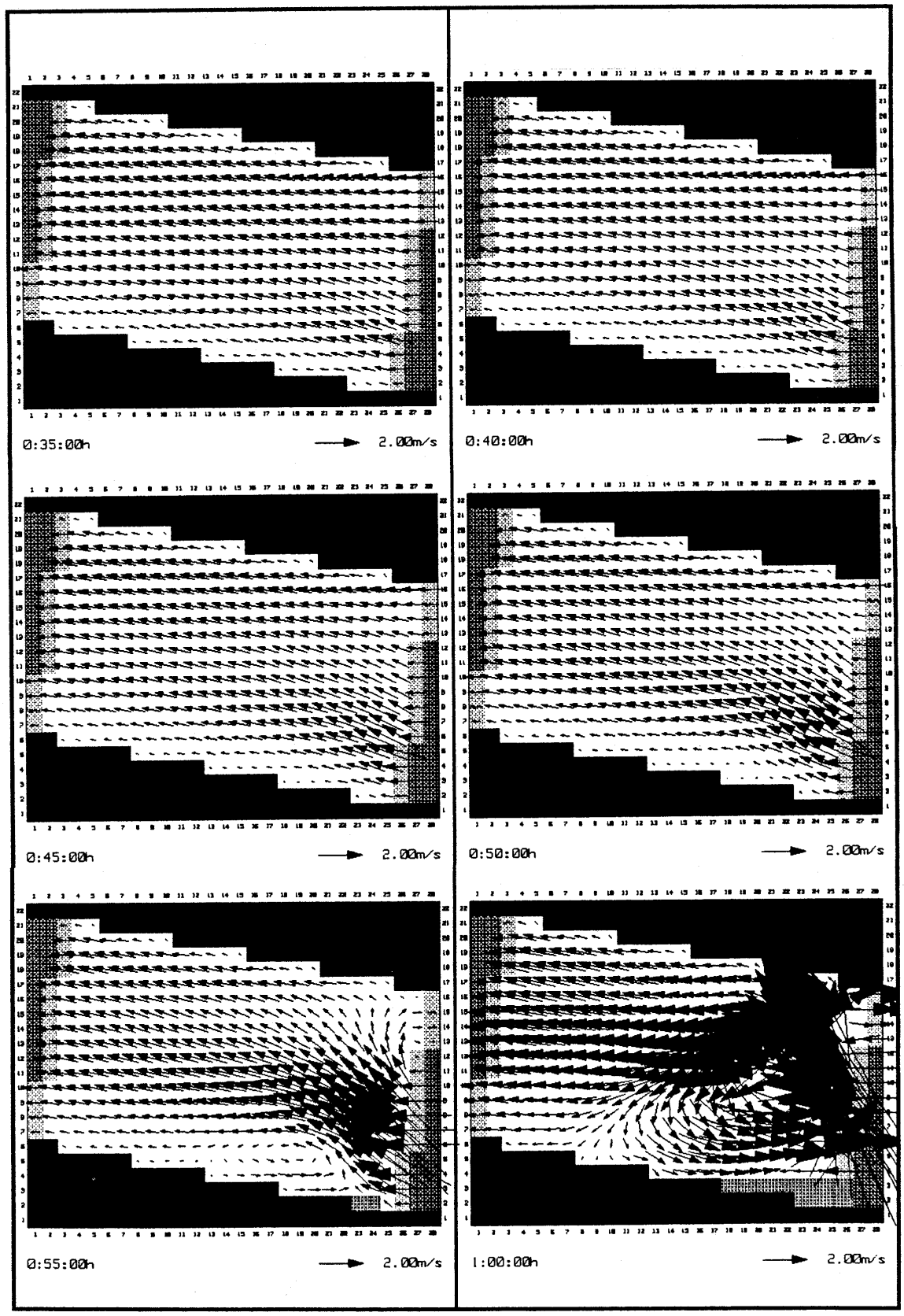


**Figure 4.10a Instability Generation at an Oblique Boundary**

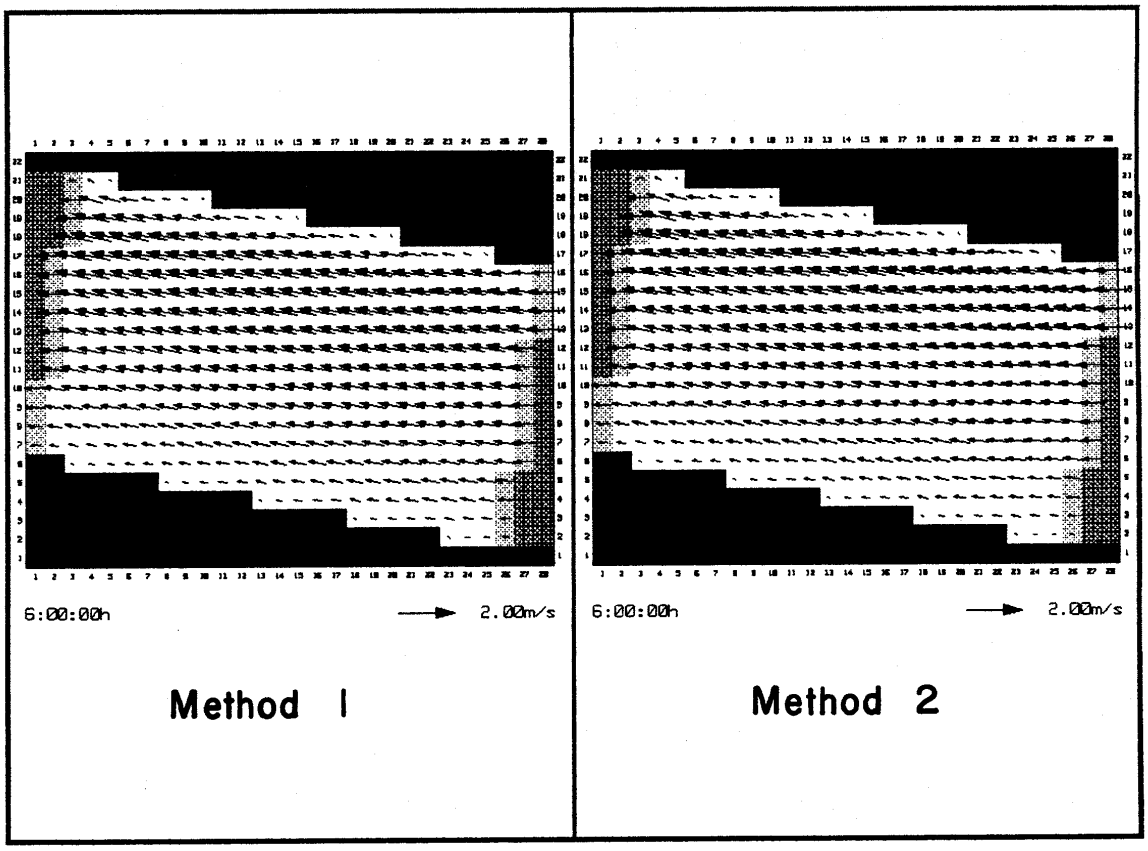


**Figure 4.10b Flow Patterns at 6 h for Methods 1 and 2 Oblique Boundary Test**

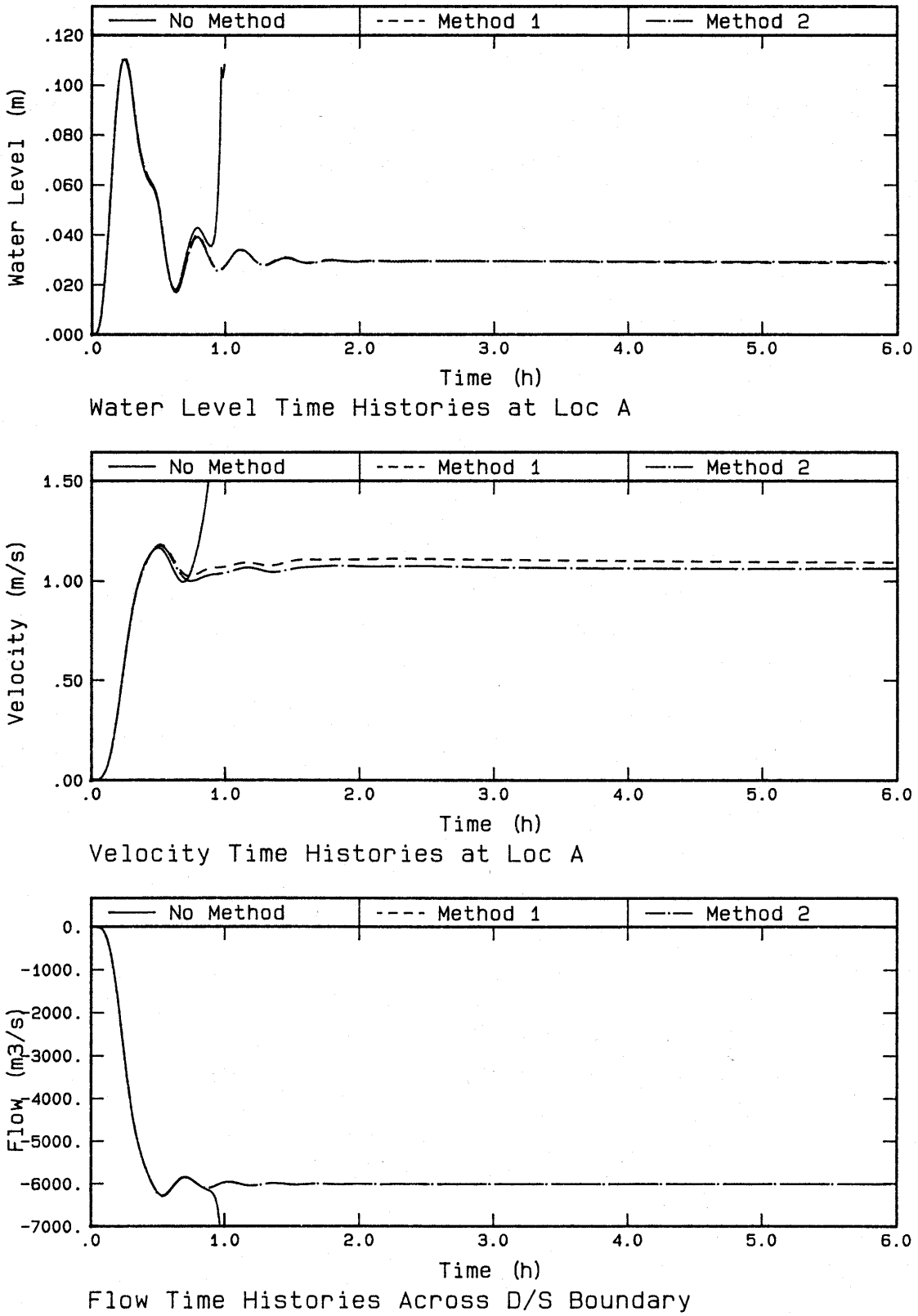


**Figure 4.10c Time Histories - Oblique Boundary Test**

# 5 CONCLUSION

A dynamically linked 2-D/1-D hydrodynamic modelling program for modelling long waves has been developed and validated.

For the 1-D scheme that of the ESTRY program was used without modification and was found to be satisfactory. For the 2-D scheme, new computer code was written based on the 2-D scheme proposed in Stelling (1984).

The 2-D scheme computer code was validated and assessed using a range of test models. The results from the testing found that:

1. Mass was conserved 100 % between internal grid elements.

2. The advection terms in the momentum equation were performing correctly.

3. Water level boundaries were extremely stable, but incorrect results can occur where only water level boundaries are specified, as the discharge across the model's boundaries is not defined.

4. Flow boundaries were highly unstable for steady state simulations, and where stable, caused a loss of mass of up to 3 % for large Courant Numbers (> 50). They showed good stability in dynamic simulations.

Three new developments of significance were achieved.

1. A method for wetting and drying of 2-D intertidal flats, which allows the continued draining of perched waters.

2. The dynamic linking of any number of 1-D network models to a 2-D model.

3. The stabilisation of water level boundaries lying obliquely to a 2-D orthogonal grid, therefore, providing maximum flexibility for locating the 2-D/1-D interface.

The wetting and drying method developed is shown to calculate the tidal prism more accurately, and to eliminate the occurrence of surges when perched waters are re-connected with the rising tide. Application in practice has shown the method to be a significant improvement over convential methods, especially in models with large areas of intertidal flats.

For dynamically linking the 1-D and 2-D schemes, a simple but effective method was used. The 1-D and 2-D boundaries at the interface are treated as normal open boundaries. A flow boundary is specified for the 1-D model and a water level boundary for the 2-D model. At the end of each computation step boundary condition data is transferred from one model to the other. For the 1-D boundary, the flow across the 2-D model boundary is specified, while for the 2-D boundary the water level from the 1-D model is used.

The conditions at the 2-D/1-D interface are that the water level is approximately horizontal, there is negligible variation in the convective acceleration terms, and the flow is perpendicular to the 2-D model boundary. These are essentially the same conditions which are applied at the open boundaries of the 1-D and 2-D schemes.

Testing has shown the 2-D/1-D link to conserve mass 100%, to have no stability problems and to not generate numerical disturbances. Application to more than twenty production models has shown it to be a very useful and powerful facility.

A key aspect in the successful application of the 2-D/1-D link was the development of a method for stabilising water level boundaries which lie obliquely to the orthogonal 2-D grid. This provides maximum flexibility for locating the interface, which in practice is extremely important, because of the irregularity of natural water bodies.

# 6 REFERENCES

**Abbott M B, Damsgaard A, Rodenhuis G S (1973)** *System 21, Jupiter, A Design System for Two-Dimensional Nearly Horizontal Flows* Journal of Hydraulic Research **11**, 1-28

**Abbott M B (1979)** Computational Hydraulics - Elements of the theory of free surface flows Pitman Publishing Limited, London, UK

**Apelt C J (1982)** *A One-Dimensional Dynamic Flow Model* Proceedings, Workshop on Applied Dynamic Flow Modelling, Brisbane, December 1982 Vol II, Brisbane, ACADS and the Institution of Engineers Australia, 1-22

**Apelt C J, Gout J J, Szewczyk A A (1974)** *Numerical Modelling of Pollutant Transport and Dispersion in Bays and Estuaries* Numerical Methods in Fluid Dynamics Pentech Press, London, UK, 307-24

**Benque J P, Cunge J A, Feuillet J, Hanguel A, Holly F M (1982a)** *New Method for Tidal Current Computation* Journal of the Waterway, Port, Coastal and Ocean Division ASCE, v108, No WW3, Aug 1982, 396-417

**Benque J P, Hanguel A, Viollet P L (1982b)** Engineering Applications of Computational Hydraulics, Vol II Pitman, London, 1982

**Collins N I (1988)** Dynamic Flow Modelling - Comparison and Evaluation of Current Models M.Eng.Sc Thesis, The University of Queensland, August 1988

**Crean P B, Murty T S, Strongach J A (1988)** *Mathematical Modelling of Tides and Estuarine Circulation* Lecture Notes on Coastal and Estuarine Studies v30, Springer-Verlag, New York, 1988

**Danish Hydraulic Institute (1983)** *Special Presentation of Mathematical Modelling* Numerical Modelling in Hydraulics and Water Resources - Special Presentations of Recent Developments Twentieth IAHR Biennial Congress, Moscow, Sep 1983

**Engelund F, Hansen E (1972)** A Monograph on Sediment Transport in Alluvial Streams Technical University of Denmark, ISBN 87 571 0422 0, 1972

**Falconer R A (1986)** *Water Quality Simulation Study of a Natural Harbor* Journal of the Waterway, Port, Coastal and Ocean Division ASCE, v112, No 1, Jan 1986, 15-34

**Falconer R A, Owens P H (1987)** *Numerical Simulation of Flooding and Drying in a Depth-Averaged Tidal Flow Model* Proc Instn Civ Engrs Part 2, **83**, Mar 1987, 161-180

**Floyd J M (1988)** Two-Dimensional Tidal Flows - Implementation of Wilders Implicit Scheme Report IT330, Hydraulics Research Ltd, Wallingford, Dec 1988

**Leendertse J J (1967)** Aspects of a Computational Model for Long Water Wave Propagation The RAND Corporation, Memorandum RH-5299-PR, Santa Monica, California

**Leendertse J J (1970)** A Water-Quality Simulation Model for Well-Mixed Estuaries and Coastal Seas: Volume 1, Principles of Computation The RAND Corporation, Memorandum RM-6230-RC, Feb 1970

**Morrison W R B, Smith P A (1978)** *A Practical Application of a Network Model* Numerical Simulation of Fluid Motion North Holland Publishing Company, Amsterdam, 1978

**Rosenberg D U van (1969)** Methods for the Numerical Solution of Partial Differential Equations American Elsevier Publishing Company, New York, 1969

**Stelling G S (1981)** *Coupling 1-D and 2-D Horizontal Flow Models* Numerical Methods for Coupled Problems Proc International Conf, Swansea, 1981, 1005-1016

**Stelling G S (1984)** On the Construction of Computational Methods for Shallow Water Flow Problems Rijkswaterstaat Communications, No 35/1984, The Hague, The Netherlands

**Stelling G S, Wiersma A K, Willemse J B T M (1986)** *Practical Aspects of Accurate Tidal Computations* Journal of Hydraulic Engineering ASCE, v112, No 9, Sep 1986, 802-817

**Syme W J (1989)** *Computer Graphic Techniques - An Essential Tool for Interpreting and Analysing a Dynamic Flow Model* WATERCOMP '89 ACADS and I.E.Aust, Melbourne, May/Jun 1989, 245-249

**Syme W J (1990a)** *Practical 1-D and 2-D Computer Modelling of Flow and Transport Processes in Rivers, Estuaries and Coastal Waters* Queensland Division Technical Papers The Institution of Engineers Australia, Vol 31, No 23, Sep 1990, 15-19

**Syme W J, Apelt C J (1990b)** *Linked Two-Dimensional/One-Dimensional Flow Modelling Using the Shallow Water Equations* Conference on Hydraulics in Civil Engineering 1990 The Institution of Engineers Australia, Sydney, Jul 1990, 28-32

**Weare T J (1979)** *Errors Arising from Irregular Boundaries in ADI Solutions of the Shallow Water Equations* International Journal for Numerical Methods in Engineering John Wiley and Sons Ltd, 1979, v14, 921-931

# APPENDIX A: ARCHITECTURE OF THE SOFTWARE

The architecture of the software developed for this study is illustrated in Diagrams A-1 to A-3 on the following pages.

Diagram A-1 shows the global structure of the software, illustrating the links between the data processing and technical computations.

Diagram A-2a represents the major steps performed each time the 2-D/1-D program is executed. Step 11 in Diagram A-2a is detailed in Diagram A-2b which depicts the computational steps carried out every half-timestep. In Diagram A-2b, Stage 1 represents the first half of the timestep and Stage 2 the second half (refer to Chapter 3 for details).

Diagram A-3 illustrates the steps involved in the 2-D/1-D link and how they interact with the computational steps given in Diagram A-2b. The diagram presents the case for Stage 1. For Stage 2 (second half of timestep) the same procedure as shown in Diagram A-3 is used, except that Stage 2 is substituted for Stage 1.

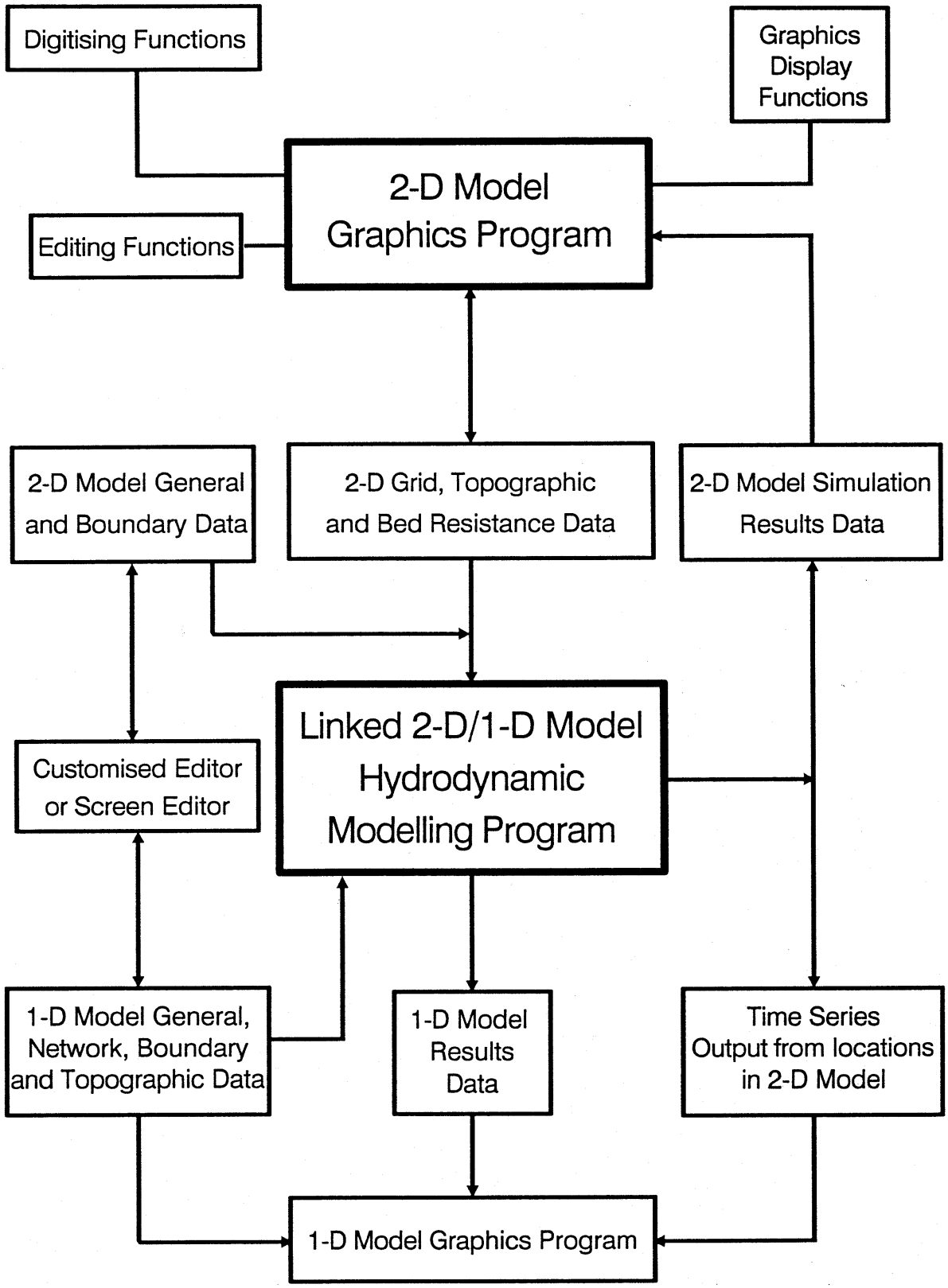


**Diagram A-1 Global Structure**

## Linked 2-D/1-D Hydrodynamic Program Steps

0 START

1 Read dimensions of 2-D model and data array sizes. Allocate memory and set pointers for dynamic arrays.

2 Read general data for 2-D model.

3 Read topographic data of 2-D model generated by graphics editor.

4 Read boundary data of 2-D model.

5 Initialise work variables and arrays.

6 Check data.

7 Set wet/dry flags.

8 Set up 1-D model. Execute ESTRY data input, dynamic memory allocation, checking and initialising procedures.

9 Initialise run-time variables.

10 Execute ESTRY run-time initialisation procedure.

11 Perform hydrodynamic computations.
(See Diagram A-2b)

12 Write time series data at selected locations.

13 Execute ESTRY data output procedures.

14 END

**Diagram A-2a Linked 2-D/1-D Hydrodynamic Program Steps**

## Hydrodynamic Computation Steps

The following steps are performed every half-timestep.

Stages 1 and 2 are defined in Chapter 3. Stage 1, Steps 1 and 2 represent the computations during the first half of a timestep, while Stage 2, Steps 1 and 2 represent those of the second half of a timestep.

**1**

t = t + Δt/2  Δt = one timestep, t = time

**2**

Retain hydrodynamic variables from previous half time-step.

**3**

Calculate 2-D model boundary values at time t.

**4**

Transfer water levels from 1-D scheme to 2-D model boundary values.

**5**

Execute wetting and drying procedures.

**6**

If first half of timestep then
  Compute Stage 1 / Step 1 of 2-D scheme.
  (Advance *v* velocities to time t.)
otherwise
  Compute Stage 2 / Step 1 of 2-D scheme.
  (Advance *u* velocities to time t.)

**7**

If first half of timestep then
  Compute Stage 1 / Step 2 of 2-D scheme.
  (Advance ζ (water levels) and *u* velocities to time t.)
otherwise
  Compute Stage 2 / Step 2 of 2-D scheme.
  (Advance ζ (water levels) and *v* velocities to time t.)

**8**

Calculate discharges across 2-D/1-D interfaces and transfer to 1-D model boundary values.

**9**

1-D Scheme Computations:
If first half of timestep then
  Execute Stage 1 ESTRY computation procedures.
otherwise
  Execute Stage 2 ESTRY computation procedures.

**10**

If end of timestep and t = save results time then
  Write 2-D results, ie. ζ, *u*, *v* and wet/dry flags, to file.
(1-D results are saved at specified times in Step 9.)

**Diagram A-2b Hydrodynamic Computation Steps**

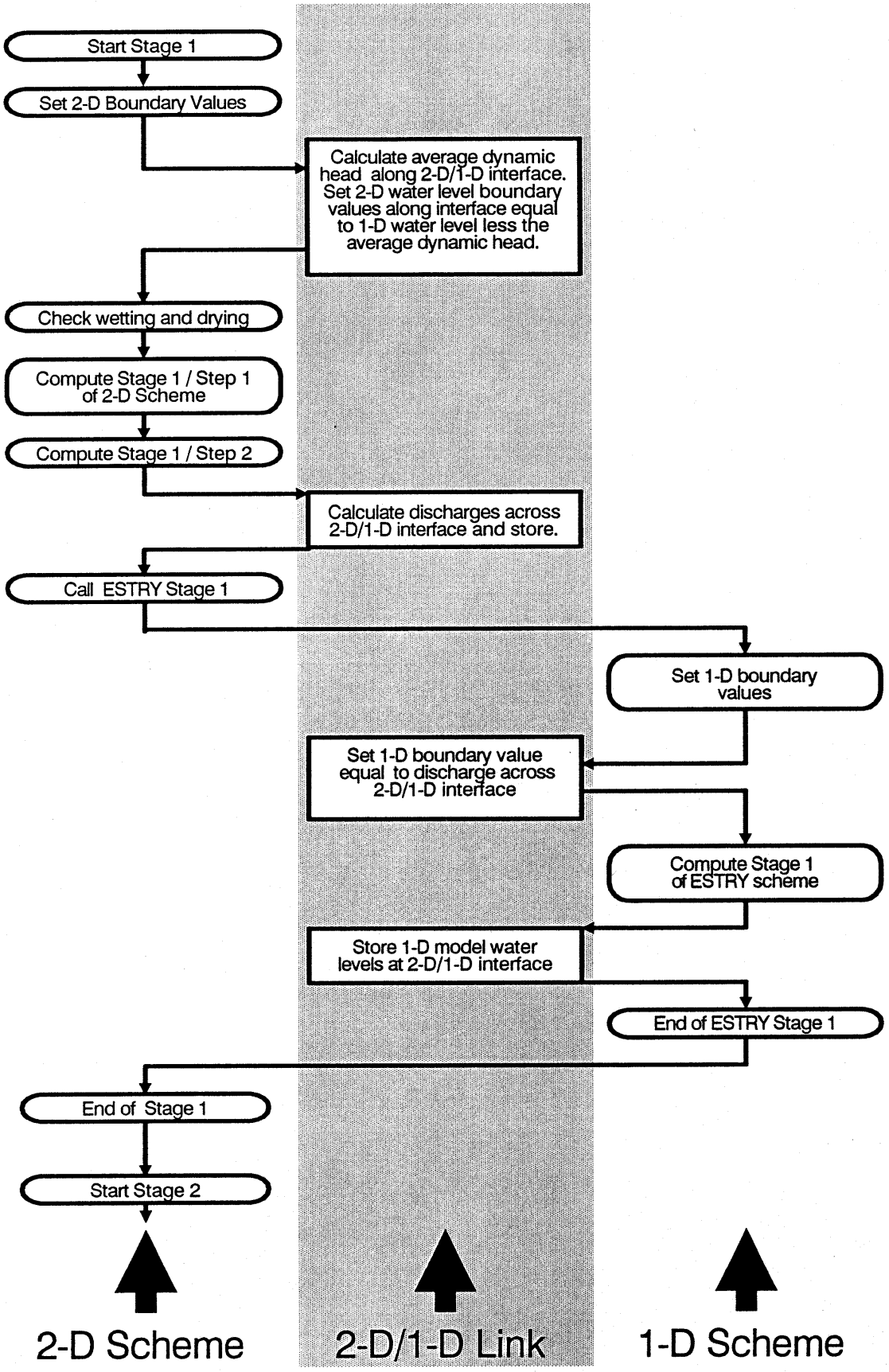


**Diagram A-3 2-D/1-D Link Structure**